

Exact Gradient Evaluation for Adaptive Quadrature Approximate Marginal Likelihood in Mixed Models for Grouped Data

Alex Stringer*

Department of Statistics and Actuarial Science, University of Waterloo

November 13, 2024

Abstract

A method is introduced for approximate marginal likelihood inference via adaptive Gaussian quadrature in mixed models with a single grouping factor. The core technical contribution is an algorithm for computing the exact gradient of the approximate log-marginal likelihood. This leads to efficient maximum likelihood via quasi-Newton optimization that is demonstrated to be faster than existing approaches based on finite-differenced gradients or derivative-free optimization. The method is specialized to Bernoulli mixed models with multivariate, correlated Gaussian random effects; here computations are performed using an inverse log-Cholesky parameterization of the Gaussian density that involves no matrix decomposition during model fitting, while Wald confidence intervals are provided for variance parameters on the original scale. Simulations give evidence of these intervals attaining nominal coverage if enough quadrature points are used, for data comprised of a large number of very small groups exhibiting large between-group heterogeneity. The Laplace approximation is well-known to give especially poor coverage and high bias for data comprised of a large number of small groups. Adaptive quadrature mitigates this, and the methods in this paper improve the computational feasibility of this more accurate method. All results may be reproduced using code available at <https://github.com/awstringer1/aghmm-paper-code>.

Keywords: Adaptive quadrature; approximate inference; grouped data; longitudinal data; mixed models

*The author gratefully acknowledges funding from the Natural Sciences and Engineering Research Council of Canada, and helpful comments from Drs. Art Owen and Audrey Bélieau.

Contents

1	Introduction	4
1.1	Background	4
2	Mixed Models and Approximate Marginal Likelihood	7
2.1	Mixed Models for Grouped Data	7
2.2	Approximate Marginal Likelihood Inference	8
2.3	Computation of the maximum approximate marginal likelihood estimator	10
3	Computations with the approximate marginal likelihood	11
3.1	Exact gradient computation	11
3.1.1	Implicit differentiation of $\hat{u}_i(\theta)$	13
3.1.2	Algorithmic differentiation of $L(\theta, u)$	13
3.2	Point Estimation	14
3.3	Confidence intervals	15
3.4	Scalar random effects	16
4	Bernoulli mixed models with multivariate Gaussian random effects	17
4.1	Likelihood calculations	17
4.2	Multivariate Gaussian random effects	18
4.3	Empirical Evaluation	21
4.3.1	Absolute performance	21
4.3.2	Relative performance	23
5	Data Analysis	24
5.1	Smoking cessation	25
5.2	Toenail fungus treatment	25
6	Discussion	27
A	Algorithms	33
A.1	Approximate marginal log-likelihood and exact gradient	34
A.2	Forward substitution	36
A.3	Multivariate Gaussian quantities	36
B	Exponential family calculations	39
C	Complete Simulation Results	41
C.1	Simulation 1: absolute performance of the new method	41
C.2	Simulation 2: relative performance of the new method	73
C.2.1	Comparison with <code>GLMMadaptive</code>	73
C.2.2	Comparison with <code>lme4</code>	82
C.2.3	Comparison with <code>glmmTMB</code>	90
C.3	Additional simulation: scalar random effects	90

D Additional details for data analyses	103
D.1 Smoking cessation	103
D.2 Toenail fungus treatment	108

1 Introduction

1.1 Background

Grouped data, including longitudinal or repeated measures data, are common in modern practice. A popular class of models for grouped data are mixed models in which observations are assumed independent conditional on latent group-specific characteristics. This conditional independence yields a joint likelihood, but because this joint likelihood includes latent variables, it cannot be used directly for inference. Likelihood inferences in mixed models are instead based on the marginal likelihood of the observed data, defined as an integral of the joint likelihood over the latent variables. In general, this integral is intractable and must be approximated, and in practice inferences about parameters are made by maximizing an approximate marginal likelihood. This paper discusses a method for accurate and efficient approximate marginal likelihood inference in mixed models for grouped data with a single grouping factor.

Intractable integrals occur routinely in statistical inference. The unique aspect of the models considered in this paper is the factoring of the marginal likelihood into a product of m low-dimensional integrals, where m is the number of groups present in the data. This structure is computationally convenient, as it enables accurate approximation of the marginal likelihood using low-dimensional (adaptive) quadrature. However, it also introduces a critical *requirement* for high accuracy that has not been fully appreciated. The marginal likelihood is a product of m integrals, and hence any approximation with fixed relative accuracy will incur error tending to ∞ as $m \rightarrow \infty$. However, $m \rightarrow \infty$ is *necessary* for consistent estimation of parameters (Nie, 2007; Jiang et al., 2022). This yields the result that as more data are obtained, estimation quality will *degrade* unless each of the m integrals are approximated with increasingly high accuracy. An integral approximation attaining arbitrarily high accuracy is required for inference about parameters in mixed models for grouped data.

Adaptive Gauss-Hermite quadrature (AGHQ; simply AQ in what follows) has been used in statistical problems for decades (Naylor and Smith, 1982; Tierney and Kadane, 1986; Liu and Pierce, 1994; Jin and Andersson, 2020), including for fitting mixed models (Pinheiro and Bates, 1995a; Pinheiro and Chao, 2006; Bates et al., 2015; Rizopoulos, 2020). The technique has recently been shown to provide arbitrarily accurate low-dimensional integral

approximations in statistical problems (Bilodeau et al., 2022), number of groups, m . and this motivates AQ as a method for fitting mixed models. However, computing the AQ approximation to the marginal likelihood even for a single parameter value is non-trivial, and hence maximizing it using numerical optimization is challenging. Current state-of-the-art approaches to fitting mixed models either use AQ with finite-differenced gradients (R package **GLMMadaptive**, Rizopoulos 2020) or derivative-free optimization (R package **lme4**, Bates et al. 2015; one-dimensional random effects only). The latter approach suffers from requiring a potentially excessive number of function evaluations (Nocedal and Wright, 2006, section 9.2) while the former suffers from the same problem as well as potential inaccuracies in the gradient evaluation (Nocedal and Wright, 2006, section 9.1), leading to computational challenges compared to methods depending on exact gradients. The core technical contribution of the present paper is an algorithm for computing the *exact* gradient of the approximate log-marginal likelihood for any number of quadrature points and random effects dimension ≥ 1 . Quasi-Newton optimization with this novel exact gradient is shown to outperform these existing approaches in terms of speed (usually by around $2 - 4 \times$) while matching or improving stability.

When run with a single quadrature point AQ is the Laplace approximation. The Laplace approximation is used extensively in marginal likelihood approximation for latent variable models and forms the basis of many classical approaches to fitting mixed models; see Breslow and Clayton (1993) and Wolfinger (1993). Exact gradient evaluation algorithms exist for the Laplace approximate marginal likelihood in general (Kristensen et al., 2016) and for mixed models (Brooks et al., 2017), and both Newton (Wood et al., 2016) and quasi-Newton (Stringer et al., 2023) optimization based on these exact gradients have been shown to be fast and stable. Unfortunately, the Laplace approximation is often not sufficiently accurate for inference in mixed models; see Joe (2008); Kim et al. (2013) and Section 4.3 of the present paper for empirical evidence. In cases where the Laplace approximation is not sufficiently accurate, these same references provide evidence that AQ can be sufficiently accurate, and the evidence from the Laplace case suggests that use of quasi-Newton optimization with an exact gradient could mitigate the computational challenges associated with this more accurate method. This observation motivates the development of the exact gradient evaluation algorithm for the AQ-approximate marginal likelihood presented in this paper.

In this paper we derive an algorithm for computing the exact gradient of the AQ-approximate marginal likelihood for mixed models with a single grouping factor. This leads to efficient quasi-Newton optimization that substantially outperforms existing approaches based on finite-differenced gradients and derivative-free optimization; specifically, in sections 4 and 5 it is shown to yield results as or more satisfactory than these existing approaches with a typical factor of $2 - 4 \times$ reduction in computation time for binary mixed models with correlated random intercepts and slopes. The procedure applies to the broad class of mixed models defined in Section 2 that includes generalized linear and non-linear mixed effects models with response distributions not limited to the exponential family and random effects distributions not limited to the Gaussian. In Section 4 we specialize the method to Bernoulli mixed models with multivariate correlated Gaussian random effects, a specific type of mixed model of substantial practical importance for which obtaining accurate inferences is known to be challenging. We use an inverse log-Cholesky parameterization of the multivariate Gaussian, such that evaluating the density requires no matrix decomposition or inversion, yielding efficient computation and closed-form derivative expressions. We then back-transform to provide Wald confidence intervals for variance parameters on the scale on which they are defined in the model, yielding interval estimates for quantities reported in practice. Simulations demonstrate that these intervals attain nominal coverage when enough quadrature points are used, even for large numbers of small groups exhibiting large heterogeneity. In contrast, as is well-known, the Laplace approximation performs poorly, exceptionally so in cases with very small groups that are common in practice. Our simulation results corroborate this observation and highlight it by presenting it in tandem with results from the AQ approximation, which is acceptably accurate. In Section 5 we apply the new procedure to two previously reported data examples, showing that the approach based on exact gradients out-performs existing approaches in computation time while returning indistinguishable inferences. This includes a comparison to the computationally demanding (but accurate) profile likelihood and bootstrap confidence intervals for variance parameters favoured by `lme4`; our Wald intervals for the variance parameters are very similar to these but 1 to 3 orders of magnitude faster to compute for a data example exhibiting very large between-subject variability.

2 Mixed Models and Approximate Marginal Likelihood

2.1 Mixed Models for Grouped Data

We consider the following class of two-level mixed models:

$$\begin{aligned} Y_{ij} \mid \mathbf{u}_i &\stackrel{\text{ind}}{\sim} F(\mu_{ij}, \boldsymbol{\phi}), \quad \mathbf{u}_i \stackrel{\text{iid}}{\sim} G(\boldsymbol{\sigma}), \\ \eta_{ij} &= h(\mu_{ij}) = \Psi(\mathbf{x}_{il}, \mathbf{v}_{ij}, \mathbf{u}_i; \boldsymbol{\beta}). \end{aligned} \tag{1}$$

Here $i = 1, \dots, m$ indexes groups and $j = 1, \dots, n_i$ indexes observations within groups which have size n_i ; when all groups are the same size, this size is denoted by $n_i \equiv n$. The $Y_{ij} \in \mathcal{Y} \subseteq \mathbb{R}$ and $\mathbf{u}_i \in \mathcal{U} \subseteq \mathbb{R}^d$ are the observed and unobserved stochastic components—data and random effects—of the model, having distributions $F(\mu_{ij}, \boldsymbol{\phi})$ and $G(\boldsymbol{\sigma})$ respectively. The corresponding densities, $f(\mu_{ij}, \boldsymbol{\phi})$ and $g(\boldsymbol{\sigma})$, are assumed to be at least three times continuously differentiable with respect to μ_{ij} , $\boldsymbol{\phi}$, and $\boldsymbol{\sigma}$. The covariates, $\mathbf{x}_{ij}, \mathbf{v}_{ij}$, are assumed fixed and known, and the regression function, Ψ , is assumed fixed and known up to unknown parameters $\boldsymbol{\beta}$, and to be at least three times continuously differentiable. The mean parameter, μ_{ij} , takes values in a space $\mathcal{M} \subseteq \mathbb{R}$ and the link function, $h : \mathcal{M} \rightarrow \mathbb{R}$, is assumed monotone and at least three times continuously differentiable. The unknown parameters, $\boldsymbol{\theta} = (\boldsymbol{\beta}, \boldsymbol{\phi}, \boldsymbol{\sigma})$, are referred to as regression coefficients, dispersion parameters, and variance parameters respectively.

The full model (Eq 1) is general, and restrictions yield more familiar models. With G a zero-mean Gaussian, F from the exponential family, and linear regression function, $\Psi(\mathbf{x}_{il}, \mathbf{v}_{ij}, \mathbf{u}_i; \boldsymbol{\beta}) = \mathbf{x}_{ij}^T \boldsymbol{\beta} + \mathbf{v}_{ij}^T \mathbf{u}_i$, the model (Eq. 1) is a generalized linear mixed model (GLMM; Breslow and Clayton 1993). If in addition F is also Gaussian, model (Eq. 1) is a linear mixed model (Bates et al., 2015). With F , and G both Gaussian and Ψ a fixed, known, nonlinear function, the model (Eq. 1) is a Gaussian non-linear mixed model (NLMM; Pinheiro and Bates 1995a; Wolfinger 1993; Vonesh 1996). The methods in Sections 2 and 3 of this paper apply to any such mixed model, while the experiments of Section 4 and data analyses of Section 5 focus on Bernoulli generalized linear mixed models with F a Bernoulli distribution, G a (multivariate) zero-mean Gaussian, and linear Ψ .

Inferences about $\boldsymbol{\theta}$ are ideally based on a marginal likelihood, $\pi(\boldsymbol{\theta}; \mathbf{y}) = \int \pi(\boldsymbol{\theta}, \mathbf{u}; \mathbf{y}) d\mathbf{u}$, where $\pi(\boldsymbol{\theta}, \mathbf{u}; \mathbf{y}) = \prod_{i=1}^m \pi_i(\boldsymbol{\theta}, \mathbf{u}_i; \mathbf{y}_i)$, $\pi_i(\boldsymbol{\theta}, \mathbf{u}_i; \mathbf{y}_i) = \prod_{j=1}^{n_i} f(y_{ij}; \mu_{ij}, \boldsymbol{\phi}) g(\mathbf{u}_i; \boldsymbol{\sigma})$, $\mathbf{y} = (\mathbf{y}_1^T, \dots, \mathbf{y}_m^T)^T \in$

\mathcal{Y}^N with $\mathbf{y}_i = (y_{i1}, \dots, y_{in_i})$, y_{ij} the observed value of Y_{ij} , $N = n_1 + \dots + n_m$, and $\mathbf{u} = (\mathbf{u}_1^T, \dots, \mathbf{u}_m^T)^T \in \mathcal{U}^{dm}$. The marginal independence of the m components of \mathbf{u} gives special structure to the integral defining the marginal likelihood:

$$\pi(\boldsymbol{\theta}; \mathbf{y}) = \int \pi(\boldsymbol{\theta}, \mathbf{u}; \mathbf{y}) d\mathbf{u} = \prod_{i=1}^m \int \pi_i(\boldsymbol{\theta}, \mathbf{u}_i; \mathbf{y}_i) d\mathbf{u}_i. \quad (2)$$

We focus on cases in which inferences cannot be based on the marginal likelihood (Eq. 2) because the m integrals defining it are intractable. This occurs for most models, the exception being those with conjugate response/random effects pairs that are chosen specifically to make these integrals tractable; see Lee and Nelder (1996). The Gaussian/Gaussian case is by far the most common such case and has been researched extensively; see Bates et al. (2015). We restrict focus in this paper to models in which the integral defining (Eq. 2) is intractable and must be approximated.

2.2 Approximate Marginal Likelihood Inference

Without conjugacy, approximations to these integrals (Eq. 2) are required, and this leads to inferences being based instead on an approximate marginal likelihood, as follows. Under the assumption that $d = \dim(\mathbf{u}_i)$ is small, the marginal likelihood involves only low-dimensional integrals. Quadrature techniques usually incur computational cost that is exponential in dimension, so evaluating m separate d -dimensional integrals is far more efficient than evaluating a single (dm) -dimensional integral. This factoring of the marginal likelihood therefore enables the use of accurate quadrature techniques for approximation, and this is well-recognized in the literature. However, this structure also *requires* the use of a highly accurate integral approximation: as $m \rightarrow \infty$, although the data contain more information about $\boldsymbol{\theta}$, the number of integrals being approximated grows, and the accuracy of the approximation to the entire marginal likelihood will decrease, leading to inaccurate inferences. A more accurate numerical method therefore may be required for data sets which have more information about $\boldsymbol{\theta}$, and this illustrates the need to choose this approximation carefully. This makes AQ especially attractive, as it can be made arbitrarily accurate as more points are added (Bilodeau et al., 2022). Adding more points comes at an increased computational burden, and the exact gradient evaluation algorithm presented in this paper reduces this burden

substantially. Let $\widehat{\mathbf{u}}(\boldsymbol{\theta}) = \arg \max_{\mathbf{u}} \pi(\boldsymbol{\theta}, \mathbf{u}; \mathbf{y}) = (\widehat{\mathbf{u}}_1(\boldsymbol{\theta})^T, \dots, \widehat{\mathbf{u}}_m(\boldsymbol{\theta})^T)^T$,

$$\widehat{\mathbf{H}}(\boldsymbol{\theta}) = -\partial_{\mathbf{u}}^2 \log \pi(\boldsymbol{\theta}, \widehat{\mathbf{u}}(\boldsymbol{\theta}); \mathbf{y}) = \text{diag} \left(\widehat{\mathbf{H}}_1(\boldsymbol{\theta}, \widehat{\mathbf{u}}_1(\boldsymbol{\theta})), \dots, \widehat{\mathbf{H}}_m(\boldsymbol{\theta}, \widehat{\mathbf{u}}_m(\boldsymbol{\theta})) \right),$$

and

$$\widehat{\mathbf{L}}_i(\boldsymbol{\theta}, \widehat{\mathbf{u}}_i(\boldsymbol{\theta})) = \widehat{\mathbf{L}}_i(\boldsymbol{\theta}, \widehat{\mathbf{u}}_i(\boldsymbol{\theta})) \widehat{\mathbf{L}}_i(\boldsymbol{\theta}, \widehat{\mathbf{u}}_i(\boldsymbol{\theta}))^T,$$

where $\widehat{\mathbf{L}}_i(\boldsymbol{\theta}, \widehat{\mathbf{u}}_i(\boldsymbol{\theta}))$ is the lower Cholesky triangle. Let $k \in \mathbb{N}$, and let $\mathcal{Q}(1, k) \subset \mathbb{R}$ be the set of nodes from a k -point Gauss-Hermite quadrature rule in one dimension, $\mathcal{Q}(d, k) = \mathcal{Q}(1, k)^d$ be the product extension of this rule to d dimensions, and $\omega_k : \mathcal{Q}(d, k) \rightarrow \mathbb{R}$ be the corresponding quadrature weights. The adaptive quadrature approximation to the marginal likelihood (Eq. 2) is:

$$\widetilde{\pi}_k^{\text{AQ}}(\boldsymbol{\theta}; \mathbf{y}) = \prod_{i=1}^m \left[|\widehat{\mathbf{L}}_i(\boldsymbol{\theta}, \widehat{\mathbf{u}}_i(\boldsymbol{\theta}))|^{-1} \sum_{\mathbf{z} \in \mathcal{Q}(d, k)} \omega_k(\mathbf{z}) \pi_i \left\{ \boldsymbol{\theta}, \widehat{\mathbf{L}}_i(\boldsymbol{\theta}, \widehat{\mathbf{u}}_i(\boldsymbol{\theta}))^{-1} \mathbf{z} + \widehat{\mathbf{u}}_i(\boldsymbol{\theta}); \mathbf{y}_i \right\} \right]. \quad (3)$$

The approximation (Eq. 3) has been used in generalized linear (Pinheiro and Chao, 2006) and non-linear (Pinheiro and Bates, 1995a) mixed models, and is available in modern software (Bates et al. 2015 for $d = 1$ only; Rizopoulos 2020).

The case $k = 1$ is called a Laplace approximation, and is considerably simpler. Here $\mathcal{Q}(d, 1) = \{\mathbf{0}\}$ and $\omega_1(\mathbf{0}) = (2\pi)^{d/2}$, and hence

$$\widetilde{\pi}_1^{\text{AQ}}(\boldsymbol{\theta}; \mathbf{y}) = (2\pi)^{(dm)/2} |\widehat{\mathbf{L}}(\boldsymbol{\theta})|^{-1} \pi \{ \boldsymbol{\theta}, \widehat{\mathbf{u}}(\boldsymbol{\theta}); \mathbf{y} \} \quad (4)$$

is recognized as the usual Laplace-approximate marginal likelihood (e.g. Wood 2011). In contrast to Eq. 3, Eq. 4 does not involve a sum over the k^d -dimensional set $\mathcal{Q}(d, k)$. The computations required to use the Laplace approximation therefore scale well with d , being at most the $O(d^3)$ operations required to compute the Cholesky factor, and even this can be reduced substantially for models with a sparse Hessian; see Rue (2001); Kristensen et al. (2016). For this reason, Eq. 4 is used ubiquitously in latent variable modeling, including for fitting mixed models (Breslow and Clayton, 1993; Wolfinger, 1993). However, in some mixed models, the Laplace approximation may fail dramatically; see Joe (2008); Kim et al. (2013); Breslow and Clayton (1993), and Section 4.3 of the present paper. Note that when the response and random effects are both Gaussian the Laplace approximation (Eq. 4) is exact, providing a connection between the methods discussed here and methods for linear mixed models (Bates et al., 2015). Again, we focus only on cases where the marginal likelihood is not tractable and must be approximated.

2.3 Computation of the maximum approximate marginal likelihood estimator

Inferences about $\boldsymbol{\theta}$ are based on the maximum approximate marginal likelihood estimator,

$$\widehat{\boldsymbol{\theta}}_k^{\text{AQ}} = \arg \max \widetilde{\pi}_k^{\text{AQ}}(\boldsymbol{\theta}; \mathbf{y}).$$

Despite its frequent applied use, few details are available in the literature regarding the computation of $\widetilde{\pi}_k^{\text{AQ}}(\boldsymbol{\theta}; \mathbf{y})$ and $\widehat{\boldsymbol{\theta}}_k^{\text{AQ}}$. The approximation, $\widetilde{\pi}_k^{\text{AQ}}(\boldsymbol{\theta}; \mathbf{y})$, is a smooth, log-concave, many-times-continuously-differentiable function of $\boldsymbol{\theta}$. Gradient-based quasi-Newton optimization is a well-established framework for such problems (Nocedal and Wright, 2006), and is widely implemented in readily-available, open-source software, including the popular `optim` function in the R language (R Core Team, 2021). It seems clear that a gradient-based approach to computing $\widehat{\boldsymbol{\theta}}_k^{\text{AQ}}$ should be preferable to other approaches. However, computing the gradient exactly—as we do in Section 3—is challenging, and a method for doing so was not available prior to the present work. A result of this lack of gradient information about $\log \widetilde{\pi}_k^{\text{AQ}}(\boldsymbol{\theta}; \mathbf{y})$ is that a variety of alternative approaches to computation of $\widetilde{\pi}_k^{\text{AQ}}(\boldsymbol{\theta}; \mathbf{y})$ —or otherwise to make inferences about $\boldsymbol{\theta}$ —have been considered in the literature.

In the Laplace case ($k = 1$), for generalized linear mixed models with Gaussian random effects, Breslow and Clayton (1993) derive a modified set of estimating equations for $\boldsymbol{\beta}$ for fixed $\boldsymbol{\sigma}$, solve them iteratively via Fisher scoring, and maximize a profile likelihood to estimate $\boldsymbol{\sigma}$; Pinheiro and Chao (2006) provide a recurrence relation and related least-squares interpretation. For $k \geq 1$, Pinheiro and Chao (2006) and Pinheiro and Bates (1995a) give formulas for the approximation for multi-level generalized linear and non-linear mixed models, respectively. However, neither latter framework includes details on how the necessary optimization should be performed, nor provide expressions or algorithms for gradient computation. McCulloch (1997) gives a Monte Carlo approximation to (Eq. 2) and corresponding versions of the EM and Newton-Raphson algorithms, and Booth and Hobert (1999) expand on and motivate the use of the Monte Carlo EM algorithm where the intractable integral defining the E-step is approximated using random sampling. Rizopoulos (2020) implements an EM algorithm in software, suggesting its use for finding initial values to further pass to a quasi-Newton optimization with finite-differenced gradients.

A common motivation that unites these previous approaches is not a preference for alter-

natives to gradient-based optimization, but rather that a lack of gradient information about $\log \tilde{\pi}_k^{\text{AQ}}(\boldsymbol{\theta}; \mathbf{y})$ simply precludes the use of this favourable approach. For the Laplace approximation ($k = 1$) only, Kristensen et al. (2016) provide an algorithmic gradient of $\log \tilde{\pi}_1^{\text{AQ}}(\boldsymbol{\theta}; \mathbf{y})$, and Stringer et al. (2023, Section 5) demonstrate its efficiency over contemporary approaches in fitting a (Bayesian) mixed model to a large set of data. We develop an algorithm for exact computation of the gradient of $\log \tilde{\pi}_k^{\text{AQ}}(\boldsymbol{\theta}; \mathbf{y})$ in Section 3, leading to efficient quasi-Newton optimization for finding $\hat{\boldsymbol{\theta}}_k^{\text{AQ}}$ for any $k \geq 1$.

3 Computations with the approximate marginal likelihood

We give an algorithm for exact computation of the gradient, $\nabla_{\boldsymbol{\theta}} \tilde{\ell}_k(\boldsymbol{\theta})$, of the approximate log-marginal likelihood, $\tilde{\ell}_k(\boldsymbol{\theta}) = \log \tilde{\pi}_k^{\text{AQ}}(\boldsymbol{\theta}; \mathbf{y})$, in Section 3.1. The technical difficulties are to differentiate “through” (a) the “inner” optimization required to find $\hat{\mathbf{u}}(\boldsymbol{\theta})$, and (b) the matrix decompositions, linear system solves, and log-determinant calculations all required to compute $\tilde{\pi}_k^{\text{AQ}}(\boldsymbol{\theta}; \mathbf{y})$ for each fixed $\boldsymbol{\theta}$. The main technical tools used are (a) implicit differentiation to account for $\hat{\mathbf{u}}(\boldsymbol{\theta})$, and (b) algorithmic differentiation of the Cholesky decomposition, $\hat{\mathbf{L}}_i(\boldsymbol{\theta}, \hat{\mathbf{u}}_i(\boldsymbol{\theta}))$, and the forward substitution required to compute $\hat{\mathbf{L}}_i(\boldsymbol{\theta}, \hat{\mathbf{u}}_i(\boldsymbol{\theta}))^{-1}\mathbf{z}$. Applying these tools effectively requires a careful organization of the computations. We discuss the use of the new gradient computations for point estimation in Section 3.2, and confidence intervals in Section 3.3. The important special case of scalar random effects (the “random intercepts” model) is treated in Section 3.4.

3.1 Exact gradient computation

We seek the gradient, $\nabla_{\boldsymbol{\theta}} \tilde{\ell}_k(\boldsymbol{\theta})$, of the approximate log-marginal likelihood, $\tilde{\ell}_k(\boldsymbol{\theta}) = \log \tilde{\pi}_k^{\text{AQ}}(\boldsymbol{\theta}; \mathbf{y})$. To begin, let

$$\tilde{\ell}_k(\boldsymbol{\theta}) = \sum_{i=1}^n \tilde{\ell}_k^i(\boldsymbol{\theta}),$$

where

$$\begin{aligned}\tilde{\ell}_k^i(\boldsymbol{\theta}) &= \tilde{\ell}_k^i\left(\boldsymbol{\theta}, \widehat{\mathbf{u}}_i(\boldsymbol{\theta}), \widehat{\mathbf{L}}_i(\boldsymbol{\theta}, \widehat{\mathbf{u}}_i(\boldsymbol{\theta}))\right), \\ \tilde{\ell}_k^i(\boldsymbol{\theta}, \mathbf{u}, \mathbf{L}) &= \log \left\{ \sum_{\mathbf{z} \in \mathcal{Q}(k, d)} g_k^i(\boldsymbol{\theta}, \mathbf{u}, \mathbf{L}; \mathbf{z}) \right\}, \\ g_k^i(\boldsymbol{\theta}, \mathbf{u}, \mathbf{L}; \mathbf{z}) &= |\mathbf{L}|^{-1} w_k(\mathbf{z}) \pi_i(\boldsymbol{\theta}, \mathbf{L}^{-1} \mathbf{z} + \mathbf{u}).\end{aligned}$$

To keep notation concise, we suppress dependency of these functions on \mathbf{y} , for example writing $\pi_i(\boldsymbol{\theta}, \mathbf{u}) \equiv \pi_i(\boldsymbol{\theta}, \mathbf{u}; \mathbf{y})$. We use the following convention for treating partial derivatives with respect to arguments of multi-variable functions. If $f : \mathbb{R}^{m+p} \rightarrow \mathbb{R}$ takes arguments $\mathbf{x} \in \mathbb{R}^m, \mathbf{y} \in \mathbb{R}^p$, then $f(\mathbf{x}; \mathbf{y})$ is the function $g : \mathbb{R}^m \rightarrow \mathbb{R}$ defined by $g(\mathbf{x}) = f(\mathbf{x}, \mathbf{y})$. This notation will help communicate the order in which terms are differentiated. For brevity we use $\partial_{\mathbf{x}} g(\mathbf{x})$ to mean $\partial g / \partial \mathbf{x}$. The remainder of this Section is dedicated to the details of the gradient computation, but note that the full algorithm is given in Algorithms 1 and 2 in Section A of the supplement.

The computations are organized as follows. We have:

$$\nabla_{\boldsymbol{\theta}} \tilde{\ell}_k^i(\boldsymbol{\theta}) = \partial_{\boldsymbol{\theta}} \tilde{\ell}_k^i\left(\boldsymbol{\theta}, \mathbf{u}, \widehat{\mathbf{L}}_i(\boldsymbol{\theta}, \mathbf{u})\right) \Big|_{\mathbf{u}=\widehat{\mathbf{u}}_i(\boldsymbol{\theta})} + \partial_{\boldsymbol{\theta}} \widehat{\mathbf{u}}_i(\boldsymbol{\theta}) \cdot \left[\partial_{\mathbf{u}} \tilde{\ell}_k^i\left(\boldsymbol{\theta}, \mathbf{u}, \widehat{\mathbf{L}}_i(\boldsymbol{\theta}, \mathbf{u})\right) \Big|_{\mathbf{u}=\widehat{\mathbf{u}}_i(\boldsymbol{\theta})} \right],$$

and

$$\partial_{(\boldsymbol{\theta}, \mathbf{u})} \tilde{\ell}_k^i(\boldsymbol{\theta}, \mathbf{u}, \widehat{\mathbf{L}}_i(\boldsymbol{\theta}, \mathbf{u})) = \partial_{(\boldsymbol{\theta}, \mathbf{u})} \tilde{\ell}_k^i(\boldsymbol{\theta}, \mathbf{u}; \mathbf{L}) \Big|_{\mathbf{L}=\widehat{\mathbf{L}}_i(\boldsymbol{\theta}, \mathbf{u})} + \partial_{(\boldsymbol{\theta}, \mathbf{u})} \tilde{\ell}_k^i(\mathbf{L}(\boldsymbol{\theta}, \mathbf{u}); \boldsymbol{\theta}, \mathbf{u}) \Big|_{\mathbf{L}=\widehat{\mathbf{L}}_i(\boldsymbol{\theta}, \mathbf{u})}.$$

Computation of $\partial_{\boldsymbol{\theta}} \widehat{\mathbf{u}}_i(\boldsymbol{\theta})$ and $\partial_{(\boldsymbol{\theta}, \mathbf{u})} \tilde{\ell}_k^i(\mathbf{L}(\boldsymbol{\theta}, \mathbf{u}); \boldsymbol{\theta}, \mathbf{u})$ are the subjects of Sections 3.1.1 and 3.1.2. The remaining terms are as follows:

$$\partial_{(\boldsymbol{\theta}, \mathbf{u})} \tilde{\ell}_k^i(\boldsymbol{\theta}, \mathbf{u}; \mathbf{L}) = \frac{\sum_{\mathbf{z} \in \mathcal{Q}(k, d)} g_k^i(\boldsymbol{\theta}, \mathbf{u}, \mathbf{L}; \mathbf{z}) \partial_{(\boldsymbol{\theta}, \mathbf{u})} \log g_k^i(\boldsymbol{\theta}, \mathbf{u}, \mathbf{L}; \mathbf{z})}{\sum_{\mathbf{z}' \in \mathcal{Q}(k, d)} g_k^i(\boldsymbol{\theta}, \mathbf{u}, \mathbf{L}; \mathbf{z}')},$$

$$\partial_{(\boldsymbol{\theta}, \mathbf{u})} \log g_k^i(\boldsymbol{\theta}, \mathbf{u}, \mathbf{L}; \mathbf{z}) = \partial_{(\boldsymbol{\theta}, \mathbf{u})} \log \pi_i(\boldsymbol{\theta}, \mathbf{u}).$$

The $\partial_{(\boldsymbol{\theta}, \mathbf{u})} \log \pi_i(\boldsymbol{\theta}, \mathbf{u})$ term is the gradient of the *joint* log-likelihood, which is assumed tractable, albeit always model-specific. Calculations for Bernoulli mixed models and multi-variate Gaussian random effects are given in Sections 4.1 and 4.2, and these are generalized to any exponential family distribution in Section B of the supplement.

3.1.1 Implicit differentiation of $\widehat{u}_i(\theta)$

Implicit differentiation to obtain $\partial_{\theta} \widehat{u}_i(\theta)$ is standard; see Kristensen et al. (2016) and Stringer et al. (2023). By definition we have $\partial_{\mathbf{u}} \log \pi_i(\theta, \widehat{\mathbf{u}}_i(\theta)) = 0$, and differentiating this equation gives

$$\widehat{\mathbf{H}}_i(\theta, \widehat{\mathbf{u}}_i(\theta)) \partial_{\theta} \widehat{\mathbf{u}}_i(\theta) = -\partial_{\theta, \mathbf{u}}^2 \log \pi_i(\theta, \widehat{\mathbf{u}}_i(\theta)).$$

At the point in Algorithm 2 (see the supplement, Section A) when $\partial_{\theta} \widehat{u}_i(\theta)$ is needed, the mode, $\widehat{\mathbf{u}}_i(\theta)$, and the Cholesky, $\widehat{\mathbf{L}}_i(\theta, \widehat{\mathbf{u}}_i(\theta))$, of the Hessian, $\widehat{\mathbf{H}}_i(\theta, \widehat{\mathbf{u}}_i(\theta))$, have already been computed, which enables efficient computation of $\partial_{\theta} \widehat{u}_i(\theta)$ via a single application of each of forward and backward substitution. In the implementation $\partial_{\theta} \widehat{u}_i(\theta)$ is never formed explicitly, but rather the matrix-vector product in which it appears is computed directly using this method.

3.1.2 Algorithmic differentiation of $L(\theta, u)$

Smith (1995) describes a reverse-mode algorithmic differentiation of any function, $f(\mathbf{L})$, of a Choleskey decomposition, $\mathbf{L} \equiv \mathbf{L}(\theta, \mathbf{u})$, of a positive-definite matrix, $\mathbf{H}(\theta, \mathbf{u}) = \mathbf{L}(\theta, \mathbf{u}) \mathbf{L}(\theta, \mathbf{u})^T$, with respect to the underlying parameters, (θ, \mathbf{u}) . We apply this algorithm to $f(\mathbf{L}) \equiv \tilde{\ell}_k^i(\mathbf{L}(\theta, \mathbf{u}); \theta, \mathbf{u})$, treating the parts of $\tilde{\ell}_k^{\text{AQ}}$ that depend on (θ, \mathbf{u}) through $\mathbf{L}(\theta, \mathbf{u})$ as variable, and all other instances of (θ, \mathbf{u}) as fixed. The required inputs to the algorithm are: (a) the computed Cholesky decomposition, \mathbf{L} ; (b) an array of derivatives, $\mathbf{M} = \partial_{(\theta, \mathbf{u})} \mathbf{H}(\theta, \mathbf{u})$, of the original matrix, $\mathbf{H}(\theta, \mathbf{u})$; and (c) the lower-triangular matrix of derivatives, $\mathbf{F} = \partial f(\mathbf{L}) / \partial \mathbf{L}$, of the function, $f(\mathbf{L})$, with respect to the elements of \mathbf{L} . In our setting, \mathbf{L} is already computed, and \mathbf{M} is model-specific; again, calculations for Bernoulli mixed models and multivariate Gaussian random effects are given in Sections 4.1 and 4.2, and generalized to the exponential family in Section B of the supplement. For $j \geq l = 1, \dots, d$, we have:

$$\begin{aligned} \mathbf{F}_{jl} &= \partial_{L_{jl}} \tilde{\ell}_k^i(\mathbf{L}; \theta, \mathbf{u}) = \frac{\sum_{\mathbf{z} \in \mathcal{Q}(k, d)} g_k^i(\theta, \mathbf{u}, \mathbf{L}; \mathbf{z}) \partial_{L_{jl}} \log g_k^i(\theta, \mathbf{u}, \mathbf{L}; \mathbf{z})}{\sum_{\mathbf{z}' \in \mathcal{Q}(k, d)} g_k^i(\theta, \mathbf{u}, \mathbf{L}; \mathbf{z}')}, \\ \partial_{L_{jl}} \log g_k^i(\theta, \mathbf{u}, \mathbf{L}; \mathbf{z}) &= -\frac{1}{L_{jj}} \mathbf{1}(j = l) + \left(\frac{\partial \mathbf{L}^{-1} \mathbf{z}}{\partial L_{jl}} \right)^T \partial_{\mathbf{u}} \log \pi_i(\theta, \mathbf{u}')|_{\mathbf{u}' = \mathbf{L}^{-1} \mathbf{z} + \mathbf{u}}. \end{aligned}$$

The d -dimensional vector $\mathbf{v} \equiv \mathbf{L}^{-1} \mathbf{z}$ is obtained for each $\mathbf{z} \in \mathcal{Q}(k, d)$ by solving the equation $\mathbf{L}\mathbf{v} = \mathbf{z}$ via forward substitution (Golub and van Loan, 1983, Algorithm 4.1-1). Accordingly,

we obtain its derivative by differentiation of this algorithm with respect to L_{jk} ; see Algorithm 3 in Section A of the supplement.

3.2 Point Estimation

With the gradient, $\nabla_{\boldsymbol{\theta}} \tilde{\ell}_k(\boldsymbol{\theta})$, of the approximate log-marginal likelihood, $\tilde{\ell}_k(\boldsymbol{\theta}) = \log \tilde{\pi}^{\text{AQ}}(\boldsymbol{\theta}; \mathbf{y})$, available, we compute the adaptive quadrature approximate maximum likelihood estimator, $\hat{\boldsymbol{\theta}}_k^{\text{AQ}} = \text{argmax}_{\boldsymbol{\theta}} \tilde{\ell}_k(\boldsymbol{\theta})$, using limited-memory BFGS (L-BFGS) quasi-Newton optimization, of the type described by Nocedal and Wright (2006, Section 6.1). Although L-BFGS is a standard algorithm, its implementation is nontrivial, specifically the step-length selection algorithm run at each quasi-Newton iteration. One option is to pass separate functions which compute $\tilde{\ell}_k(\boldsymbol{\theta})$ and $\nabla_{\boldsymbol{\theta}} \tilde{\ell}_k(\boldsymbol{\theta})$ into a pre-existing implementation of this algorithm, such as in the `optim` function in the R language (R Core Team, 2021); this strategy is taken by the `GLMMadaptive` package of Rizopoulos (2020), and the `lme4` package of Bates et al. (2015) implements its derivative-free approach in a similar manner. However, we note two opportunities for efficiency that this leaves unrealized:

- (a) Computation of $\tilde{\ell}_k(\boldsymbol{\theta})$ occurs as a byproduct of computation of $\nabla_{\boldsymbol{\theta}} \tilde{\ell}_k(\boldsymbol{\theta})$, so the log-likelihood is available at no additional cost once the gradient has been computed. This is not the case when derivatives are computed by finite-differences (`GLMMadaptive`), and not relevant when using derivative-free optimization (`lme4`).
- (b) Each evaluation of $\tilde{\ell}_k(\boldsymbol{\theta})$ requires m inner optimizations to find $\hat{\mathbf{u}}_1(\boldsymbol{\theta}), \dots, \hat{\mathbf{u}}_m(\boldsymbol{\theta})$. Within an iterative outer optimization, the values of these modes from the previous iteration should be used as starting values for the subsequent iteration, reducing the number of inner optimization steps.

To implement these efficiencies without completely re-implementing L-BFGS and the step-size selection algorithms, we use the flexible implementation of L-BFGS provided at <https://github.com/yixuan/LBFGSpp/> (accessed 05/2023), which implements the step-length selection strategy of Nocedal and Wright (2006, Section 3.5).

Starting values are required to run the L-BFGS optimization; these are somewhat model-specific, and we offer some general guidance here that we used in the experiments and data

analyses of Sections 4 and 5, where we fit Bernoulli generalized linear mixed models with correlated multivariate Gaussian random effects. We recommend to (a) fit an ordinary generalized linear model and use the estimated $\hat{\boldsymbol{\beta}}$ as a starting value for $\boldsymbol{\beta}$; (b) set $\hat{\mathbf{u}}_i(\boldsymbol{\theta}) = \mathbf{0}$ (the mean of G) for each i ; and (c) set $\boldsymbol{\sigma} = 1$ for variance parameters and 0 for covariance parameters (i.e. if the random effects are mean-zero Gaussian with covariance matrix $\boldsymbol{\Sigma}(\boldsymbol{\sigma})$, we set $\boldsymbol{\Sigma}(\boldsymbol{\sigma}) = I_d$). We did not observe any sensitivity to this choice of starting values in our experiments, although caution should be taken if attempting to generalize these recommendations to other models.

The availability of $\nabla_{\boldsymbol{\theta}}\tilde{\ell}_k(\boldsymbol{\theta})$ also leads immediately to an approximate Hessian, computed as a simple finite-differenced Jacobian of the gradient. For $\epsilon > 0$, define the $p \times p$ matrix $\tilde{\mathbf{H}} = [\tilde{\mathbf{d}}_1 : \dots : \tilde{\mathbf{d}}_p]$, where $: \dots :$ denotes column-wise concatenation, $p = \dim(\boldsymbol{\theta})$, and

$$\tilde{\mathbf{d}}_j = \frac{\nabla_{\boldsymbol{\theta}}\tilde{\ell}_k(\theta_1, \dots, \theta_j + \epsilon, \dots, \theta_p) - \nabla_{\boldsymbol{\theta}}\tilde{\ell}_k(\boldsymbol{\theta})}{\epsilon}, j = 1, \dots, p.$$

At termination of the L-BFGS algorithm, we run Newton's method from the terminal point, using $\tilde{\mathbf{H}}$ in place of the Hessian of $\tilde{\ell}_k(\boldsymbol{\theta})$. We found that the terminal point from L-BFGS is usually satisfactory, in which case a single iteration of Newton's method is run, at a marginal computational cost of p additional gradient evaluations to evaluate $\tilde{\mathbf{H}}$ (which is also required for confidence intervals; see Section 3.3), plus the $O(p^3)$ cost of a system solve involving it (recall that $p = \dim(\boldsymbol{\theta})$ is generally small). In some cases, however, the terminal point from L-BFGS is not satisfactory, and we observe that in almost all such cases, the Newton iterations starting from it produce a satisfactory estimate. This was the strategy used to produce all the simulation and data analysis results in Sections 4 and 5.

3.3 Confidence intervals

With $\tilde{\mathbf{H}}$ available, an approximate $(1 - \alpha)100\%$ Wald confidence interval for the j^{th} component of $\boldsymbol{\theta}$, θ_j , for $j = 1, \dots, p$ is given by

$$(\hat{\boldsymbol{\theta}}_k^{\text{Aq}})_j \pm z_{1-\alpha/2} \left(\tilde{\mathbf{H}}^{-1} \right)_{jj}^{1/2},$$

where z_α satisfies $P(Z < z_\alpha) = \alpha$ for $Z \sim N(0, 1)$ and $0 < \alpha < 1$.

Computing $\tilde{\mathbf{H}}$ involves p evaluations of $\nabla_{\boldsymbol{\theta}}\tilde{\ell}_k(\boldsymbol{\theta})$, using the novel gradient calculations from Section 3.1. The evaluation speed is orders of magnitude faster than that of computing

$\widehat{\boldsymbol{\theta}}_k^{\text{AQ}}$, and hence the cost of computing the Wald intervals is negligible compared to that of the point estimates. For moderate p , it is efficient to simply directly invert $\widetilde{\mathbf{H}}$ and take its diagonal elements; for larger p , the methods of e.g. Rue and Martino (2007) for determining the diagonal of a matrix inverse from its Cholesky decomposition could be applied, although we did not have need for this. The value of $\epsilon = 10^{-8}$ used in our experiments (Section 4.3) was sufficient to achieve the nominal empirical coverages reported there. We remark that the use of a single finite-difference operation for computing the Hessian as the Jacobian of the gradient is now possible due to the gradient being available exactly, reducing the computational cost of this step.

In cases where the final objects of inferential interest are not the elements of $\boldsymbol{\theta}$ directly, but rather some transformation of them, $\widetilde{\mathbf{H}}^{-1}$ is used as an input to a Delta-method confidence interval. Such situations are model-specific; see Section 4.2 for the Bernoulli/Gaussian mixed model case.

3.4 Scalar random effects

When $d = 1$, implementation of the approximate marginal likelihood and gradient computations simplifies considerably. When $\mathbf{u} \equiv u$ is a scalar the computations can be performed using simple floating point types—rather than vector and matrix types—for all \mathbf{u} -dependent quantities, improving implementation efficiency. The $d = 1$ case includes the random-intercepts model, which is of considerable interest in its own right, and is the only case for which AQ is implemented in the popular **lme4** software (Bates et al., 2015); efficient implementation of the present procedure is therefore required for comparison against this established method, as well as being of independent interest.

The steps of the novel gradient evaluation procedure remain the same. Because \mathbf{L} is now a scalar, $\mathbf{L} \equiv L = (H)^{1/2}$ where $H = -\partial_{u^2}^2 \log \pi(\boldsymbol{\theta}, \widehat{u}(\boldsymbol{\theta}); \mathbf{y})$. The algorithm of Smith (1995) is no longer needed, and the corresponding term simplifies to

$$\partial_{(\boldsymbol{\theta}, u)} \widetilde{\ell}_i^{\text{AQ}}(\mathbf{L}; \boldsymbol{\theta}, u) = (F_{11})(\mathbf{M})/(2L),$$

where $\mathbf{M} = \partial_{(\boldsymbol{\theta}, u)} H$ is now a $(p + 1)$ -dimensional vector. The \mathbf{L} -derivative of Section 3.1.2 simplifies to:

$$\partial_L \log g_k^i(\boldsymbol{\theta}, \mathbf{u}, \mathbf{L}; \mathbf{z}) = -\frac{1}{L} - \frac{z}{L^2} \partial_u \log \pi_i(\boldsymbol{\theta}, u')|_{u' = z/L + u}.$$

4 Bernoulli mixed models with multivariate Gaussian random effects

An important special case of Eq. 1 is the Bernoulli mixed model:

$$Y_{ij} \mid \mathbf{u}_i \stackrel{\text{ind}}{\sim} \text{Bern}(p_{ij}), \quad \mathbf{u}_i \stackrel{\text{iid}}{\sim} \text{N}\{\mathbf{0}, \Sigma(\boldsymbol{\sigma})\}, \quad \log \frac{p_{ij}}{1 - p_{ij}} = \mathbf{x}_{ij}^T \boldsymbol{\beta} + \mathbf{v}_{ij}^T \mathbf{u}_i. \quad (5)$$

The model (Eq. 5) is commonly used for longitudinal/repeated measures binary outcomes (Kim et al., 2013; Breslow and Clayton, 1993; Hedeker et al., 2018) and is prominent in ecology (Bolker et al., 2008) and psychology (Bono et al., 2021). Fitting the model (Eq. 5) is challenging: beyond the challenges with fitting any mixed model described in Sections 2 and 3, a parameterization of $\Sigma(\boldsymbol{\sigma})$ that leads to stable and efficient optimization, but produces estimates and confidence intervals for those estimates on an interpretable scale is required. In this Section, we give the details of applying the methods of Sections 2 and 3 to this important model. This both serves to give the details for one important case, and also to illustrate the steps required to apply the methods in this paper to specific models. We note that the multivariate Gaussian calculations given in Section 4.2 apply to any mixed model with correlated multivariate Gaussian random effects, and are hence of independent interest.

4.1 Likelihood calculations

The approximate log-marginal likelihood is a sum over groups, $\tilde{\ell}_k(\boldsymbol{\theta}) = \sum_{i=1}^m \tilde{\ell}_k^i(\boldsymbol{\theta})$, and same for its gradient. Accordingly, we give calculations for a single group. The likelihood derivative calculations up to order 2 are standard, however we repeat them here to illustrate the form of the third-order derivatives required, and for consistency of notation.

The log-likelihood calculations corresponding to Eq. 5 are

$$\begin{aligned} \ell_i(\boldsymbol{\theta}, \mathbf{u}) &= \log \pi_i(\boldsymbol{\theta}, \mathbf{u}_i; \mathbf{y}_i) = \sum_{j=1}^{n_i} y_{ij} \eta_{ij} - \log(1 + e^{\eta_{ij}}), \\ \frac{\partial \ell_i(\boldsymbol{\theta}, \mathbf{u})}{\partial(\boldsymbol{\beta}, \mathbf{u})} &= \left(\frac{\partial \ell_i}{\partial \boldsymbol{\eta}_i} \right)^T [\mathbf{X}_i : \mathbf{V}_i], \quad \frac{\partial \ell_i}{\partial \eta_{ij}} = y_{ij} - \frac{e^{\eta_{ij}}}{1 + e^{\eta_{ij}}} \\ \frac{\partial^2 \ell_i(\boldsymbol{\theta}, \mathbf{u})}{\partial(\boldsymbol{\beta}, \mathbf{u}) \partial(\boldsymbol{\beta}, \mathbf{u})^T} &= [\mathbf{X}_i : \mathbf{V}_i]^T \left(\frac{\partial^2 \ell_i}{\partial \boldsymbol{\eta}_i \partial \boldsymbol{\eta}_i^T} \right) [\mathbf{X}_i : \mathbf{V}_i], \quad \frac{\partial^2 \ell_i}{\partial \eta_{ij}^2} = -\frac{e^{\eta_{ij}}}{1 + e^{\eta_{ij}}} \left(1 - \frac{e^{\eta_{ij}}}{1 + e^{\eta_{ij}}} \right), \end{aligned}$$

where $\boldsymbol{\eta}_i = (\eta_{i1}, \dots, \eta_{in_i})^T \in \mathbb{R}^{n_i}$, $\mathbf{X}_i = [\mathbf{x}_{i1} : \dots : \mathbf{x}_{in_i}] \in \mathbb{R}^{n_i \times q}$, and $\mathbf{V}_i = [\mathbf{v}_{i1} : \dots : \mathbf{v}_{in_i}] \in \mathbb{R}^{n_i \times d}$. Define $\mathbf{H}_i^y = -\partial^2 \ell_i(\boldsymbol{\theta}, \mathbf{u}) / \partial \mathbf{u} \partial \mathbf{u}^T$; we seek the third-order derivative matrices $\partial \mathbf{H}_i^y / \partial \theta_l$. These are zero for components of $\boldsymbol{\theta}$ corresponding to $\boldsymbol{\sigma}$, and for \mathbf{u} and $\boldsymbol{\beta}$ are given by

$$\begin{aligned}\frac{\partial \mathbf{H}_i^y}{\partial \mathbf{u}_l} &= \sum_{j=1}^{n_i} \frac{\partial^3 \ell_i}{\partial \eta_{ij}^3} \mathbf{v}_{ij} \mathbf{v}_{ij}^T v_{ijl}, \quad \frac{\partial \mathbf{H}_i^y}{\partial \boldsymbol{\beta}_l} = \sum_{j=1}^{n_i} \frac{\partial^3 \ell_i}{\partial \eta_{ij}^3} \mathbf{v}_{ij} \mathbf{v}_{ij}^T x_{ijl}, \\ \frac{\partial^3 \ell_i}{\partial \eta_{ij}^3} &= \frac{e^{\eta_{ij}}}{1 + e^{\eta_{ij}}} \left(1 - \frac{e^{\eta_{ij}}}{1 + e^{\eta_{ij}}}\right) \left(1 - 2 \frac{e^{\eta_{ij}}}{1 + e^{\eta_{ij}}}\right).\end{aligned}$$

These are a special case of the calculations for general exponential family distributions, which follow similarly; see Section B of the supplement.

4.2 Multivariate Gaussian random effects

We require a parameterization of the Normal density that leads to efficient and stable optimization. In particular, $\boldsymbol{\Sigma}$ is required to be symmetric and positive-definite, and it is preferable to impose this via re-parameterization rather than employing constrained optimization techniques; see Pinheiro and Bates (1995b). However, the final desired output of the procedure is point and interval estimates for variance components on a scale that is interpretable in the context of the original problem. While point estimates for the unique elements of $\boldsymbol{\Sigma}$ are straightforward to obtain via invariance of maximum likelihood to general transformations, obtaining interval estimates via the Delta method requires innovation.

We use the following “inverse log-Cholesky” parameterization of $\boldsymbol{\Sigma}$:

$$\boldsymbol{\Sigma}^{-1}(\boldsymbol{\sigma}) = \mathbf{A} \mathbf{D} \mathbf{A}^T, \quad \mathbf{D} = \text{diag}(e^{\delta_1}, \dots, e^{\delta_d}), \quad \text{lower.tri}(\mathbf{A}) = \boldsymbol{\phi}, \quad \boldsymbol{\sigma} = (\boldsymbol{\delta}, \boldsymbol{\phi}),$$

where \mathbf{D} is diagonal and \mathbf{A} is unit lower-triangular so that $\dim(\boldsymbol{\phi}) = r = d(d-1)/2$ and hence $\dim(\boldsymbol{\sigma}) = s = d(d+1)/2$. The covariance parameters, $\boldsymbol{\phi}$, represent the lower triangle of \mathbf{A} in column-major order excluding the diagonal, so $\phi_1 = \mathbf{A}_{21}, \phi_2 = \mathbf{A}_{31}$, and so on.

Because $\mathbf{D} > 0$, $\boldsymbol{\Sigma}^{-1}$ is symmetric and positive-definite, and hence $\boldsymbol{\Sigma}$ is as well. The free parameters, $\boldsymbol{\sigma}$, are unconstrained, and—again, because $\mathbf{D} > 0$ —uniquely determine $\boldsymbol{\Sigma}^{-1}$ (Golub and van Loan, 1983). In this parameterization the random effects density is

$$\log g(\mathbf{u}; \boldsymbol{\sigma}) = \text{const} + \frac{1}{2} \sum_{j=1}^d \delta_j - \frac{1}{2} \mathbf{u}^T \mathbf{A} \mathbf{D} \mathbf{A}^T \mathbf{u}. \quad (6)$$

Note that our log-Cholesky parameterization differs from those of Rizopoulos (2020), Bates et al. (2015), and Pinheiro and Bates (1995b) in that we transform Σ^{-1} instead of Σ . The reason to do this is because evaluation of the density and its derivatives in this parameterization requires only basic matrix operations, avoiding inverses, determinants, system solves, and any such computation that would involve performing a matrix decomposition at every evaluation. This structure leads to efficient computations involving the density, and hence improves efficiency of the optimization.

We seek the three derivatives required to implement Algorithm 2 (see the supplement, Section A), and it will be convenient to express Eq. 6 directly in terms of \mathbf{u} , $\boldsymbol{\delta}$, and $\boldsymbol{\phi}$. We first note that the product, $\mathbf{A}^T \mathbf{u}$, can be expressed explicitly in terms of $\boldsymbol{\phi}$, \mathbf{u} , and a unique $d \times r$ selection matrix, $\mathbf{S}(\mathbf{u})$, as $\mathbf{A}^T \mathbf{u} = \mathbf{u} + \mathbf{S}(\mathbf{u})\boldsymbol{\phi}$; see Section 1.3 of the supplement for full details. This yields the following derivative expressions:

$$\begin{aligned} \frac{\partial \log g}{\partial \mathbf{u}} &= -\mathbf{u}^T \mathbf{A} \mathbf{D} \mathbf{A}^T, & \frac{\partial^2 \log g}{\partial \mathbf{u} \partial \mathbf{u}^T} &= -\mathbf{A} \mathbf{D} \mathbf{A}^T. \\ \frac{\partial \log g}{\partial \delta_j} &= \frac{1}{2} \left[1 - \exp(\delta_j) \{ \mathbf{u} + \mathbf{S}(\mathbf{u})\boldsymbol{\phi} \}_j^2 \right], & \frac{\partial^2 \log g}{\partial \delta_j^2} &= -\frac{1}{2} \exp(\delta_j) \{ \mathbf{u} + \mathbf{S}(\mathbf{u})\boldsymbol{\phi} \}_j^2, \\ \frac{\partial \log g}{\partial \boldsymbol{\phi}} &= -\{ \mathbf{u} + \mathbf{S}(\mathbf{u})\boldsymbol{\phi} \}^T \mathbf{D} \mathbf{S}(\mathbf{u}). & \frac{\partial^2 \log g}{\partial \boldsymbol{\phi} \partial \boldsymbol{\phi}^T} &= -\mathbf{S}(\mathbf{u})^T \mathbf{D} \mathbf{S}(\mathbf{u}). \end{aligned}$$

The cross terms are as follows:

$$\begin{aligned} \frac{\partial}{\partial \delta_j} \frac{\partial \log g}{\partial \mathbf{u}} &= -\exp(\delta_j) (\mathbf{A}^T \mathbf{u})_j \mathbf{A}_j, \\ \frac{\partial^2 \log g}{\partial \boldsymbol{\phi} \partial u_j} &= - \left[\mathbf{u}^T \mathbf{D} \left\{ \frac{d\mathbf{S}(\mathbf{u})}{du_j} \right\} + (\mathbf{D} \mathbf{S}(\mathbf{u}))_j + \boldsymbol{\phi}^T \mathbf{S}(\mathbf{u})^T \mathbf{D} \left\{ \frac{d\mathbf{S}(\mathbf{u})}{du_j} \right\} + \boldsymbol{\phi}^T \left\{ \frac{d\mathbf{S}(\mathbf{u})^T}{du_j} \right\} \mathbf{D} \mathbf{S}(\mathbf{u}) \right], \\ \frac{\partial}{\partial \delta_j} \frac{\partial \log g}{\partial \boldsymbol{\phi}} &= -\exp(\delta_j) \{ \mathbf{u} + \mathbf{S}(\mathbf{u})\boldsymbol{\phi} \}_j^T \mathbf{S}(\mathbf{u})_j. \end{aligned}$$

Given these novel expressions involving $\mathbf{S}(\mathbf{u})$ for the density and its derivatives, the third-order derivatives required to implement the procedure in the present paper are now straightforward to obtain. Let

$$\mathbf{H}^u = -\frac{\partial \log g}{\partial \mathbf{u} \partial \mathbf{u}^T} = \mathbf{A} \mathbf{D} \mathbf{A}^T.$$

We seek derivatives of the elements of \mathbf{H}^u with respect to $\mathbf{u}, \boldsymbol{\delta}, \boldsymbol{\phi}$. Clearly $(\partial/\partial \mathbf{u}) \mathbf{H}^u = 0$ as Eq. 6 is a quadratic function of \mathbf{u} . For the variance parameters,

$$\frac{\partial}{\partial \delta_l} \mathbf{H}^u = \exp(\delta_l) \mathbf{A}_l \mathbf{A}_l^T, \quad \frac{\partial}{\partial \phi_l} \mathbf{H}^u = \mathbf{A} \mathbf{D} \frac{\partial \mathbf{A}^T}{\partial \phi_l} + \frac{\partial \mathbf{A}}{\partial \phi_l} \mathbf{D} \mathbf{A}^T.$$

The remaining computational details pertaining to these expressions are given in Section A of the supplement.

While this log-Cholesky parameterization of Σ^{-1} is useful for model fitting, point and interval estimates for elements of Σ are required on the original scale for interpretation. Point estimates are obtained in a straightforward manner by invoking the invariance of maximum likelihood to transformations, and simply computing $\tilde{\Sigma} = \tilde{\mathbf{A}}\tilde{\mathbf{D}}\tilde{\mathbf{A}}^T$, where $\tilde{\mathbf{A}}$ and $\tilde{\mathbf{D}}$ are \mathbf{A} and \mathbf{D} evaluated at the approximate MLEs, $\tilde{\boldsymbol{\phi}}$ and $\tilde{\boldsymbol{\delta}}$, obtained by indexing the appropriate components of $\hat{\boldsymbol{\theta}}_k^{\text{AQ}}$. Interval estimates require innovation, and here we provide delta method Wald intervals for Σ_{ij} based on Wald intervals for $\tilde{\boldsymbol{\phi}}$ and $\tilde{\boldsymbol{\delta}}$. Define $\sigma_{ij} = \Sigma_{ij}$ and $\tilde{\sigma}_{ij} = \tilde{\Sigma}_{ij}$. We use the approximation

$$\text{Var}(\tilde{\sigma}_{ij}) \approx \mathbf{J}_{ij}^T \text{Var}(\tilde{\boldsymbol{\delta}}, \tilde{\boldsymbol{\phi}}) \mathbf{J}_{ij},$$

where $\text{Var}(\tilde{\boldsymbol{\delta}}, \tilde{\boldsymbol{\phi}})$ is the appropriate block of $\tilde{\mathbf{H}}^{-1}$ (the inverse of the approximate Hessian; see Section 3.3), and

$$\mathbf{J}_{ij}^T = \frac{\partial \tilde{\sigma}_{ij}}{\partial (\tilde{\boldsymbol{\delta}}, \tilde{\boldsymbol{\phi}})}$$

is the Jacobian of the map $(\tilde{\boldsymbol{\delta}}, \tilde{\boldsymbol{\phi}}) \rightarrow \tilde{\sigma}_{ij}$. The dimension of $(\tilde{\boldsymbol{\delta}}, \tilde{\boldsymbol{\phi}})$ is $s = d(d+1)/2$, the dimension of \mathbf{J}_{ij} is $s \times 1$, and the dimension of $\text{Var}(\tilde{\boldsymbol{\delta}}, \tilde{\boldsymbol{\phi}})$ is $s \times s$. We require an expression for $\mathbf{J}_{ij}^T = (\partial \tilde{\sigma}_{ij} / \partial (\tilde{\boldsymbol{\delta}}, \tilde{\boldsymbol{\phi}})_1, \dots, \partial \tilde{\sigma}_{ij} / \partial (\tilde{\boldsymbol{\delta}}, \tilde{\boldsymbol{\phi}})_s)$. This is given as follows:

$$\frac{\partial \Sigma_{ij}^{-1}}{\partial \delta_l} = \exp(\delta_l) \mathbf{A}_{il} \mathbf{A}_{jl}, \quad \frac{\partial \Sigma_{ij}^{-1}}{\partial \phi_l} = \sum_{t=1}^d \exp(\delta_t) \left\{ \frac{d\mathbf{A}_{it}}{d\phi_l} \mathbf{A}_{jt} + \mathbf{A}_{it} \frac{d\mathbf{A}_{jt}}{d\phi_l} \right\}, \quad \frac{\partial \Sigma}{\partial (\tilde{\boldsymbol{\delta}}, \tilde{\boldsymbol{\phi}})_l} = -\Sigma \frac{\partial \Sigma^{-1}}{\partial (\tilde{\boldsymbol{\delta}}, \tilde{\boldsymbol{\phi}})_l} \Sigma.$$

Because d is assumed small enough for quadrature to be computationally efficient in the first place, d and s are small enough that matrix computations, including explicit inversion, can be performed naively at minimal computational cost. For example, a random slopes model (see Eq. 14) has $d = 2$ and $s = 3$, leading to negligible computational burden relative to that required to obtain $\hat{\boldsymbol{\theta}}_k^{\text{AQ}}$.

The only quantities for which further detail is required are the selection matrix, $\mathbf{S}(\mathbf{u})$, its derivative-vector/matrix products, $\mathbf{D}\{d\mathbf{S}(\mathbf{u})/d\mathbf{u}_j\}$ and $\{d\mathbf{S}(\mathbf{u})^T/d\mathbf{u}_j\}\mathbf{D}$, and the derivative matrices, $d\mathbf{A}_{it}/d\phi_l$. We offer Algorithms 4–6 in Section A of the supplement which describe computation of these quantities. Our algorithmic approach to these computations avoids complicated higher-order tensor algebra, despite the procedure depending on third-order

derivatives of multivariable functions. The result is an efficient implementation of the whole procedure that involves only matrix and vector algebra.

Finally, for the variances, $\tilde{\sigma}_{ii}$, we compute Wald intervals on the log-scale as $\log \tilde{\sigma}_{ii} \pm z_{1-\alpha/2} \text{se}(\log \tilde{\sigma}_{ii})$, where $\text{se}(\log \tilde{\sigma}_{ii}) = \text{Var}(\log \tilde{\sigma}_{ii})^{1/2}$ and

$$\text{Var}(\log \tilde{\sigma}_{ii}) \approx \text{Var}(\tilde{\sigma}_{ii})/\tilde{\sigma}_{ii},$$

and then obtain an interval for σ_{ii} by exponentiating this interval. This ensures that the lower bounds always remain positive, and generally appears to give more accurate intervals.

4.3 Empirical Evaluation

Two sets of simulations offer empirical evidence that: (a) inferences about $\boldsymbol{\theta}$ using $\widehat{\boldsymbol{\theta}}_k^{\text{AQ}}$ are accurate for some k , and that there are compelling cases where $k > 1$ is required, motivating the need for novel methods to make such inferences efficiently; and (b) the novel methods of Section 3 and the setup of the present Section yield computations that are fast and stable relevant to existing, established methods. On the former point, $k > 1$ is seen to be most impactful for cases involving any or all of large m , small n , or large $\boldsymbol{\sigma}$; the Laplace approximation ($k = 1$) gives exceptionally poor inferences in these cases, and this is mitigated by choosing large enough k . On the latter point, we find evidence that the proposed method yields results at least as favourable as existing methods in shorter amounts of time. We strongly emphasize that the proposed methods do not *compete* with existing methods that already give favourable results, but rather that they *complement* existing methods by replacing cumbersome derivative-free optimization or finite difference-based gradient calculations with exact gradient calculations, typically yielding a factor of 2 – 4 reduction in computing time.

4.3.1 Absolute performance

We use a similar simulation setup to Breslow and Clayton (1993), considering the following model:

$$Y_{ij} \mid \mathbf{u}_i \stackrel{\text{ind}}{\sim} \text{Bern}(p_{ij}), \mathbf{u}_i \stackrel{\text{iid}}{\sim} \text{N}\{\mathbf{0}, \boldsymbol{\Sigma}(\boldsymbol{\sigma})\}, \log \frac{p_{ij}}{1 - p_{ij}} = \beta_0 + \beta_1 x_i + \beta_2 t_j + \beta_3 x_i t_j + u_{i1} + u_{i2} t_j. \quad (7)$$

This is model (5) with $\mathbf{x}_{ij} \equiv (x_i, t_j)^\top$ and $\mathbf{v}_{ij} = (1, t_j)^\top$. The group-specific covariate, x_i , takes value 1 for half the groups and value 0 for the other half. The measurement-specific covariate, t_j , takes values on an equally-spaced grid of length n_i from -3 to 3 . We consider all combinations of $m = \{100, 200, 500, 1000\}$, $n = \{3, 5, 7, 9\}$, and $k = \{1, 3, \dots, 23, 25\}$. Breslow and Clayton (1993) considered only $m = 100$, $n = 7$, and $k = 1$, concluding that the PQL approach based on the Laplace approximation appeared negatively biased for binary data; they do not assess coverage of confidence intervals. Our simulations recover the claim about bias and provide additional evidence that confidence intervals based on the Laplace approximation achieve very poor coverage, but that $k \gg 1$ mitigates these shortcomings.

We deliberately focus on small n because this situation appears to be common in practice but yields the least accurate integral approximations, and so is of importance in the present context. We would expect that for larger n , the Laplace approximation ($k = 1$) would be adequate, and hence we do not focus on this case.

For the variance matrix, we choose

$$\Sigma(\boldsymbol{\sigma}) = \begin{pmatrix} \sigma_1^2 & \sigma_{12} \\ \sigma_{12} & \sigma_2^2 \end{pmatrix} = \begin{pmatrix} 2 & 1 \\ 1 & 1 \end{pmatrix},$$

which gives $\text{Corr}(u_{i1}, u_{i2}) \approx 0.71$. These variance components are on the logit scale, and hence this can be considered a very difficult situation of random effects having high variance and high correlation. Breslow and Clayton (1993) consider $\text{Corr}(u_{i1}, u_{i2}) = 0$ only, and smaller $\sigma_1^2 = 0.5, \sigma_2^2 = 0.25$. Finally, we use $\boldsymbol{\beta} = (-2.5, -0.15, 0.1, 0.2)^\top$, which yields imbalanced responses due to the low value for β_0 . This further increases the difficulty of making inferences. Overall, this is a challenging simulation setup.

We report complete and detailed performance results for all seven parameters in Section C of the supplement. Here we report results for β_0 , σ_1 , and σ_{12} , which were parameters for which we observed the largest differences in inferences for different values of k . We conclude that for all parameters and combinations of m and n , it appears possible to choose a large enough k such that inferences based on $\hat{\boldsymbol{\theta}}_k^{\text{AQ}}$ have low bias and nominal interval coverage. This is especially relevant to practice, as—unlike m and n —the practitioner may always increase k , and the novel methods in the present paper make doing so much faster and easier. The simulation study in Section 4.3.2 reports computational comparisons to existing methods.

Results are presented in Figure 1. We report the absolute bias, $\text{Bias}(\theta; k) = \mathbb{E}\hat{\theta}_k^{\text{AQ}} - \theta$, for

β_0 and σ_{12} , and the relative bias, $\text{Rel. Bias}(\theta; k) = \mathbb{E}\widehat{\theta}_k^{\text{AQ}}/\theta$, for σ_1^2 . The bias is exceptionally high for the Laplace approximation ($k = 1$), which is consistent with comments made by Breslow and Clayton (1993). The distribution of the bias appears to converge to one centred at 0 as k is increased. We report the empirical coverage proportions and lengths (which are of course simply scalar multiples of the standard errors) of the Wald intervals (Sections 3.3 and 4.2) for the same parameters. Similar to the bias, the coverages appear to converge to nominal as k is increased, with poor performance for lower k . For σ_{12} , the improved performance of $k = 1$ relative to $k = 3$ is attributed to the $k = 1$ intervals being far wider than those for $k = 3$, which appear too narrow relative to higher k . We emphasize that the conclusion here is that we appear to be able to always choose a large enough k to provide valid inferences. The novel methods in the present paper make such computations more convenient for the practitioner.

4.3.2 Relative performance

We perform a second simulation study to attempt to isolate the impact of using the new, exact gradient computations on computational time and estimation quality. To this end, we simulate datasets from the model (14) and fit this model using both the new approach and the **GLMMadaptive** R package (Rizopoulos, 2020; R Core Team, 2021). Because the **lme4** software does not fit models with multivariate random effects by AQ with $k > 1$, we also consider the following random intercepts model:

$$Y_{ij} \mid u_i \stackrel{\text{ind}}{\sim} \text{Bern}(p_{ij}), \quad u_i \stackrel{\text{iid}}{\sim} \text{N}(0, \sigma^2), \quad \log \frac{p_{ij}}{1 - p_{ij}} = \beta_0 + \beta_1 x_i + u_i. \quad (8)$$

Model (15) is model (14) with $\beta_2 = \beta_3 = \sigma_2 = 0$, and we set $\boldsymbol{\beta} = (-2.5, -.15)$ and $\sigma^2 = 2$. We use model (15) to compare the new approach to **lme4**, where we use the alternative efficient scalar implementation of the new approach briefly described in Section 3.4. We include only the results for the combination of $m = 1000$ and $n = 5$ shown also in Figure 1; again, the complete analysis presented in Section D of the supplementary materials.

Figure 2 shows boxplots of (a) the relative computation times, (b) the difference in minimized approximate base-10 average negative log-likelihood values, $-\widetilde{\ell}_k^{\text{AQ}}(\widehat{\boldsymbol{\theta}}_k^{\text{AQ}})/(N \log 10)$, and (c) the difference in base-10 logarithms of the 2-norm of the exact gradient of the minimized average approximate negative log-likelihood values, $\log_{10} \|\nabla \widetilde{\ell}_k^{\text{AQ}}(\widehat{\boldsymbol{\theta}}_k^{\text{AQ}})\|_2/(N \log 10)$, for the

new approach against each of `GLMMadaptive` and `lme4`. Positive values indicate that each existing approach returned an MLE, $\hat{\boldsymbol{\theta}}_k^{\text{AQ}}$, having a higher minimized negative log-likelihood value, or higher gradient norm at the minimum than the new approach; in all metrics, a higher value therefore means that the new method performed favourably compared to an existing method. We find that the new approach tends to give results that are at least as favourable as existing methods with a typical factor of $2 - 4$ reduction in computation time than each existing method, with slight variations for different values of k . The expanded simulations in Section C of the supplementary materials show that this tends to hold across different values of m and n .

Both `GLMMadaptive` and `lme4` return comparable satisfactory results to the new method. The new method returns these results in a shorter computation time. This suggests that the use of exact gradients has the potential to speed up optimization for mixed models, compared to finite-differenced gradients (`GLMMadaptive`) or derivative-free optimization techniques (`lme4`). The absolute computation times of the chosen examples are mostly a few seconds on the hardware used; however, the relative computation times are expected to hold for larger sets of data for which the absolute computation times are also larger.

We remark as well that our implementation of this procedure is young and potentially naive, while the other two are quite mature and efficient; it is implausible that these gains in speed are due to a superior implementation of the methods, since it is implausible that the present implementation is in any way superior to these robust and mature software packages. The most plausible explanation for the difference in empirical performance is that the use of exact gradients and quasi-Newton L-BFGS minimization is appreciably computationally favourable to the use of derivative-free optimization methods or finite-differenced gradient-based quasi-Newton optimization in approximate likelihood inference for mixed models.

5 Data Analysis

We present two re-analyses of mixed models previously reported in the literature. The first provides an example of multivariate random effects, where small n with moderate m leads to very different inferences for different k . The second provides the same for scalar random effects, in the presence of very large between-subject heterogeneity.

5.1 Smoking cessation

Hedeker et al. (2018) provide data from a study by Gruder et al. (1993) on the associations between social support and smoking cessation. The data consist of binary indicators, Y_{ij} , with $Y_{ij} = 1$ indicating smoking cessation, from $i = 1, \dots, m = 489$ subjects at $j = 1, \dots, n_i \in \{1, 2, 3, 4\}$ follow-up times after a televised intervention. Subjects were randomly assigned to receive social support ($x_i = 1$) or not ($x_i = 0$) and followed up at $t_j = 0, 6, 12$, or 24 months post-intervention (note the t_j values in the data are normalized). The following model is considered:

$$Y_{ij} \mid \mathbf{u}_i \stackrel{\text{ind}}{\sim} \text{Bern}(p_{ij}), \mathbf{u}_i \stackrel{\text{iid}}{\sim} N\{\mathbf{0}, \Sigma(\boldsymbol{\sigma})\}, \log \frac{p_{ij}}{1 - p_{ij}} = \beta_0 + \beta_1 x_i + \beta_2 t_j + \beta_3 x_i t_j + u_{i1} + u_{i2} t_j. \quad (9)$$

The random intercept, u_{i1} , is included to account for potentially different baseline propensity for cessation among subjects and the random slope, u_{i2} , is included because the correlations between cessation at each time point appear nonzero; see Hedeker et al. (2018) for details.

We fit this model using our new approach and **GLMMadaptive**; recall that **lme4** does not fit the random slopes model with $k > 1$. Inspection of their SAS code reveals that Hedeker et al. (2018) used $k = 11$; this choice of estimator is not discussed by them. We fit the model with k between 1 and 25, and observe that results appear to stop changing for $k \geq 17$ or so.

Figure 3 (a) – (c) shows the estimated variance components from both methods; regression coefficients were essentially the same from both procedures and are shown in Section D of the supplement. Of particular note is the very large estimate for $\hat{\sigma}_1^2$. In all cases, when k is large enough, inferences stop changing. For σ_{12} and to a lesser extent σ_2^2 , the large- k intervals are smaller from the new method than **GLMMadaptive**; combined with the nominal coverage of these intervals for this parameter in the simulations, this can be regarded as an advantage of the new method.

Figure 3 (d) shows the relative computation times of **GLMMadaptive** compared to the new method over 500 repetitions of the fit. Although it varies with k , the new method is usually around 4 – 5 times, and in uncommon cases up to 10 times faster than **GLMMadaptive**. It was never less than 2.5 times faster.

5.2 Toenail fungus treatment

Lesaffre and Spiessens (2001) report measurements of a binary indicator, Y_{ij} , with $Y_{ij} = 1$

indicating the absence of toenail infection, from $i = 1, \dots, m = 294$ subjects who were given an oral treatment for toenail infection ($x_i = 1$) or not ($x_i = 0$) and followed up at $j = 1, \dots, n_j \in \{1, \dots, 7\}$ times $t_j = -3, \dots, 3$. They fit the random intercepts model:

$$Y_{ij} \mid u_i \stackrel{\text{ind}}{\sim} \text{Bern}(p_{ij}), \quad u_i \stackrel{\text{iid}}{\sim} N(0, \sigma^2), \quad \log \frac{p_{ij}}{1 - p_{ij}} = \beta_0 + \beta_1 x_i + \beta_2 t_j + \beta_3 x_i t_j + u_{i1}. \quad (10)$$

The purpose of the analysis by Lesaffre and Spiessens (2001) was to investigate the sensitivity of inferences to the choice of k ; although focus was on non-adaptive Gauss-Hermite quadrature, they also use AQ, concluding that inferences appear to stop changing around $k = 10$ or so. We fit this model to these data using our new method, **lme4**, and **GLMMadaptive** to investigate performance and choice of k .

Figure 4 shows the results of fitting the model (10) to the toenail infection treatment data of Lesaffre and Spiessens (2001). For β , the point estimates and Wald confidence intervals for all methods level off for large enough k and are in agreement with each other. The point where inferences stop changing is around $k = 17$ or so, higher than the $k = 10$ suggested by Lesaffre and Spiessens (2001). For σ , the point estimates for all three methods are also in agreement for large k . Note the exceptionally large estimate of $\hat{\sigma} \approx 4$, indicating massive between-subject heterogeneity.

The **lme4** software includes options to compute accurate bootstrap and profile likelihood intervals for the variance components. The bootstrap in particular should be accurate at any sample size and for any values of σ . While the Wald intervals provided by our approach and **GLMMadaptive** are found to be accurate in the examples shown here, they may be inaccurate for smaller N . However, the difference in computation time is large: the profile approach takes around 60 times longer than the point estimates and Wald intervals computed using the new approach. A reviewer points out that the availability of the exact gradient could potentially be used to speed up the computation of profile likelihood intervals. The bootstrap with 200 samples took between 1300 – 1600 times longer than the new approach. Figure 4 (c) shows all the intervals; for large enough k the Wald, profile, and bootstrap agree closely for these data.

Figure 4 (d) shows the relative computation times of **lme4** and **GLMMadaptive** compared to the new approach, across 500 repetitions of the fit. The new approach is mostly between 2 and 8 times faster than these established approaches, and is never slower. Note that these

time comparisons for `lme4` do not include confidence intervals for σ .

6 Discussion

The restriction to mixed models with a single grouping factor is necessary for the developments in this paper. The core aspect of the model that was considered is the factoring of the marginal likelihood into a product of m low dimensional integrals; any model in which this does not occur will require further innovation in order to apply accurate low-dimensional quadrature techniques. Pinheiro and Chao (2006) apply adaptive quadrature in multi-level mixed models, and it would be interesting to derive the gradient algorithm presented in this paper to this case. It remains unclear whether it is possible to derive a procedure for fitting mixed models with more general random effects structure using AQ.

We conjecture here that it is not possible to develop a quadrature-based procedure that works for *all* mixed model random effects structures by showing an example where it does not appear possible, as follows. Consider a model with crossed random effects as defined by Ghosh et al. (2022, Eq. 1):

$$\begin{aligned} Y_{ij} \mid u_i, v_j &\stackrel{\text{ind}}{\sim} F(\mu_{ij}, \boldsymbol{\phi}), \quad u_i \stackrel{\text{iid}}{\sim} N(0, \sigma_u^2), \quad v_j \stackrel{\text{iid}}{\sim} N(0, \sigma_v^2), \\ \eta_{ij} = h(\mu_{ij}) &= \beta_0 + \mathbf{x}_{ij}^T \boldsymbol{\beta} + u_i + v_j. \end{aligned} \tag{11}$$

The marginal likelihood corresponding to Eq. 11 is (Ghosh et al., 2022, Eq. 5) $\pi(\boldsymbol{\theta}; \mathbf{y}) = \int \pi(\boldsymbol{\theta}, \mathbf{u}, \mathbf{v}) d\mathbf{u} d\mathbf{v}$, where $\mathbf{u} = (u_1, \dots, u_R)^T$ and $\mathbf{v} = (v_1, \dots, v_C)^T$ with R, C very large and total sample size $N \ll RC$. Crucially, $\pi(\boldsymbol{\theta}; \mathbf{y})$ does not factor over the random effects, and low-dimensional quadrature cannot be applied as it can for the model considered in this paper.

Every mixed model analysis in which inferences are obtained by maximizing an approximate marginal likelihood where the approximation is adaptive quadrature must specify a number of quadrature points, k , for which estimates will be reported. There is currently no clear principle upon which to base this important choice. However, the simulations of the previous Section demonstrate that it does have a substantial effect on the quality of inferences. Choosing a k that is too high was never observed to lead to substantially worse inferences than one that is too low, and simply increases computation time. Choosing a

k that is too low, however, can clearly lead to dramatically inappropriate inferences. We therefore recommend to choose a k high enough that inferences appear to stop changing as k is further increased. We are certainly not the first to suggest this as a strategy for choosing k ; in fact, we were unable to find a published simulation study or data analysis which used these methods and reported choosing k in any other way. Development of a more principled strategy for choosing k may be regarded as an open problem.

Automatic differentiation (AD) is an established tool for obtaining exact gradients, and C++ implementations are accessible in R via the Stan Math library (Carpenter et al., 2015, 2017) and the Template Model Builder (TMB; Kristensen et al. 2016). Naive automatic differentiation of $\log \tilde{\pi}_k^{\text{AQ}}(\boldsymbol{\theta}; \mathbf{y})$ is challenging due to the inner optimization required to compute $\hat{\mathbf{u}}(\boldsymbol{\theta})$, the third derivatives involved in differentiating the Hessian determinant, and the matrix algorithms required to compute the Hessian determinant and solve the triangular system required to scale the quadrature nodes. The glmmTMB software (Brooks et al., 2017), through the TMB software (Kristensen et al., 2016), provides efficient automatic differentiation of $\log \tilde{\pi}_1^{\text{AQ}}(\boldsymbol{\theta}; \mathbf{y})$; we include a brief comparison in Section C of the supplementary materials. The proposed gradient evaluation algorithm in Section 3 uses algorithmic differentiation to differentiate through the Cholesky and forward solve algorithms, as well as implicit differentiation for $\hat{\mathbf{u}}(\boldsymbol{\theta})$. These contributions could plausibly lead to an efficient implementation of automatic differentiation for $\log \tilde{\pi}_k^{\text{AQ}}(\boldsymbol{\theta}; \mathbf{y})$.

References

Bates, D., Mächler, M., Bolker, B., and Walker, S. (2015). Fitting Linear Mixed-Effects Models Using lme4. *Journal of Statistical Software*, 67(1):1–48.

Bilodeau, B., Stringer, A., and Tang, Y. (2022). Stochastic Convergence Rates and Applications of Adaptive Quadrature in Bayesian Inference.

Bolker, B. M., Brooks, M. E., Clark, C. J., Geange, S. W., Poulsen, J. R., Stevens, M. H. H., and White, J.-S. S. (2008). Generalized Linear Mixed Models: A Practical Guide for Ecology and Evolution. *Trends in Ecology and Evolution*, 42(3):127–135.

Bono, R., Alarcon, R., and Blanca, M. J. (2021). Report Quality of Generalized Linear Mixed Models in Psychology: A Systematic Review. *Frontiers in Psychology*, 12.

Booth, J. and Hobert, J. (1999). Maximizing Generalized Linear Mixed Model Likelihoods with an Automated Monte Carlo EM Algorithm. *Journal of the Royal Statistical Society, Series B (Methodology)*, 61(1):265–285.

Breslow, N. E. and Clayton, D. G. (1993). Approximate Inference in Generalized Linear Mixed Models. *Journal of the American Statistical Association*, 88(421):9–25.

Brooks, M. E., Kristensen, K., Benthem, K. J. v., Magnusson, A., Berg, C. W., Nielsen, A., Skaug, H. J., Maechler, M., and Bolker, B. M. (2017). glmmTMB Balances Speed and Flexibility Among Packages for Zero-Inflated Generalized Linear Mixed Modeling. *The R Journal*, 9(2):378–400.

Carpenter, B., Gelman, A., Hoffman, M. D., Lee, D., Goodrich, B., Betancourt, M., Brubaker, M., Guo, J., Li, P., and Riddell, A. (2017). Stan: A probabilistic programming language. *Journal of statistical software*, 76(1).

Carpenter, B., Hoffman, M. D., Brubaker, M., Lee, D., Li, P., and Betancourt, M. (2015). The stan math library: Reverse-mode automatic differentiation in c++. *arXiv preprint arXiv:1509.07164*.

Ghosh, S., Hastie, T., and Owen, A. B. (2022). Scalable logistic regression with crossed random effects. *Electronic Journal of Statistics*, 16:4604–4635.

Golub, G. H. and van Loan, C. F. (1983). *Matrix computations*. The Johns Hopkins University Press, Baltimore, Maryland.

Gruder, C. L., Mermelstein, R. J., and Kirkendol, S. e. a. (1993). Effects of social support and relapse prevention training as adjuncts to a televised smoking cessation intervention. *Journal of Consulting and Clinical Psychology*, 61:113–120.

Hedeker, D., du Toit, S. H., Demirtas, H., and Gibbons, R. D. (2018). A Note on Marginalization of Regression Parameters from Mixed Models of Binary Outcomes. *Biometrics*, 74(1):354–361.

Jiang, J., Wand, M., and Bhaskaran, A. (2022). Usable and precise asymptotics for generalized linear mixed model analysis and design. *Journal of the Royal Statistical Society, Series B (Methodology)*, 84:55–82.

Jin, S. and Andersson, B. (2020). A Note on the Accuracy of Adaptive Gauss-Hermite Quadrature. *Biometrika*, 107(3):737–744.

Joe, H. (2008). Accuracy of Laplace Approximation for Discrete Response Mixed Models. *Computational Statistics and Data Analysis*, 52:5066–5074.

Kim, Y., Choi, Y.-K., and Emery, S. (2013). Logistic regression with multiple random effects: A simulation study of estimation methods and statistical packages. *The American Statistician*, 67(3):171–182.

Kristensen, K., Nielson, A., Berg, C. W., Skaug, H., and Bell, B. M. (2016). TMB: automatic differentiation and Laplace approximation. *Journal of statistical software*, 70(5).

Lee, Y. and Nelder, J. A. (1996). Hierarchical Generalized Linear Models (with discussion). *Journal of the Royal Statistical Society, Series B (Methodology)*, 587(4):619–678.

Lesaffre, E. and Spiessens, B. (2001). On the Effect of the Number of Quadrature Points in a Logistic Random-Effects Model: An Example. *Journal of the Royal Statistical Society, Series C (Applied Statistics)*, 50(3):325–335.

Liu, Q. and Pierce, D. A. (1994). A Note on Gauss-Hermite Quadrature. *Biometrika*, 81(3):624–629.

McCulloch, C. E. (1997). Maximum Likelihood Algorithms for Generalized Linear Mixed Models. *Journal of the American Statistical Association*, 92(437):162–170.

Naylor, J. C. and Smith, A. F. M. (1982). Applications of a Method for the Efficient Computation of Posterior Distributions. *Journal of the Royal Statistical Society, Series C (Applied Statistics)*, 31(3):214–225.

Nie, L. (2007). Convergence Rate of MLE in Generalized Linear and Nonlinear Mixed-Effects Models: Theory and Applications. *Journal of Statistical Planning and Inference*, 137:1787–1804.

Nocedal, J. and Wright, S. J. (2006). *Numerical Optimization*. Springer, New York, NY.

Pinheiro, J. and Chao, E. (2006). Efficient Laplacian and Adaptive Gaussian Quadrature Algorithms for Multilevel Generalized Linear Mixed Models. *Journal of Computational and Graphical Statistics*, 15(1):58–81.

Pinheiro, J. C. and Bates, D. M. (1995a). Approximations to the Log-Likelihood Function in the Nonlinear Mixed Effects Models. *Journal of Computational and Graphical Statistics*, 4(1):12–35.

Pinheiro, J. C. and Bates, D. M. (1995b). Unconstrained parametrizations for variance-covariance matrices. *Statistics and Computing*, 6:289–296.

R Core Team (2021). *R: A Language and Environment for Statistical Computing*. R Foundation for Statistical Computing, Vienna, Austria.

Rizopoulos, D. (2020). *GLMMadaptive: Generalized Linear Mixed Models using Adaptive Gaussian Quadrature*.

Rue, H. (2001). Fast sampling of Gaussian Markov random fields. *Journal of the Royal Statistical Society, Series B: Statistical Methodology*, 63(2):325–338.

Rue, H. and Martino, S. (2007). Approximate Bayesian inference for hierarchical Gaussian Markov random field models. *Journal of Statistical Planning and Inference*, 137:3177 – 3192.

Smith, S. P. (1995). Differentiation of the Cholesky Algorithm. *Journal of Computational and Graphical Statistics*, 4(2):134–147.

Stringer, A., Brown, P., and Stafford, J. (2023). Fast, acalable approximations to posterior distributions in extended latent Gaussian models. *Journal of Computational and Graphical Statistics*, 32(1).

Tierney, L. and Kadane, J. B. (1986). Accurate Approximations to Posterior Moments and Marginal Densities. *Journal of the American Statistical Association*, 81(393):82–86.

Vonesh, E. F. (1996). A Note on the use of Laplace's Approximation for Nonlinear Mixed Effect Models. *Biometrika*, 83(2):447–452.

Wolfinger, R. (1993). Laplace's approximation for nonlinear mixed models. *Biometrika*, 80(4):791–795.

Wood, S. (2011). Fast stable restricted maximum likelihood and marginal likelihood estimation of semiparametric generalized linear models. *Journal of the Royal Statistical Society, Series B (Statistical Methodology)*, 73(1):3 – 36.

Wood, S., Pya, N., and Säfken, B. (2016). Smoothing parameter and model selection for general smooth models. *Journal of the American Statistical Association*, 111:1548 – 1575.

A Algorithms

This section gives algorithms for:

1. Evaluating the approximate log-marginal likelihood, $\tilde{\ell}_k(\boldsymbol{\theta})$, and its (exact) gradient, $\nabla_{\boldsymbol{\theta}}\tilde{\ell}_k(\boldsymbol{\theta})$.
2. Evaluating the derivative of the solution, \mathbf{v} , to the lower-triangular system, $\mathbf{L}\mathbf{v} = \mathbf{z}$, with respect to the elements of (the lower triangle of) \mathbf{L} .
3. Evaluating vector products and their derivatives involving the matrix quantities $\mathbf{S}(\mathbf{u})$ and \mathbf{A} required to implement models with the parameterization of the multivariate Gaussian given in Section 4.2 of the main manuscript.

A.1 Approximate marginal log-likelihood and exact gradient

Data:

$$\mathbf{y}_i \in \mathbb{R}^{n_i}, i = 1, \dots, m;$$

$$N = n_1 + \dots + n_m;$$

$$\mathbf{X} \in \mathbb{R}^{N \times q}; \mathbf{Z} \in \mathbb{R}^{N \times d};$$

$$\boldsymbol{\beta} \in \mathbb{R}^q;$$

$$\boldsymbol{\phi} \in \mathbb{R}^w;$$

$$\boldsymbol{\sigma} \in \mathbb{R}^s;$$

$$\pi(\boldsymbol{\theta}, \mathbf{u}; \mathbf{y}) \text{ joint likelihood, } \mathbf{y} = (\mathbf{y}_1, \dots, \mathbf{y}_m) \in \mathbb{R}^N;$$

$$\mathbf{g}(\boldsymbol{\theta}, \mathbf{u}; \mathbf{y}) = \partial \log \pi(\boldsymbol{\theta}, \mathbf{u}; \mathbf{y}) / \partial (\boldsymbol{\theta}, \mathbf{u});$$

$$\mathbf{H}(\boldsymbol{\theta}, \mathbf{u}; \mathbf{y}) = \partial^2 \log \pi(\boldsymbol{\theta}, \mathbf{u}; \mathbf{y}) / \partial (\boldsymbol{\theta}, \mathbf{u}) \partial (\boldsymbol{\theta}, \mathbf{u})^T;$$

$$\mathbf{M}(\boldsymbol{\theta}, \mathbf{u}; \mathbf{y}) = (\mathbf{M}_1, \dots, \mathbf{M}_p) \in \mathbb{R}^{d \times d \times p}, \mathbf{M}_l = \partial \mathbf{H}(\boldsymbol{\theta}, \mathbf{u}; \mathbf{y}) / \partial (\boldsymbol{\theta}, \mathbf{u})_l, l = 1, \dots, p;$$

$$k \in \mathbb{N}, \mathcal{Q}(k, 1) = \{z_1, \dots, z_k\} \subset \mathbb{R}, \omega_k : \mathcal{Q}(k, 1) \rightarrow \mathbb{R}^+.$$

Set:

$$\boldsymbol{\theta} = (\boldsymbol{\beta}, \boldsymbol{\phi}, \boldsymbol{\sigma}) \in \mathbb{R}^p;$$

$$\mathbf{u} = \mathbf{0} \in \mathbb{R}^d;$$

$$\tilde{\ell}_k(\boldsymbol{\theta}) = 0;$$

$$\nabla_{\boldsymbol{\theta}} \tilde{\ell}_k(\boldsymbol{\theta}) = \mathbf{0} \in \mathbb{R}^p$$

$$\boldsymbol{\eta}_i = \boldsymbol{\eta}'_i = \boldsymbol{\eta}''_i = \mathbf{0} \in \mathbb{R}^{n_i}, i \in \{1, \dots, m\};$$

$$\mathcal{Q}(k, d) = \mathcal{Q}(k, 1)^d;$$

$$\omega_k(\mathbf{z}) = \omega_k(z_1) \times \dots \times \omega_k(z_d);$$

$$\mathbf{v} = \mathbf{0} \in \mathbb{R}^{k^d}, \mathbf{g}_1 = \mathbf{0} \in \mathbb{R}^{p+d}, \mathbf{g}_2 = \mathbf{0} \in \mathbb{R}^{p+d}, \mathbf{g}_3 = \mathbf{0} \in \mathbb{R}^{p+d}, \mathbf{g}_4 = \mathbf{0} \in \mathbb{R}^p;$$

$$\mathbf{F} \in \mathbb{R}^{d \times d} \text{ lower-triangular;}$$

$$\mathbf{w}^L \in \mathbb{R}^{k^d \times d(d+1)/2};$$

$$\mathbf{w}^u \in \mathbb{R}^{k^d \times p}.$$

Result: Input to Algorithm 2.

Algorithm 1: Quantities required to compute the approximate log-marginal likelihood, $\tilde{\ell}_k(\boldsymbol{\theta})$, and its exact gradient, $\nabla_{\boldsymbol{\theta}} \tilde{\ell}_k(\boldsymbol{\theta})$; see Algorithm 2 for computations.

Data: Output of Algorithm 1.

Result: $\tilde{\ell}_k(\boldsymbol{\theta}) \in \mathbb{R}$, $\nabla_{\boldsymbol{\theta}} \tilde{\ell}_k(\boldsymbol{\theta}) = \partial \tilde{\ell}_k(\boldsymbol{\theta}) / \partial \boldsymbol{\theta}^T \in \mathbb{R}^p$

for $i = 1, \dots, m$ **do**

 Let $t_1 = 0$.

 Compute $\hat{\mathbf{u}}_i(\boldsymbol{\theta})$ via Newton's method.

 Compute $\widehat{\mathbf{H}}_i(\boldsymbol{\theta}, \hat{\mathbf{u}}_i(\boldsymbol{\theta})) = -\partial^2 \log \pi_i(\boldsymbol{\theta}, \hat{\mathbf{u}}_i(\boldsymbol{\theta})) / \partial \mathbf{u}_i \partial \mathbf{u}_i^T$;

 Compute $\widehat{\mathbf{L}}_i(\boldsymbol{\theta}, \hat{\mathbf{u}}_i(\boldsymbol{\theta}))$, lower Cholesky triangle of $\widehat{\mathbf{H}}_i(\boldsymbol{\theta}, \hat{\mathbf{u}}_i(\boldsymbol{\theta}))$;

 Compute $\log |\widehat{\mathbf{L}}_i(\boldsymbol{\theta}, \hat{\mathbf{u}}_i(\boldsymbol{\theta}))| = \log \widehat{\mathbf{L}}_i(\boldsymbol{\theta}, \hat{\mathbf{u}}_i(\boldsymbol{\theta}))_{11} + \dots + \log \widehat{\mathbf{L}}_i(\boldsymbol{\theta}, \hat{\mathbf{u}}_i(\boldsymbol{\theta}))_{dd}$;

 Compute $\mathbf{M}(\boldsymbol{\theta}, \hat{\mathbf{u}}_i(\boldsymbol{\theta}); \mathbf{y}_i)$;

 Set $\mathbf{w}^L = \mathbf{0}$.

for $j = 1, \dots, |\mathcal{Q}(k, d)|$ **do**

 Compute $\widehat{z}_j(\boldsymbol{\theta}) = \widehat{\mathbf{L}}_i(\boldsymbol{\theta}, \hat{\mathbf{u}}_i(\boldsymbol{\theta}))^{-1} z_j + \hat{\mathbf{u}}_i(\boldsymbol{\theta})$;

 Set $\mathbf{v}_j = \log \pi_i(\boldsymbol{\theta}, \widehat{z}_j(\boldsymbol{\theta}); \mathbf{y}_i) + \log \omega_k(z_j) - \log |\widehat{\mathbf{L}}_i(\boldsymbol{\theta}, \hat{\mathbf{u}}_i(\boldsymbol{\theta}))|$;

 Set $\mathbf{w}_{j,.}^u = \partial \log \pi_i(\boldsymbol{\theta}, \widehat{z}_j(\boldsymbol{\theta}); \mathbf{y}_i) / \partial \mathbf{u}_i$;

 Compute $\widehat{\mathbf{L}}_i(\boldsymbol{\theta}, \hat{\mathbf{u}}_i(\boldsymbol{\theta}))^{-1} \mathbf{z}$ and

$\mathbf{t}_2 \equiv (\partial \widehat{\mathbf{L}}_i(\boldsymbol{\theta}, \hat{\mathbf{u}}_i(\boldsymbol{\theta}))^{-1} \mathbf{z} / \partial L_{11}, \dots, \partial \widehat{\mathbf{L}}_i(\boldsymbol{\theta}, \hat{\mathbf{u}}_i(\boldsymbol{\theta}))^{-1} \mathbf{z} / \partial L_{dd})^T$ via Algorithm 3;

 Set $\mathbf{w}_{j,.}^L = \mathbf{t}_2^T \mathbf{w}_{j,1:d}^u$;

end

 Set $t_1 = \log \sum_{j=1}^{|\mathcal{Q}(k, d)|} \exp(\mathbf{v}_j)$;

 Increment $\tilde{\ell}_k(\boldsymbol{\theta}) += t_1$;

 Set $\mathbf{g}_1 = \sum_{j=1}^{|\mathcal{Q}(k, d)|} \mathbf{w}_{j,.}^u \exp(\mathbf{v}_j)$;

 Set $\text{lower.tri}(\mathbf{F}) = \sum_{j=1}^{|\mathcal{Q}(k, d)|} \mathbf{w}_{j,.}^L \exp(\mathbf{v}_j)$;

$\mathbf{g}_2 = \partial \tilde{\ell}_k^i(\mathbf{L}(\boldsymbol{\theta}, \hat{\mathbf{u}}_i(\boldsymbol{\theta})); \boldsymbol{\theta}, \hat{\mathbf{u}}_i(\boldsymbol{\theta})) / \partial (\boldsymbol{\theta}, \mathbf{u}_i)$, via the algorithm from Section 2.3.1 of Smith (1995) (see Section 3.1.2 of the main manuscript);

 Set $\mathbf{g}_3 = \mathbf{g}_1 + \mathbf{g}_2$;

 Set $\mathbf{g}_4 = (\mathbf{g}_3)_{(d+1):(d+p)} + \left[\widehat{\mathbf{L}}_i(\boldsymbol{\theta}, \hat{\mathbf{u}}_i(\boldsymbol{\theta}))^{-1} \widehat{\mathbf{H}}_i(\boldsymbol{\theta}, \hat{\mathbf{u}}_i(\boldsymbol{\theta}))_{1:d, (d+1):(d+p)} \right]^T$;

 Increment $\nabla_{\boldsymbol{\theta}} \tilde{\ell}_k(\boldsymbol{\theta}) += \mathbf{g}_4 \times \exp(-t_1)$.

end

Algorithm 2: Computation of the approximate log-marginal likelihood, $\tilde{\ell}_k(\boldsymbol{\theta})$, and its exact gradient, $\nabla_{\boldsymbol{\theta}} \tilde{\ell}_k(\boldsymbol{\theta})$; see Algorithm 1 for setup and definitions.

A.2 Forward substitution

Data: $\mathbf{L} \in \mathbb{R}^{d \times d}$, lower triangular, $\mathbf{z} \in \mathbb{R}^d$, $r \geq s \in \{1, \dots, d\}$.

Result: $\mathbf{z} \rightarrow \mathbf{L}^{-1}\mathbf{z}$, $\mathbf{g} = \partial_{L_{kl}} \mathbf{L}^{-1}\mathbf{z}$

Set $\mathbf{g} = \mathbf{0} \in \mathbb{R}^d$;

for $i = 1, \dots, d$ **do**

for $j = 1, \dots, i - 1$ **do**

$z_i \leftarrow z_i - L_{ij}z_j$;

$g_i \leftarrow g_i - L_{ij}g_j$;

if $i = r, j = s$ **then**

$g_i \leftarrow g_i - z_j$;

end

end

$z_i = z_i / L_{ii}$;

$g_i = g_i / L_{ii}$;

if $i = r = s$ **then**

$g_i = g_i - z_i / L_{ii}$

end

end

Algorithm 3: Forward substitution with derivative. The input vector \mathbf{z} is overwritten with $\mathbf{L}^{-1}\mathbf{z}$, and the vector \mathbf{g} contains the d -dimensional vector $\partial_{L_{rs}} \mathbf{L}^{-1}\mathbf{z}$ where r, s index the lower triangle of \mathbf{L} in column-major order, $L_{11}, L_{1,2}, \dots, L_{dd}$.

A.3 Multivariate Gaussian quantities

This section contains algorithms for evaluating

- The selection matrix, $\mathbf{S}(\mathbf{u})$, such that $\mathbf{A}^T \mathbf{u} = \mathbf{u} + \mathbf{S}(\mathbf{u})\boldsymbol{\phi}$ (Algorithm 4),
- The derivative matrix $\partial \mathbf{S}(\mathbf{u}) / \partial u_j$, $j = 1, \dots, d$ (Algorithm 5), and
- The derivative matrix $\partial \mathbf{A} / \partial \phi_j$, $j = 1, \dots, d(d-1)/2$ (Algorithm 6).

These details are required to implement the multivariate Gaussian calculations from Section 4.2 of the main manuscript.

Algorithm 4 shows how to obtain the selection matrix, $\mathbf{S}(\mathbf{u})$, such that

$$\mathbf{A}^T \mathbf{u} = \mathbf{u} + \mathbf{S}(\mathbf{u})\boldsymbol{\phi},$$

where

$$\mathbf{A} = \begin{pmatrix} 1 & & & & \\ \phi_1 & 1 & & & \\ \phi_2 & \phi_d & 1 & & \\ \vdots & \vdots & \vdots & 1 & \\ \phi_{d-1} & \cdots & \cdots & \phi_r & 1 \end{pmatrix}.$$

An example is helpful to illustrate this construction. Let $d = 3$ so $\mathbf{u} = (u_1, u_2, u_3)^T$, $r = 3(3 - 1)/2 = 3$ and hence $\boldsymbol{\phi} = (\phi_1, \phi_2, \phi_3)^T$. Then

$$\begin{aligned} \mathbf{A}^T \mathbf{u} &= \begin{pmatrix} 1 & \phi_1 & \phi_2 \\ 0 & 1 & \phi_3 \\ 0 & 0 & 1 \end{pmatrix} \begin{pmatrix} u_1 \\ u_2 \\ u_3 \end{pmatrix} \\ &= \begin{pmatrix} u_1 + \phi_1 u_2 + \phi_2 u_3 \\ u_2 + \phi_3 u_3 \\ u_3 \end{pmatrix} \\ &= \mathbf{u} + \begin{pmatrix} u_2 & u_3 & 0 \\ 0 & 0 & u_3 \\ 0 & 0 & 0 \end{pmatrix} \boldsymbol{\phi}. \end{aligned}$$

Hence, with $d = 3$, we have

$$\mathbf{S}(\mathbf{u}) = \begin{pmatrix} u_2 & u_3 & 0 \\ 0 & 0 & u_3 \\ 0 & 0 & 0 \end{pmatrix}.$$

Further, it is clear that $\partial \mathbf{S}(\mathbf{u}) / \partial u_j$ will be a matrix containing 0 and 1 only, with a 1 located wherever u_j is. An advantage of the following algorithmic construction of $\mathbf{S}(\mathbf{u})$ is that differentiation of this algorithm immediately yields an algorithm for computing the matrix $\partial \mathbf{S}(\mathbf{u}) / \partial u_j$ for any $j = 1, \dots, d$; see Algorithm 5.

Data: $\mathbf{u} \in \mathbb{R}^d$

Result: $\mathbf{S}(\mathbf{u}) \in \mathbb{R}^{d \times d(d-1)/2}$

Set $r = d(d-1)/2$; **for** $k = 0, \dots, r-1$ **do**

```

if  $(k+1)\%(d-i) == 0$  then
   $i \leftarrow i+1;$ 
   $j \leftarrow i+1;$ 
end
 $\mathbf{S}(\mathbf{u})_{i,k} \leftarrow u_j;$ 
 $j \leftarrow j+1;$ 
end

```

Algorithm 4: Obtain the matrix, $\mathbf{S}(\mathbf{u})$, such that $\mathbf{A}^T \mathbf{u} = \mathbf{u} + \mathbf{S}(\mathbf{u})\phi$. Note: 0-based indexing.

Data: $\mathbf{u} \in \mathbb{R}^d$, $l \in \{0, \dots, d-1\}$.

Result: $\partial \mathbf{S}(\mathbf{u}) / \partial u_l \in \mathbb{R}^{d \times d(d-1)/2}$

Set $s = d(d-1)/2$;

for $k = 0, \dots, s-1$ **do**

```

if  $(k+1)\%(d-i) == 0$  then
   $i \leftarrow i+1;$ 
   $j \leftarrow i+1;$ 
end
if  $j == l$  then
   $\mathbf{S}(\mathbf{u})_{i,k} \leftarrow 1;$ 
end
 $j \leftarrow j+1;$ 

```

end

Algorithm 5: Obtain the matrix $\partial \mathbf{S}(\mathbf{u}) / \partial u_l$ for $l = 0, \dots, d-1$. Note: 0-based indexing.

The final details required are the derivative matrices, $\partial \mathbf{A} / \partial \phi_l$ and $\partial \mathbf{A}^T / \partial \phi_l$. These are also matrices of only 0 and 1 and we determine them algorithmically. Specifically, the matrix $\partial \mathbf{A} / \partial \phi_l$ is a matrix of all 0 except for a 1 at index (i, j) such that $d(j-1) - j(j-1)/2 + (i-j) = l$. To determine the (i, j) location of ϕ_l , we simply invert this relation; see Algorithm 6.

A note on implementation: we do not actually compute the matrix $\partial \mathbf{A} / \partial \phi_l$ when computing products of the form $\partial \mathbf{A} / \partial \phi_l \mathbf{D} \mathbf{A}^T$. Instead we compute (i, j) from Algorithm 6 and use that the product $\partial \mathbf{A} / \partial \phi_l \mathbf{D} \mathbf{A}^T$ is the $d \times d$ matrix formed by placing the j^{th} row of $\mathbf{D} \mathbf{A}^T$

in the i^{th} row of the $d \times d$ -dimensional zero matrix, and $\mathbf{A}\mathbf{D}\partial\mathbf{A}^T/\partial\phi_l$ is its transpose. These are formed directly.

Data: $d \in \mathbb{N}, l \in \{1, \dots, d\}$

Result: (i, j) such that $j \in \{1, \dots, d-1\}, i \in \{j+1, \dots, d\}$, and

$$l = d(j-1) - j(j-1)/2 + (i-j)$$

Set $i = 1, j = 0$;

while $j < d$ **do**

```

if  $l == d(j-1) - j(j-1)/2 + (i-j)$  then
|   return  $(i, j)$ ;
end
i  $\leftarrow i + 1$ ;
if  $i > d$  then
|    $j \leftarrow j + 1$ ;
|    $i \leftarrow j + 1$ ;
end

```

end

Algorithm 6: Return the location, (i, j) , of ϕ_l in \mathbf{A} , for $l = 1, \dots, d(d-1)/2$.

B Exponential family calculations

The calculations for Bernoulli generalized linear mixed models given in Section 4.1 of the main manuscript are an important special case of the generalized linear mixed model with exponential family response. While the Bernoulli case is of specific interest to readers and the model used in all the experiments in the paper, the strategy for obtaining the calculations for general exponential family responses is identical; the former really is a special case of the latter. We give those calculations here, as follows.

The model is:

$$\begin{aligned}
Y_{ij} \mid \mathbf{u}_i &\stackrel{\text{ind}}{\sim} F(\mu_{ij}, \boldsymbol{\phi}), \quad \mathbf{u}_i \stackrel{\text{iid}}{\sim} G(\boldsymbol{\sigma}), \\
\eta_{ij} &= h(\mu_{ij}) = \mathbf{x}_{ij}^T \boldsymbol{\beta} + \mathbf{v}_{ij}^T \mathbf{u}_i.
\end{aligned} \tag{12}$$

The response distribution, $F(\mu_{ij}, \boldsymbol{\phi})$, belongs to the exponential family if its density is

$$f(y_{ij}; \mu_{ij}, \boldsymbol{\phi}) = \exp \left\{ \frac{y_{ij}\eta_{ij} - b(\eta_{ij})}{\phi} \right\} c(y_{ij}; \boldsymbol{\phi}), \tag{13}$$

for known functions b, c , where $\boldsymbol{\phi} = \phi$ is a single dispersion parameter, and $\eta_{ij} = h(\mu_{ij})$ as in

Eq. 12. We treat the dispersion parameter, ϕ , as fixed and known; the most common case where this must be estimated is when the response is Gaussian, in which case the methods in this paper are not relevant, as the marginal likelihood is tractable.

We have

$$\begin{aligned}\log f(y_{ij}; \mu_{ij}, \phi) &= \frac{y_{ij}\eta_{ij} - b(\eta_{ij})}{\phi} + \log c(y_{ij}; \phi), \\ \nabla_{\boldsymbol{\theta}} \log f(y_{ij}; \mu_{ij}, \phi) &= \frac{y_{ij} - b'(\eta_{ij})}{\phi} \mathbf{x}_{ij}, \\ \nabla_{\mathbf{u}_i} \log f(y_{ij}; \mu_{ij}, \phi) &= \frac{y_{ij} - b'(\eta_{ij})}{\phi} \mathbf{v}_{ij}, \\ \nabla_{\boldsymbol{\theta}\boldsymbol{\theta}^T}^2 \log f(y_{ij}; \mu_{ij}, \phi) &= -\frac{b''(\eta_{ij})}{\phi} \mathbf{x}_{ij} \mathbf{x}_{ij}^T, \\ \nabla_{\mathbf{u}_i \mathbf{u}_i^T}^2 \log f(y_{ij}; \mu_{ij}, \phi) &= -\frac{b''(\eta_{ij})}{\phi} \mathbf{v}_{ij} \mathbf{v}_{ij}^T, \\ \nabla_{\mathbf{u}_i \boldsymbol{\theta}^T}^2 \log f(y_{ij}; \mu_{ij}, \phi) &= -\frac{b''(\eta_{ij})}{\phi} \mathbf{v}_{ij} \mathbf{x}_{ij}^T.\end{aligned}$$

The above expressions are standard and immediate, and recover the corresponding expressions in Section 4.1 of the main manuscript. We also require third derivatives of the log-likelihood. We seek the $(p+d) \times (p+d) \times (p+d)$ -dimensional tensor

$$\mathbf{M}(\boldsymbol{\theta}, \mathbf{u}) = \partial_{(\boldsymbol{\theta}, \mathbf{u})} \mathbf{H}_{ij}^y(\boldsymbol{\theta}, \mathbf{u}_i),$$

where

$$\mathbf{H}_{ij}^y(\boldsymbol{\theta}, \mathbf{u}_i) = -\nabla_{\mathbf{u}_i \mathbf{u}_i^T}^2 \log f(y_{ij}; \mu_{ij}, \phi) = \nabla_{\mathbf{u}_i \mathbf{u}_i^T}^2 \frac{b''(\eta_{ij})}{\phi} \mathbf{v}_{ij} \mathbf{v}_{ij}^T.$$

We have

$$\begin{aligned}\frac{\partial}{\partial \beta_l} \mathbf{H}_{ij}^y(\boldsymbol{\theta}, \mathbf{u}_i) &= -\frac{b'''(\eta_{ij})}{\phi} \mathbf{v}_{ij} \mathbf{v}_{ij}^T x_{ijl} \\ \frac{\partial}{\partial u_l} \mathbf{H}_{ij}^y(\boldsymbol{\theta}, \mathbf{u}_i) &= -\frac{b'''(\eta_{ij})}{\phi} \mathbf{v}_{ij} \mathbf{v}_{ij}^T v_{ijl}.\end{aligned}$$

This completes the calculations required to implement Algorithm 2 for any exponential family distribution.

C Complete Simulation Results

C.1 Simulation 1: absolute performance of the new method

In Section 4 we performed the following simulation study. For each combination of $m = \{100, 200, 500, 1000\}$, $n = \{3, 5, 7, 9\}$, and $k = \{1, 3, \dots, 23, 25\}$, we generated 1000 datasets from the model

$$Y_{ij} \mid \mathbf{u}_i \stackrel{\text{ind}}{\sim} \text{Bern}(p_{ij}), \quad \mathbf{u}_i \stackrel{\text{iid}}{\sim} \text{N}\{\mathbf{0}, \Sigma(\boldsymbol{\sigma})\}, \quad \log \frac{p_{ij}}{1 - p_{ij}} = \beta_0 + \beta_1 x_i + \beta_2 t_j + \beta_3 x_i t_j + u_{i1} + u_{i2} t_j, \quad (14)$$

where x_i takes value 1 for half the groups and value 0 for the other half, and t_j takes values on an equally-spaced grid of length n_i from -3 to 3 . We used $\boldsymbol{\beta} = (-2.5, -1.5, .1, .2)^T$ and

$$\Sigma(\boldsymbol{\sigma}) = \begin{pmatrix} \sigma_1^2 & \sigma_{12} \\ \sigma_{12} & \sigma_2^2 \end{pmatrix} = \begin{pmatrix} 2 & 1 \\ 1 & 1 \end{pmatrix}.$$

We fit the model using the new procedure, and compute and report bias (for $\boldsymbol{\beta}$ and σ_{12}) and relative bias (for σ_1^2 and σ_2^2), as well as the lengths and empirical coverage proportions of Wald confidence intervals. The complete simulation results are too extensive to report in the main manuscript, so we report them here.

The bias plots, Figures 5 – 14, report boxplots of $\hat{\theta} - \theta$ (bias) or $\hat{\theta}/\theta$ (relative bias) as appropriate, where each point is the realized value of this statistic from one simulated set of data and model fit.

The coverage plots, Figures 15 – 21, report $X(\theta)/B$ where $B = 1000$ and

$$X(\theta) = \sum_{b=1}^B \mathbf{1} \left[\theta \in \left\{ \hat{\theta} - 2 \times \text{s.e.}(\hat{\theta}), \hat{\theta} + 2 \times \text{s.e.}(\hat{\theta}) \right\} \right]$$

is the number of simulated sets of data for which the Wald interval contained the true value of θ . The intervals drawn around the lines are confidence intervals for this Binomial proportion and are calculated as

$$\{X(\theta)/B\} \pm 2 \times \sqrt{\frac{\{X(\theta)/B\}(1 - \{X(\theta)/B\})}{B}}.$$

The length plots, Figures 22 – 31, report

$$4 \times \text{s.e.}(\hat{\theta}),$$

which is the length of the Wald confidence interval for θ .

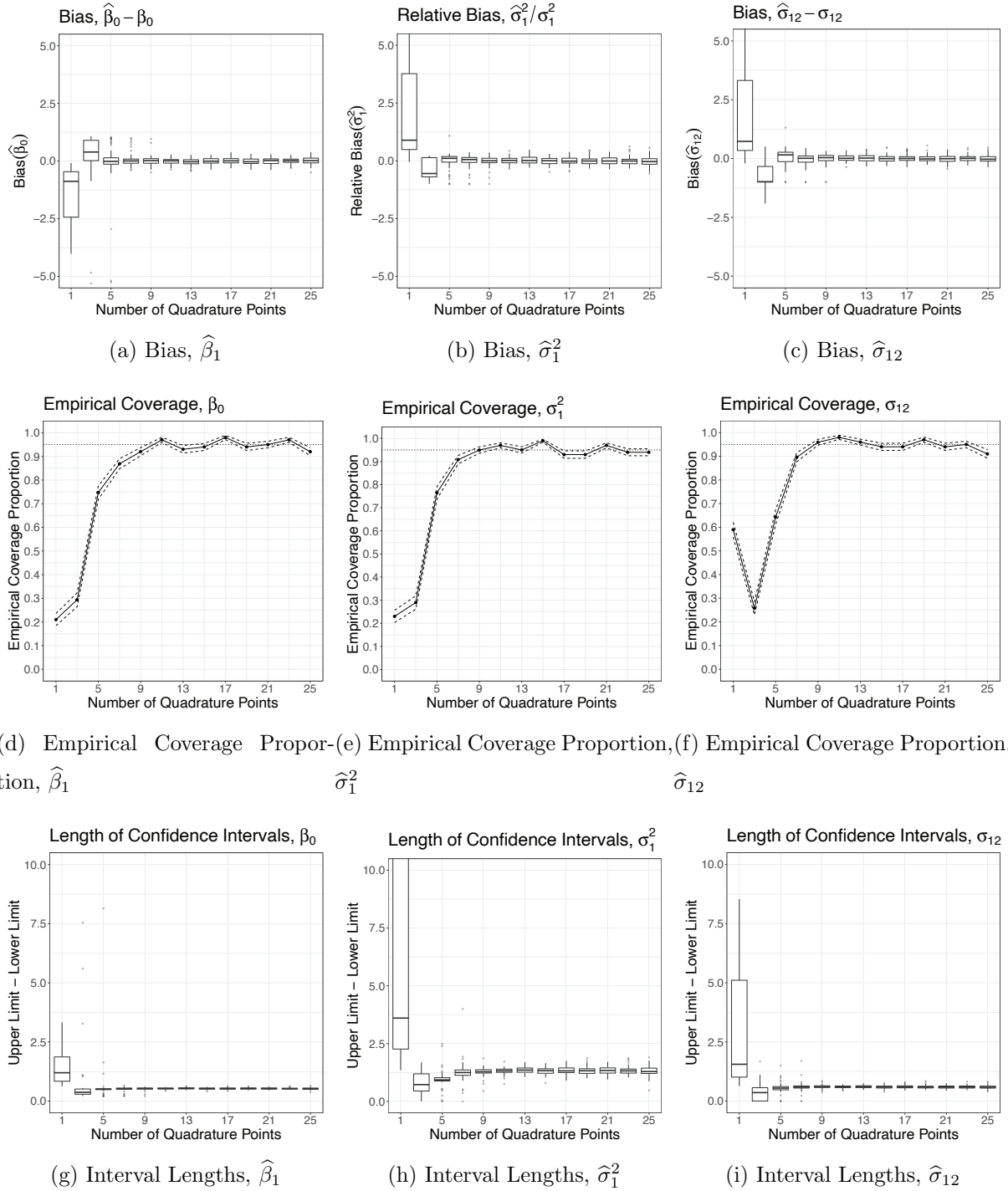


Figure 1: Simulation results for 1000 sets of data generated from model (14) using $m = 1000$ and $n = 5$, and with large variance components ($\sigma_1^2 = 2, \sigma_{12} = 1$) and imbalanced binary response ($\beta_0 = -2.5$, logit scale). In all cases, taking k large enough yields low bias and intervals attaining nominal coverage. Lower $k < 11$ or so yields higher bias, low coverage, and wide intervals, with the Laplace approximation ($k = 1$) yielding exceptionally poor inferences.

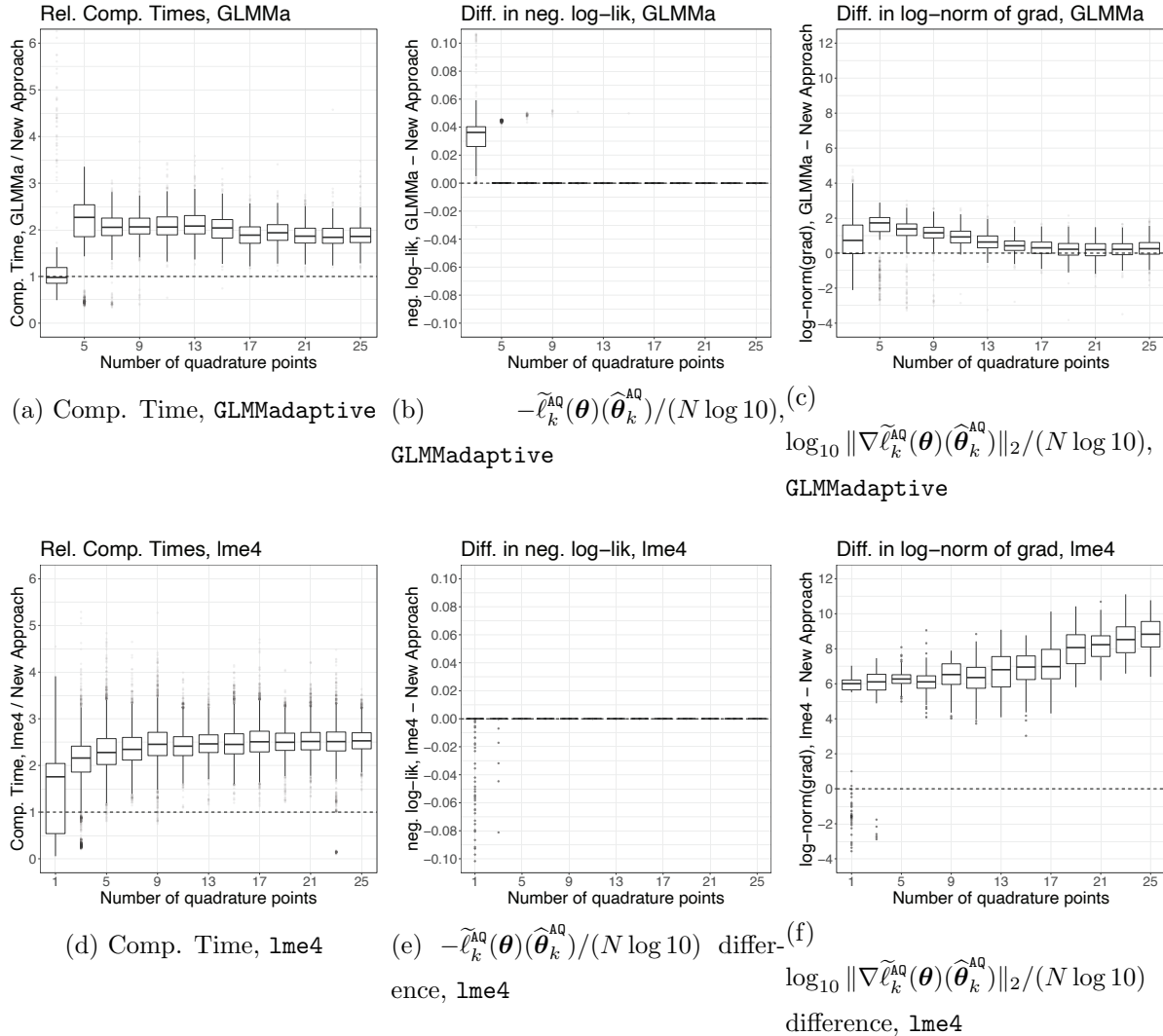


Figure 2: Simulation results for 500 sets of data generated from model (14) (**GLMMadaptive**, a-c) and 1000 sets of data generated from model (15) (**lme4**, d-f) using $m = 1000$ and $n = 5$, and with large variance components ($\sigma_1^2 = 2, \sigma_{12} = 1$) and imbalanced binary response ($\beta_0 = -2.5$, logit scale). Plots (b,e) and (c,f) show the differences in base-10 average minimized negative log-likelihood, $-\tilde{\ell}_k^{\text{AQ}}(\boldsymbol{\theta})(\hat{\boldsymbol{\theta}}_k^{\text{AQ}})/(N \log 10)$, and base-10 log of the 2-norm of the gradient of the average log-likelihood at the minimum, $\log_{10} \|\nabla \tilde{\ell}_k^{\text{AQ}}(\boldsymbol{\theta})(\hat{\boldsymbol{\theta}}_k^{\text{AQ}})\|_2 / (N \log 10)$, for each existing method minus the new method. Positive values indicate that the new approach performed favourably. Because both **GLMMadaptive** and **lme4** give satisfactory performance in absolute terms (see the supplement, Section C), the fact that the new method performs mostly as well or better can be interpreted as the new method not sacrificing performance in order to achieve its 2 – 4 times speed-up in computation time (a,d).

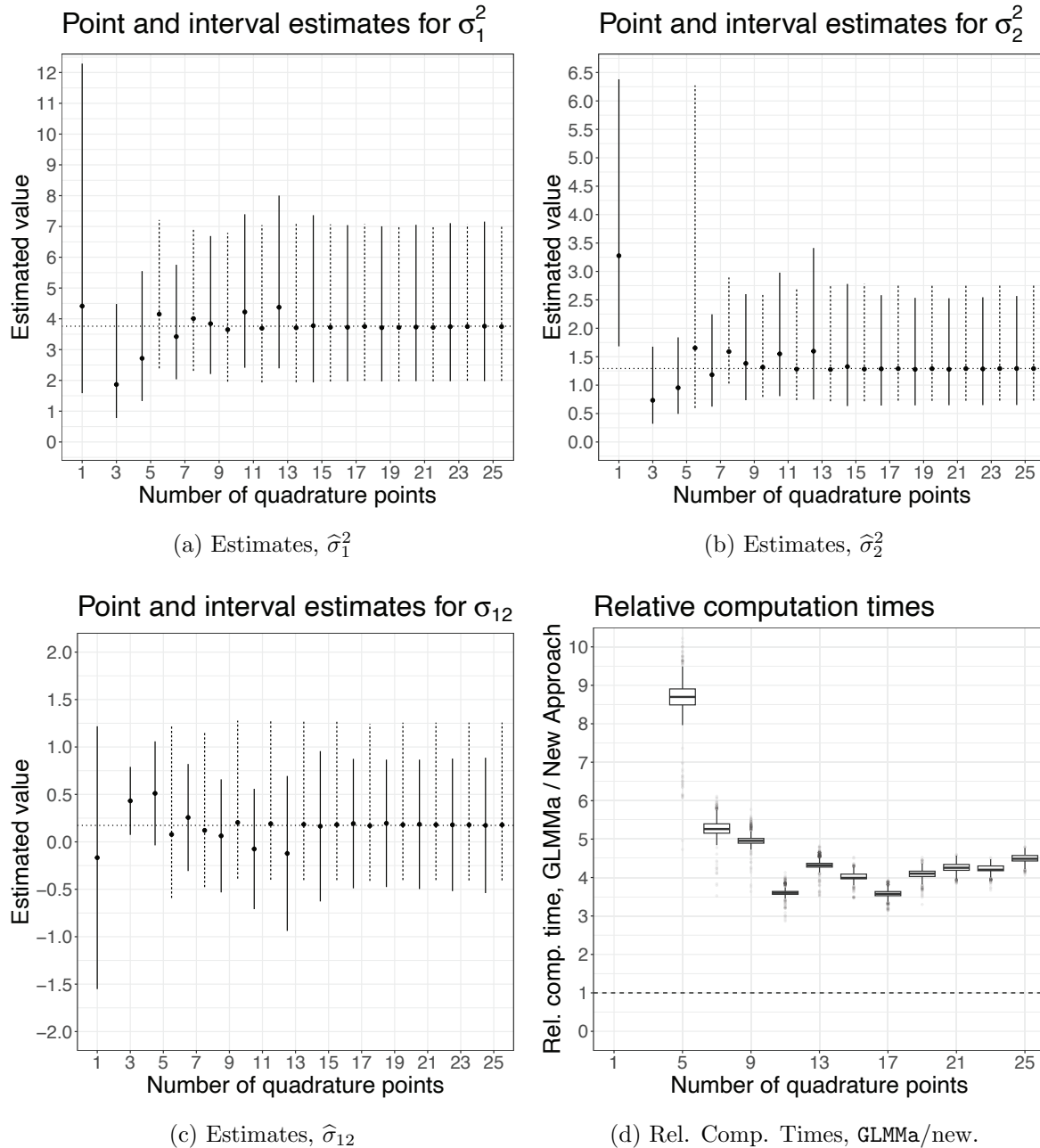


Figure 3: Results for the smoking cessation data of Section 5.1. (a) – (c): Parameter estimates for variance components from the new approach (—) and GLMMadaptive (---). In all cases, the estimates stop changing after some k for both methods. The new approach returns a non-singular Hessian for all k , while GLMMadaptive does so for $k > 3$. For σ_2^2 and σ_{12} , the intervals for large k are narrower for the new method than for GLMMadaptive, much so in the case of σ_{12} . (d): relative computation times for GLMMadaptive relative to the new approach, based on 500 repetitions of the fit. The new approach is between 2.5 and 10 times faster than GLMMadaptive for this problem, with some variability across values of k .

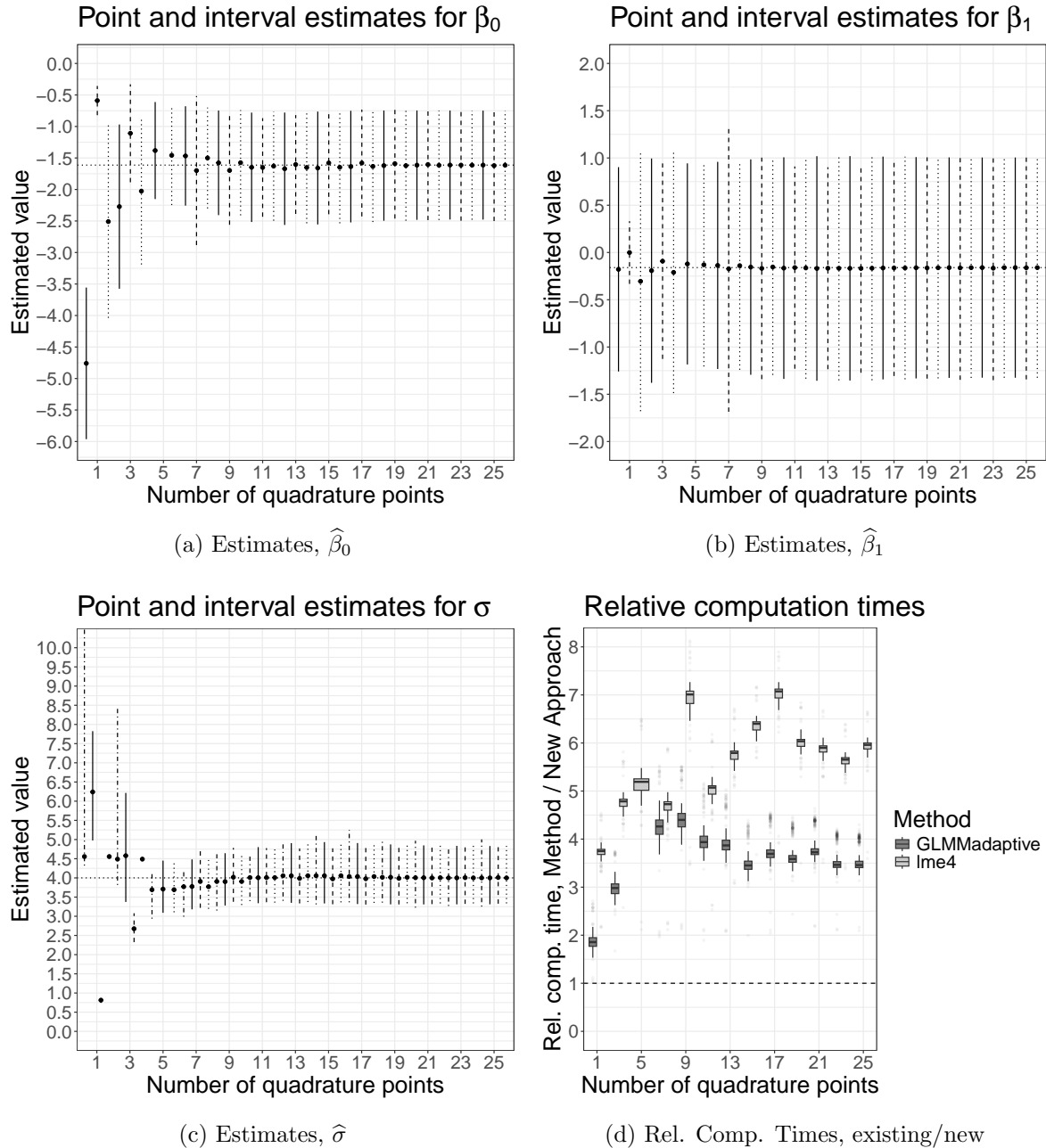


Figure 4: Results for the toenail infection treatment data of Section 5.2. (a) – (b): Parameter estimates for regression coefficients from the new approach (—), GLMMadaptive (---), and lme4 (···), with Wald confidence intervals. (c): Parameter estimates for the between-subject standard deviation, σ , from the new approach (—), GLMMadaptive (---), lme4 with profile likelihood (···), and lme4 with bootstrap intervals based on 200 fits (·—·). For large enough k , there is very little difference between the Wald intervals and the profile and bootstrap intervals for σ . (d): relative computation times for GLMMadaptive and lme4 (point estimation only) relative to the new approach, based on 500 repetitions of the fit. The new approach is 45 between 2.5 and 10 times faster than GLMMadaptive, and up to 7 times faster than lme4 for this problem, with some variability across values of k .

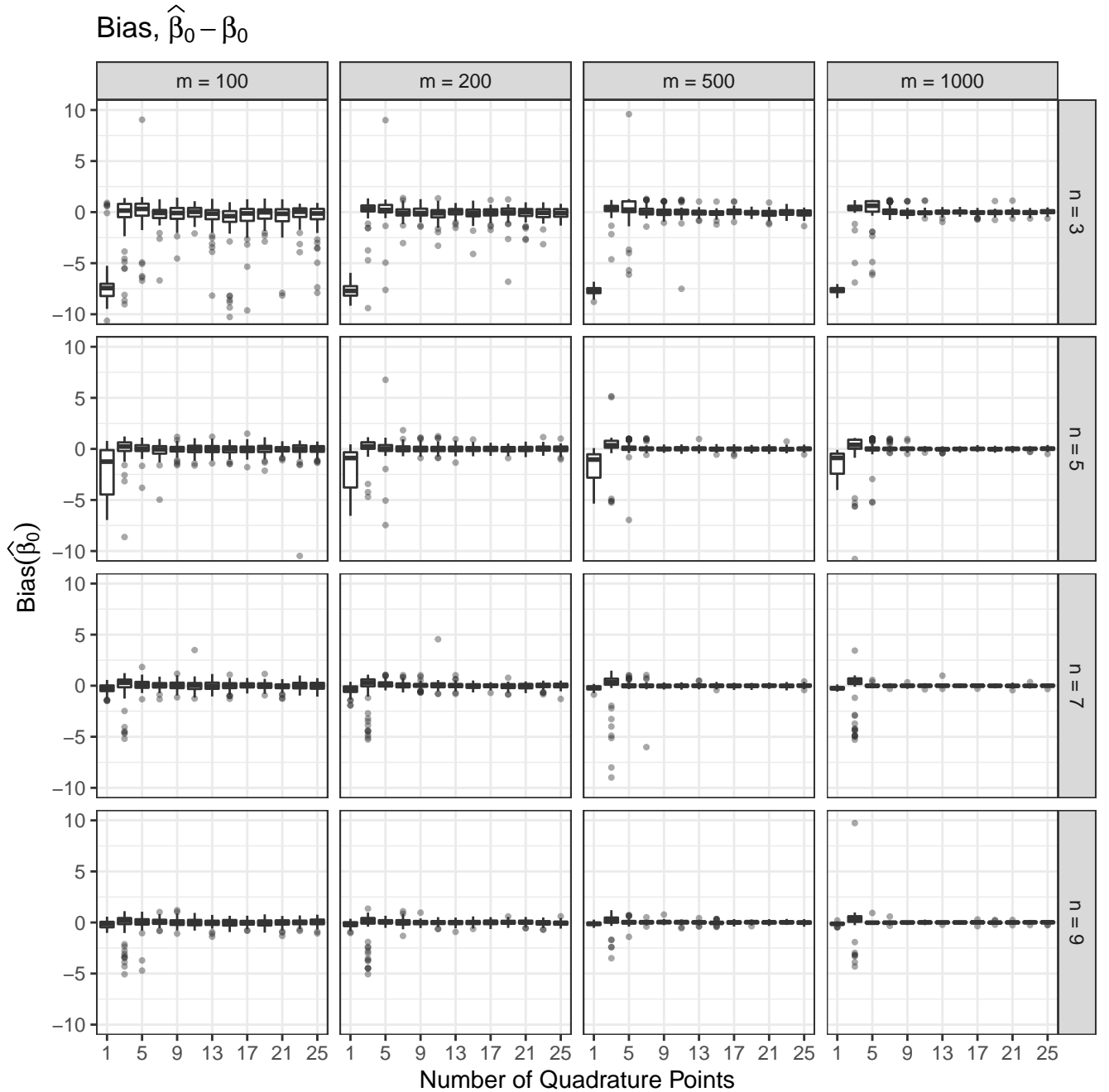


Figure 5: Empirical bias, $\hat{\beta}_0 - \beta_0$, for β_0 in the simulation study of Section 4.3 in the main manuscript, where 1000 sets of data were generated from the random-slopes model (14). The Laplace approximation ($k = 1$) exhibits high bias for lower $n = 3, 5$. Small numbers of quadrature points, $k < 5$ or so, appear to yield a higher number of outlying bias results. Higher numbers of quadrature points appear to give accurate integral approximations: even in the challenging case of $m = 1000$ and $n = 3$, the larger k results appear to have low bias. For $n = 3$ and lower m , the results are less stable, although this case would be expected to be challenging even if an exact likelihood could be used. 16

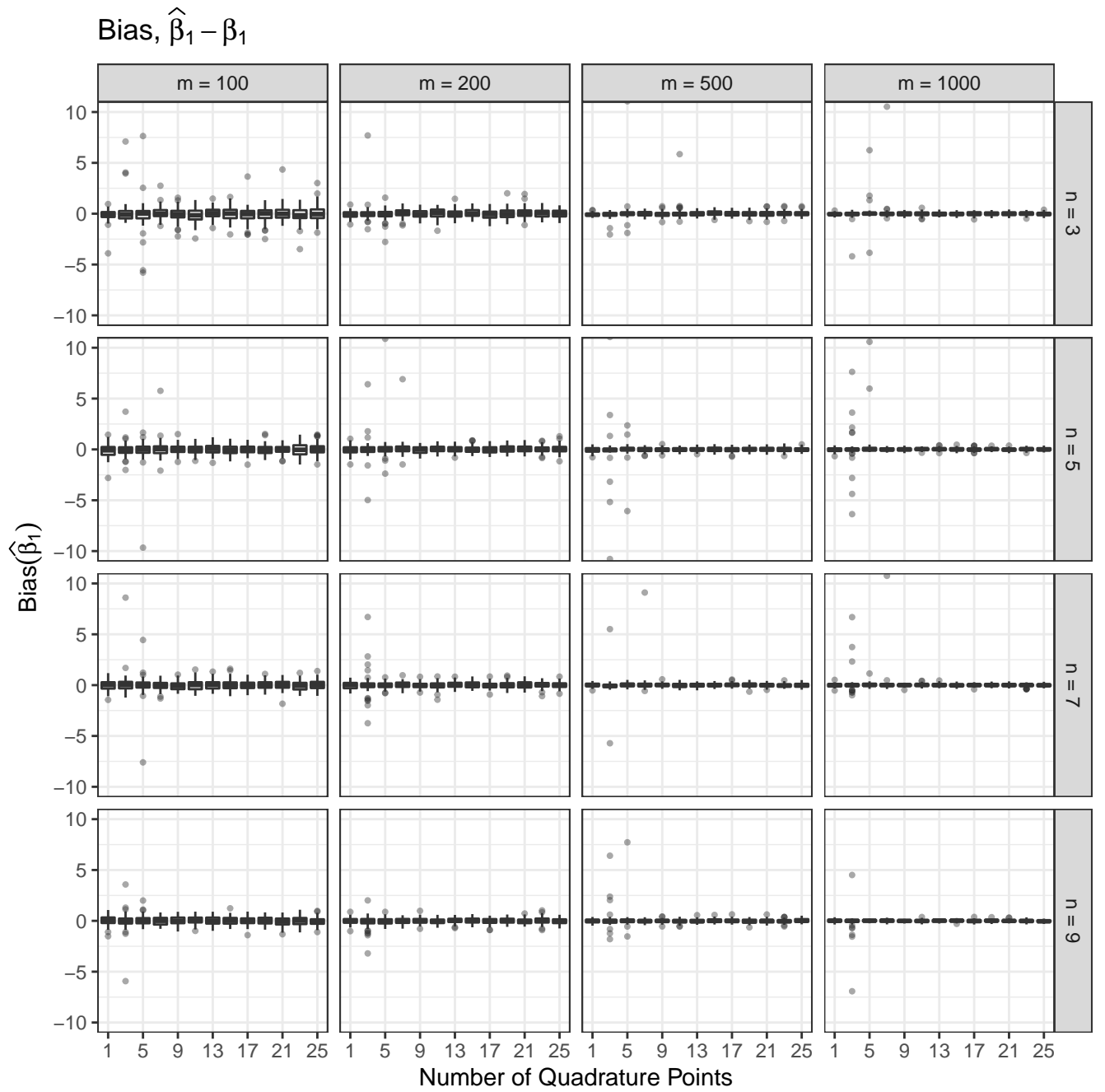


Figure 6: Empirical bias, $\hat{\beta}_1 - \beta_1$, for β_1 in the simulation study of Section 4.3 in the main manuscript, where 1000 sets of data were generated from the random-slopes model (14). All combinations of m, n, k appear to yield generally low bias, with a small number of outliers. Inference for β_1 is not expected to be very challenging in this model, and these results are not surprising.

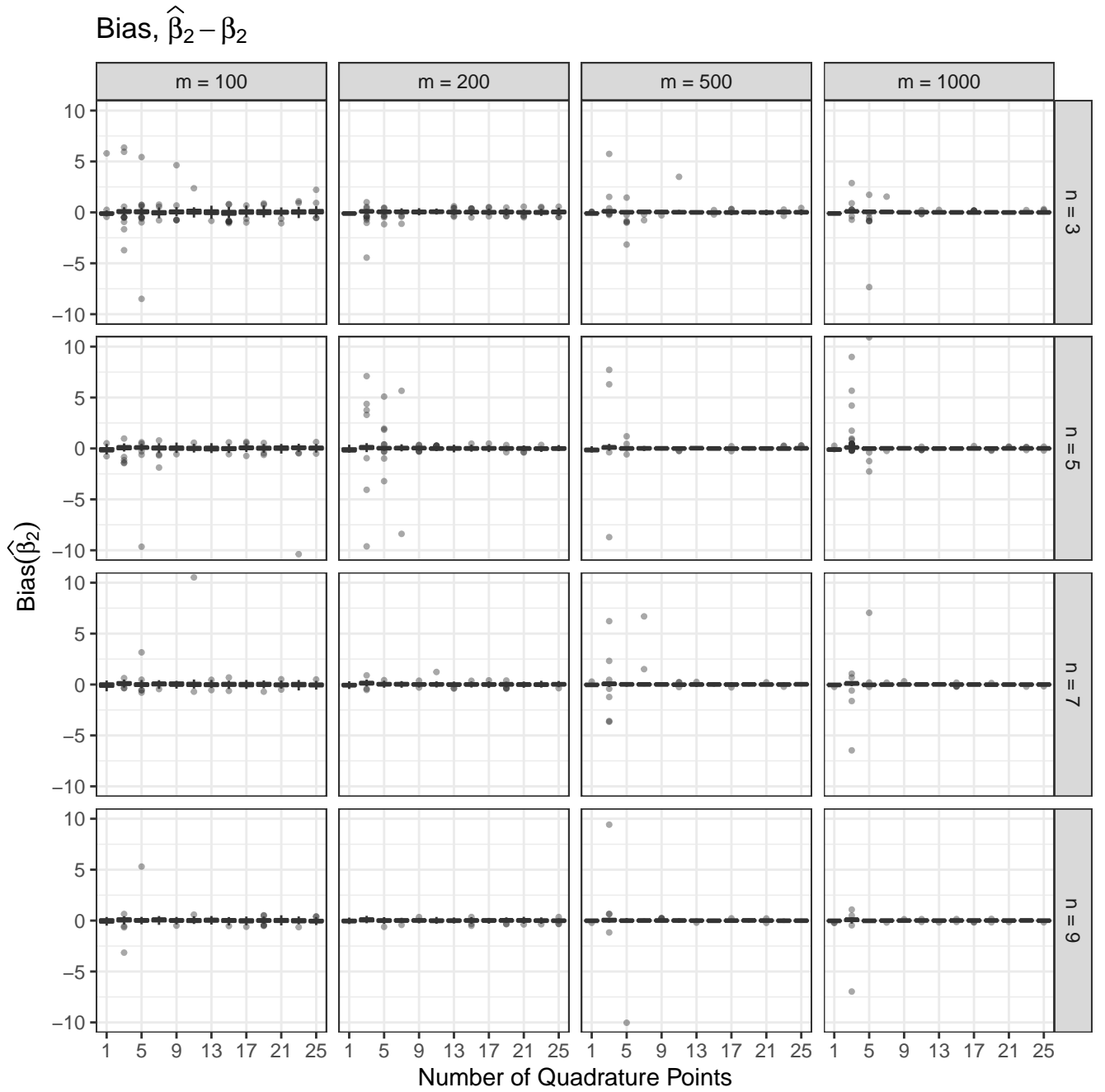


Figure 7: Empirical bias, $\hat{\beta}_2 - \beta_2$, for β_2 in the simulation study of Section 4.3 in the main manuscript, where 1000 sets of data were generated from the random-slopes model (14). All combinations of m, n, k appear to yield generally low bias, with a small number of outliers. Inference for β_2 is not expected to be very challenging in this model, and these results are not surprising.

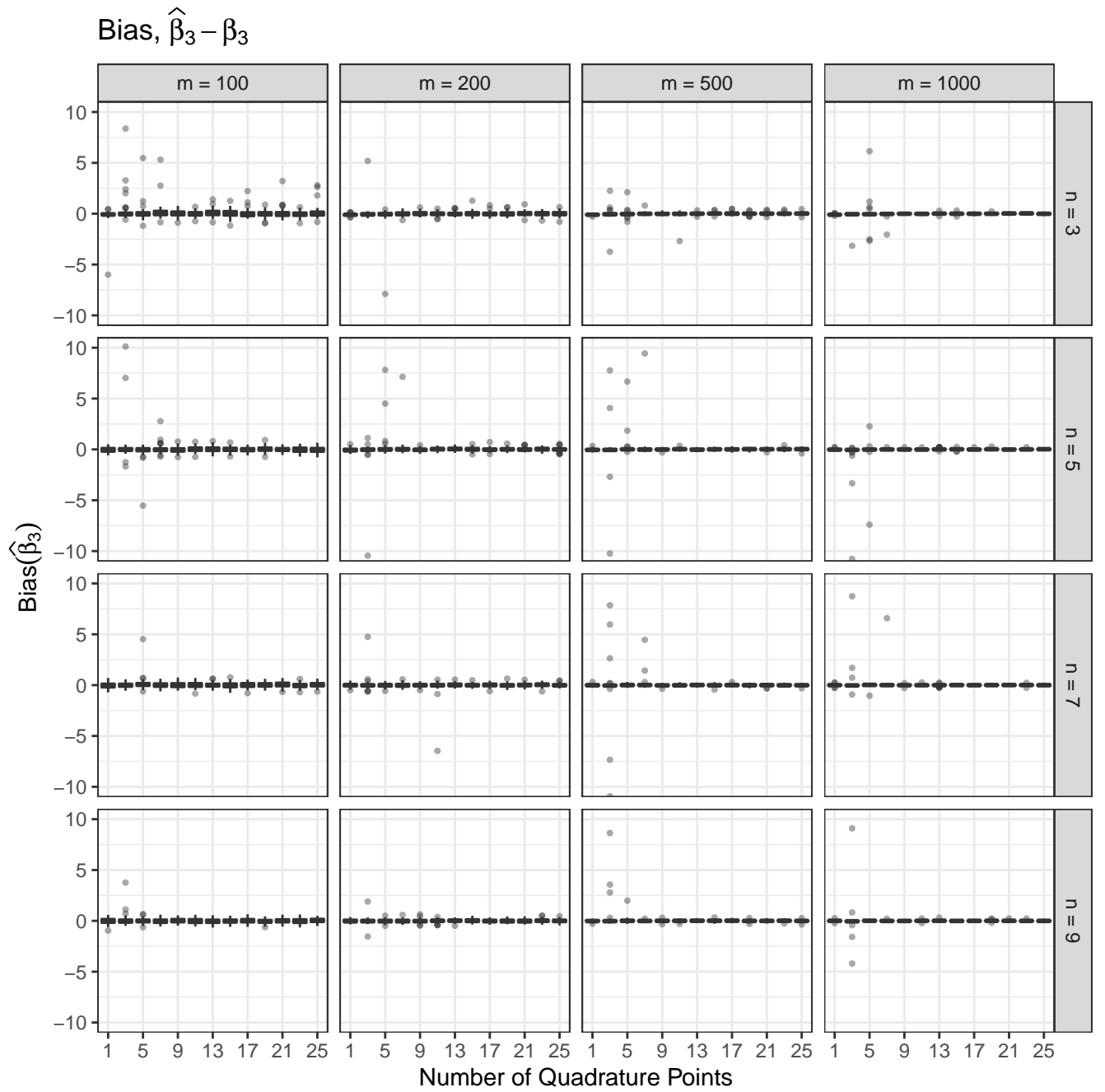


Figure 8: Empirical bias, $\hat{\beta}_3 - \beta_3$, for β_3 in the simulation study of Section 4.3 in the main manuscript, where 1000 sets of data were generated from the random-slopes model (14). All combinations of m, n, k appear to yield generally low bias, with a small number of outliers. Inference for β_3 is not expected to be very challenging in this model, and these results are not surprising.

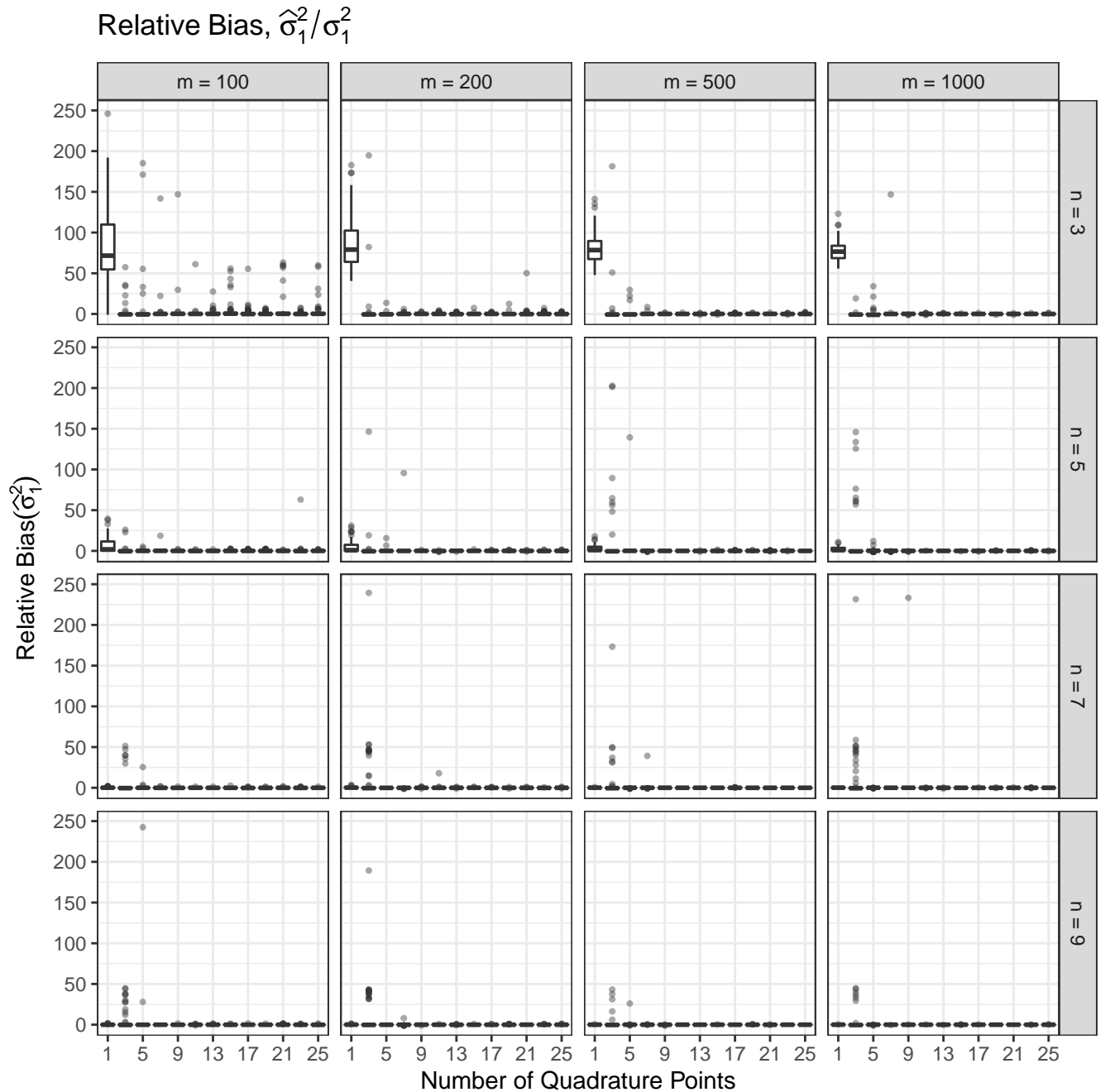


Figure 9: Empirical relative bias, $\hat{\sigma}_1^2/\sigma_1^2$, for σ_1^2 in the simulation study of Section 4.3 in the main manuscript, where 1000 sets of data were generated from the random-slopes model (14). The y-axis range is very large so that the scale of the relative bias for the Laplace approximation with low n is visible. A larger k leads to greatly reduced bias across values of m and n .

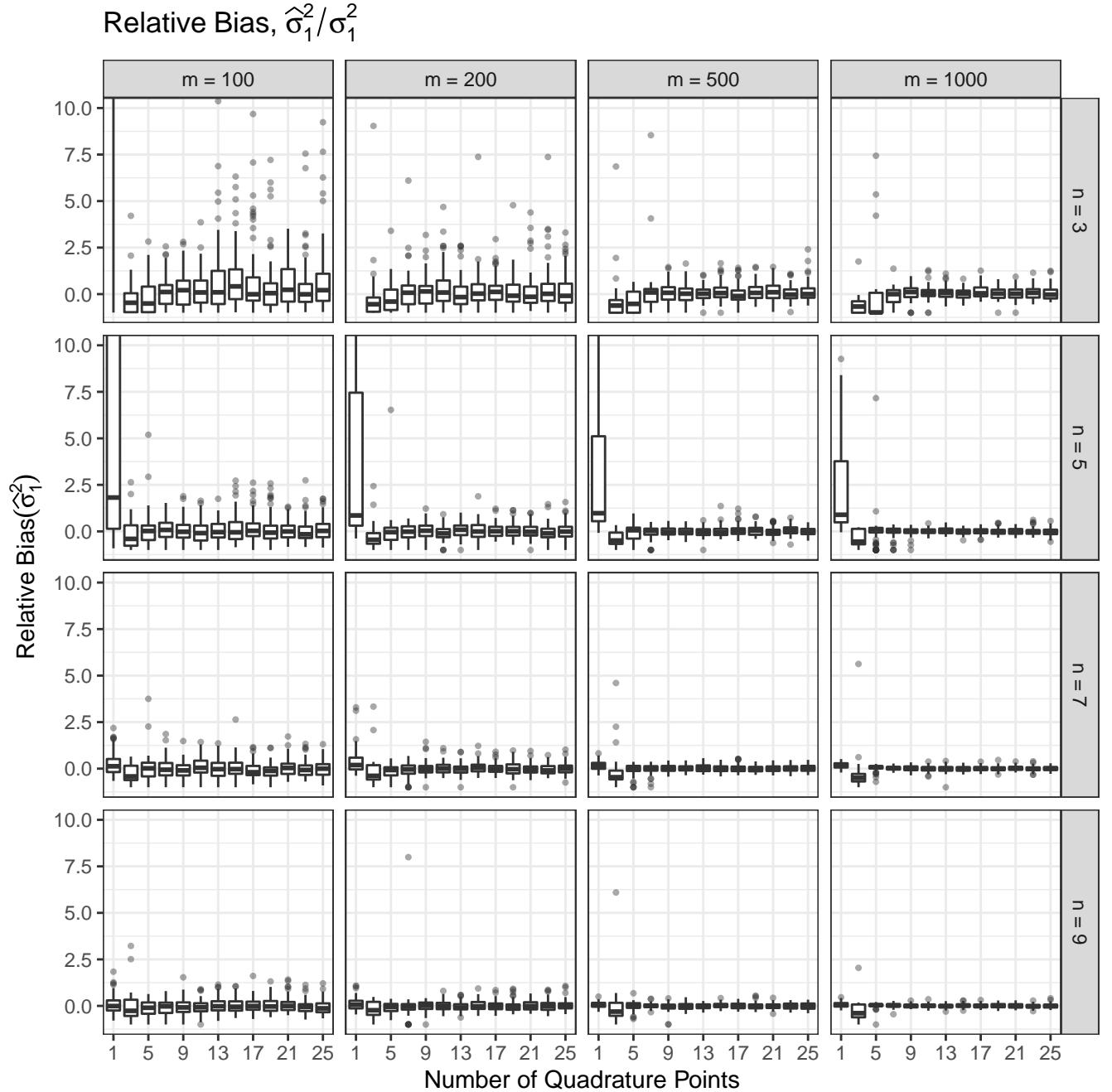


Figure 10: Empirical relative bias, $\hat{\sigma}_1^2 / \sigma_1^2$, for σ_1^2 in the simulation study of Section 4.3 in the main manuscript, where 1000 sets of data were generated from the random-slopes model (14). The y-axis range is zoomed in so that the pattern in bias across all m, n, k is visible, except for the massive biases incurred with $n = 3$ and $k = 1$. For all n , $k = 1$ exhibits positive bias and $k = 3$ exhibits negative bias, on average, with larger n diminishing this effect. However, larger k yields small bias for estimating σ_1^2 for all values of m, n , even large m with small n , where the likelihood should be the most difficult to approximate accurately. The true value, $\sigma_1^2 = 2$ on the logit scale, sgn can be regarded as very large and difficult to estimate accurately.

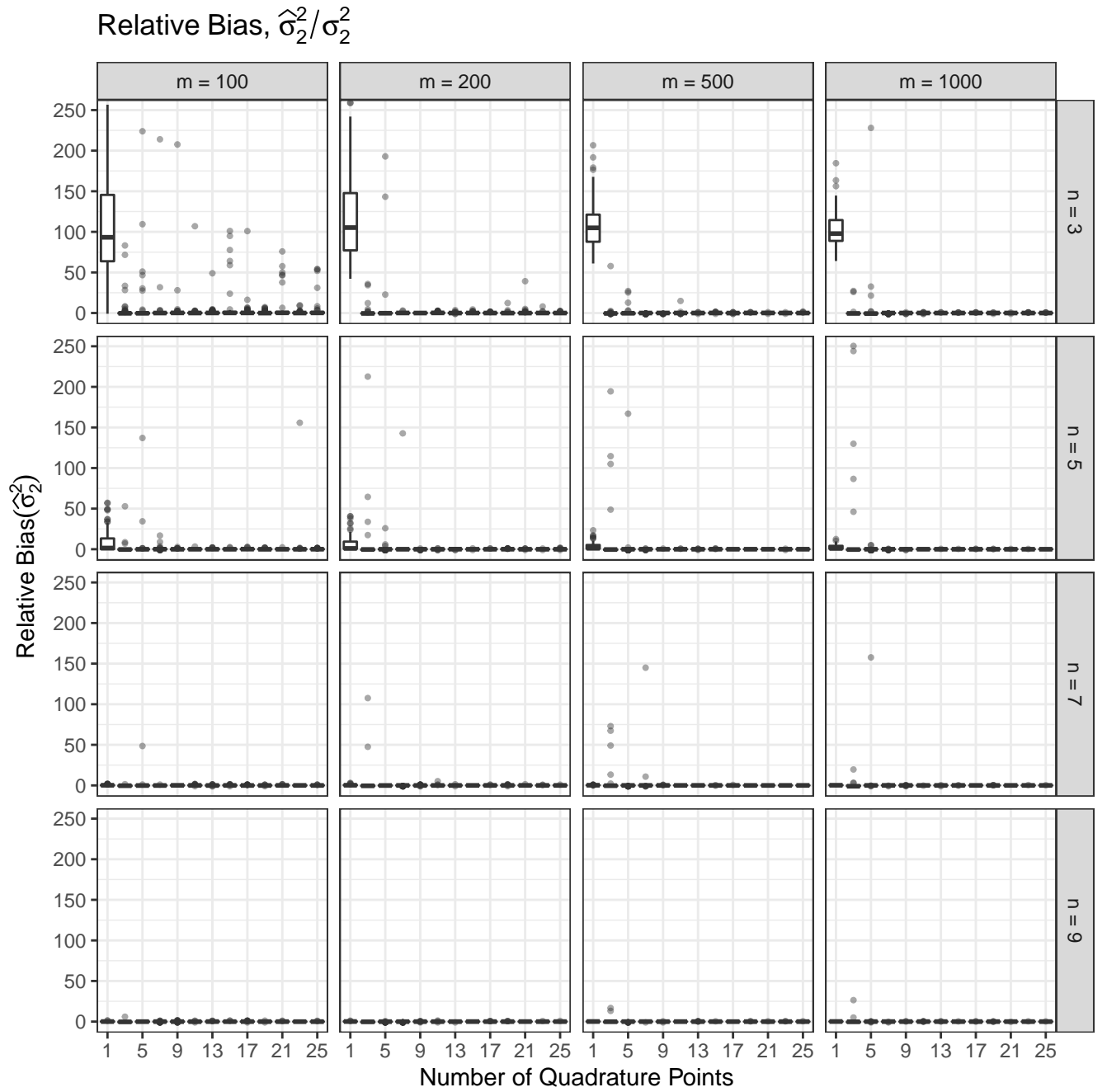


Figure 11: Empirical relative bias, $\hat{\sigma}_2^2/\sigma_2^2$, for σ_2^2 in the simulation study of Section 4.3 in the main manuscript, where 1000 sets of data were generated from the random-slopes model (14). The y-axis range is very large so that the scale of the relative bias for the Laplace approximation with low n is visible. A larger k leads to greatly reduced bias across values of m and n .

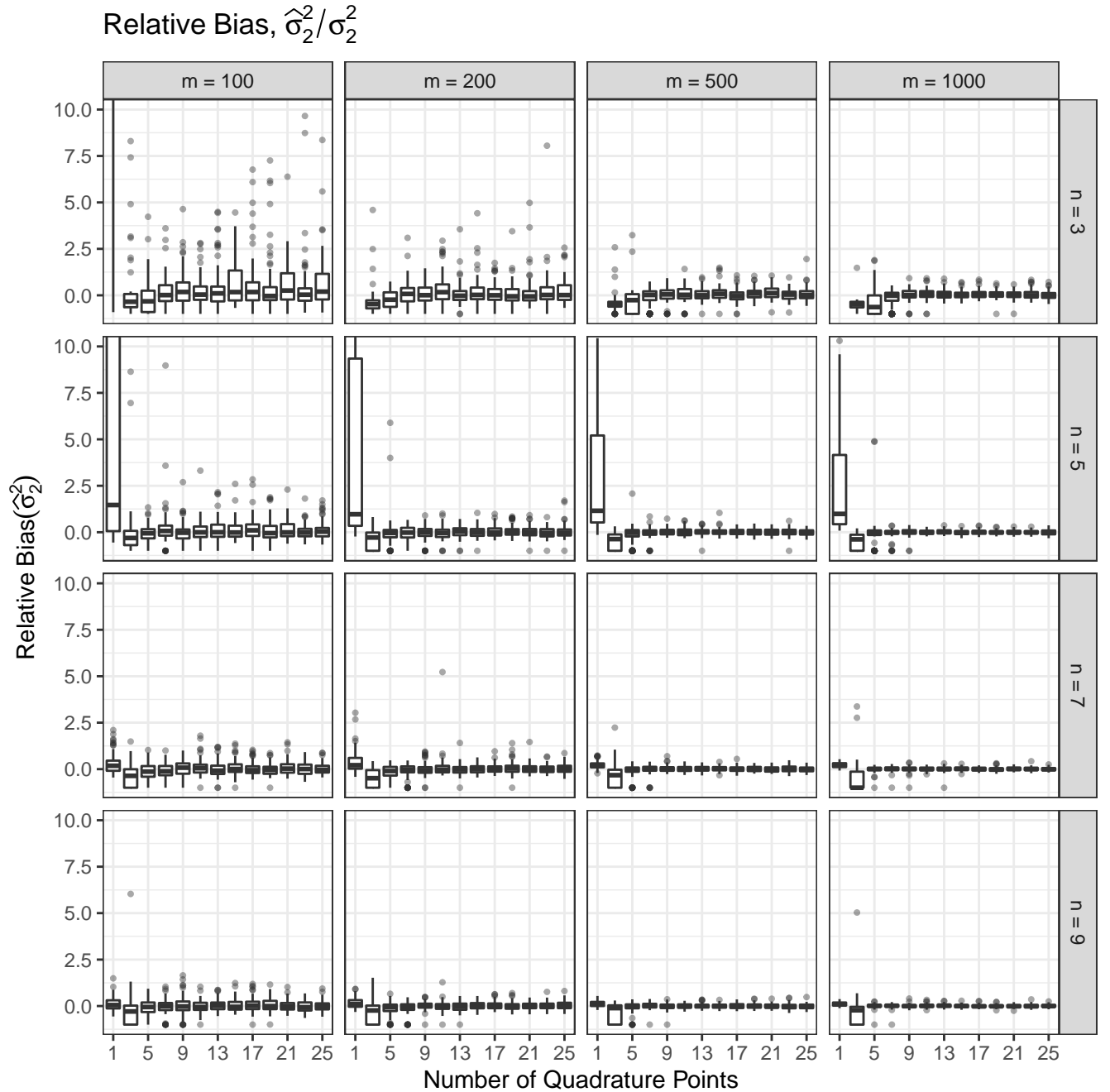


Figure 12: Empirical relative bias, $\hat{\sigma}_2^2 / \sigma_2^2$, for σ_2^2 in the simulation study of Section 4.3 in the main manuscript, where 1000 sets of data were generated from the random-slopes model (14). The y-axis range is zoomed in so that the pattern in bias across all m, n, k is visible, except for the massive biases incurred with $n = 3$ and $k = 1$. For all n , $k = 1$ exhibits positive bias and $k = 3$ exhibits negative bias, on average, with larger n diminishing this effect. However, larger k yields small bias for estimating σ_2^2 for all values of m, n , even large m with small n , where the likelihood should be the most difficult to approximate accurately.

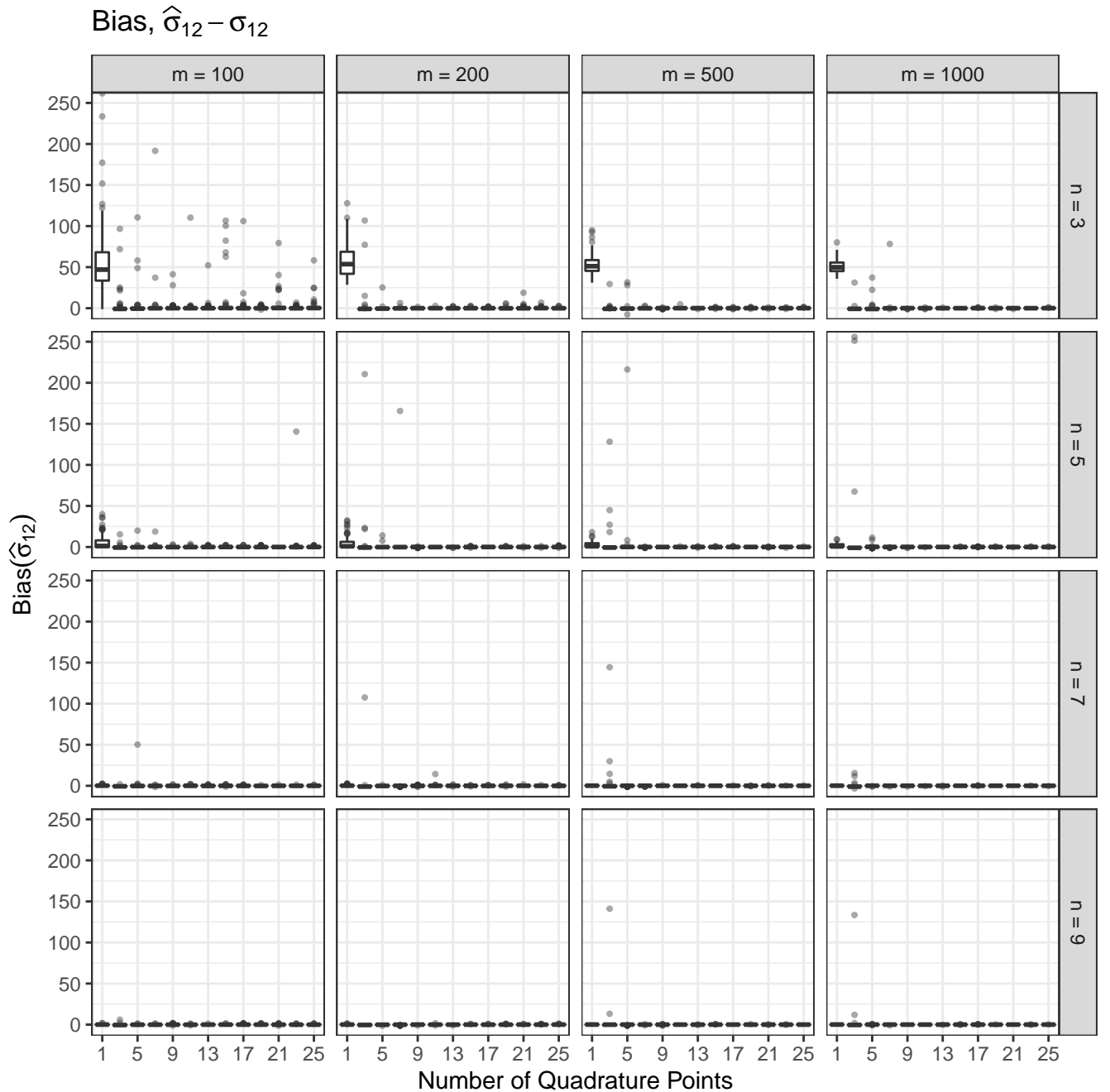


Figure 13: Empirical bias, $\hat{\sigma}_{12} - \sigma_{12}$, for σ_{12} in the simulation study of Section 4.3 in the main manuscript, where 1000 sets of data were generated from the random-slopes model (14). The y-axis range is very large so that the scale of the relative bias for the Laplace approximation with low n is visible. A larger k leads to greatly reduced bias across values of m and n .

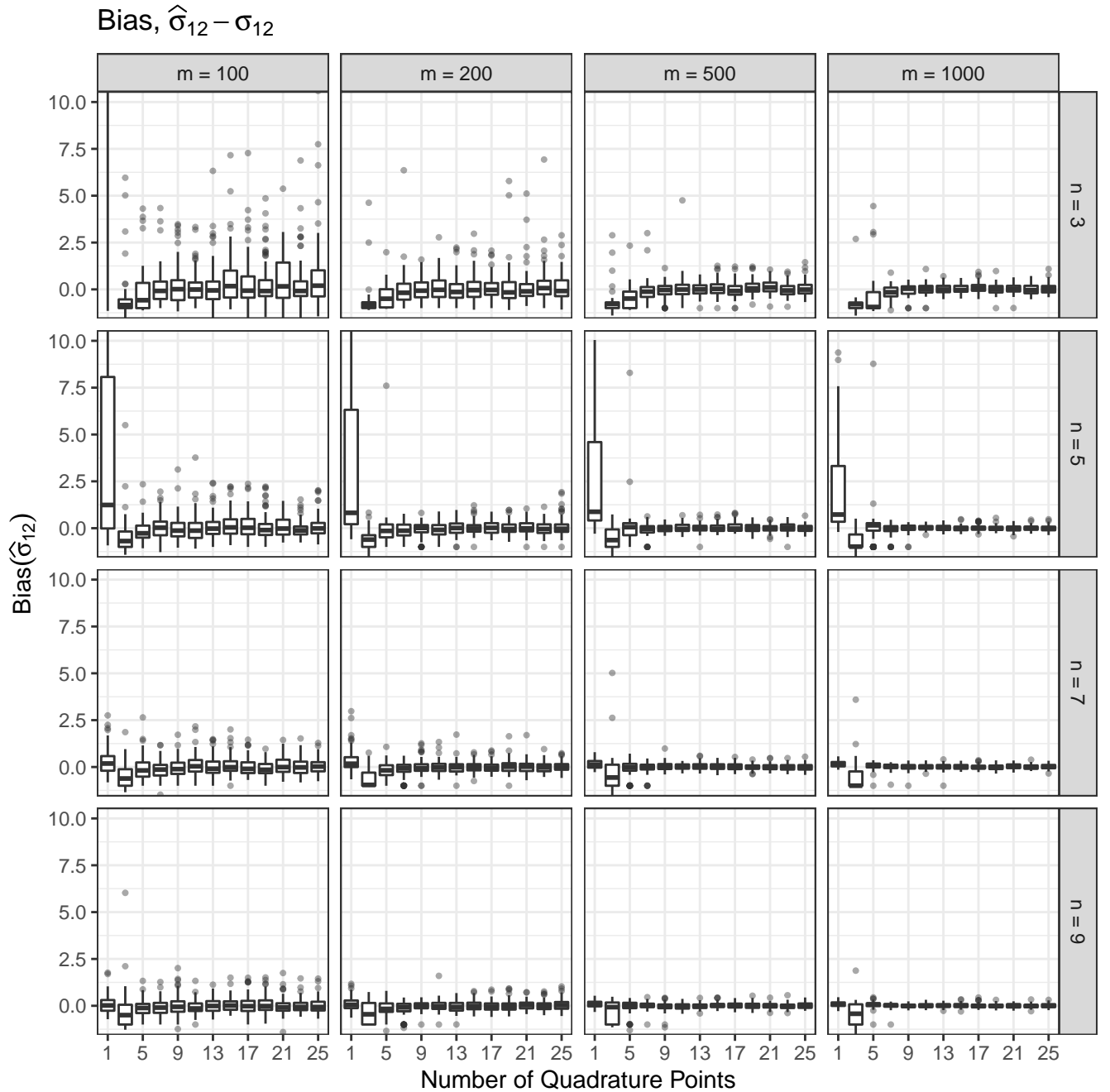


Figure 14: Empirical bias, $\hat{\sigma}_{12} - \sigma_{12}$, for σ_{12} in the simulation study of Section 4.3 in the main manuscript, where 1000 sets of data were generated from the random-slopes model (14). The y-axis range is zoomed in so that the pattern in bias across all m, n, k is visible, except for the massive biases incurred with $n = 3$ and $k = 1$. For all n , $k = 1$ exhibits positive bias and $k = 3$ exhibits negative bias, on average, with larger n diminishing this effect. However, larger k yields small bias for estimating σ_2^2 for all values of m, n , even large m with small n , where the likelihood should be the most difficult to approximate accurately.

Empirical Coverage, β_0

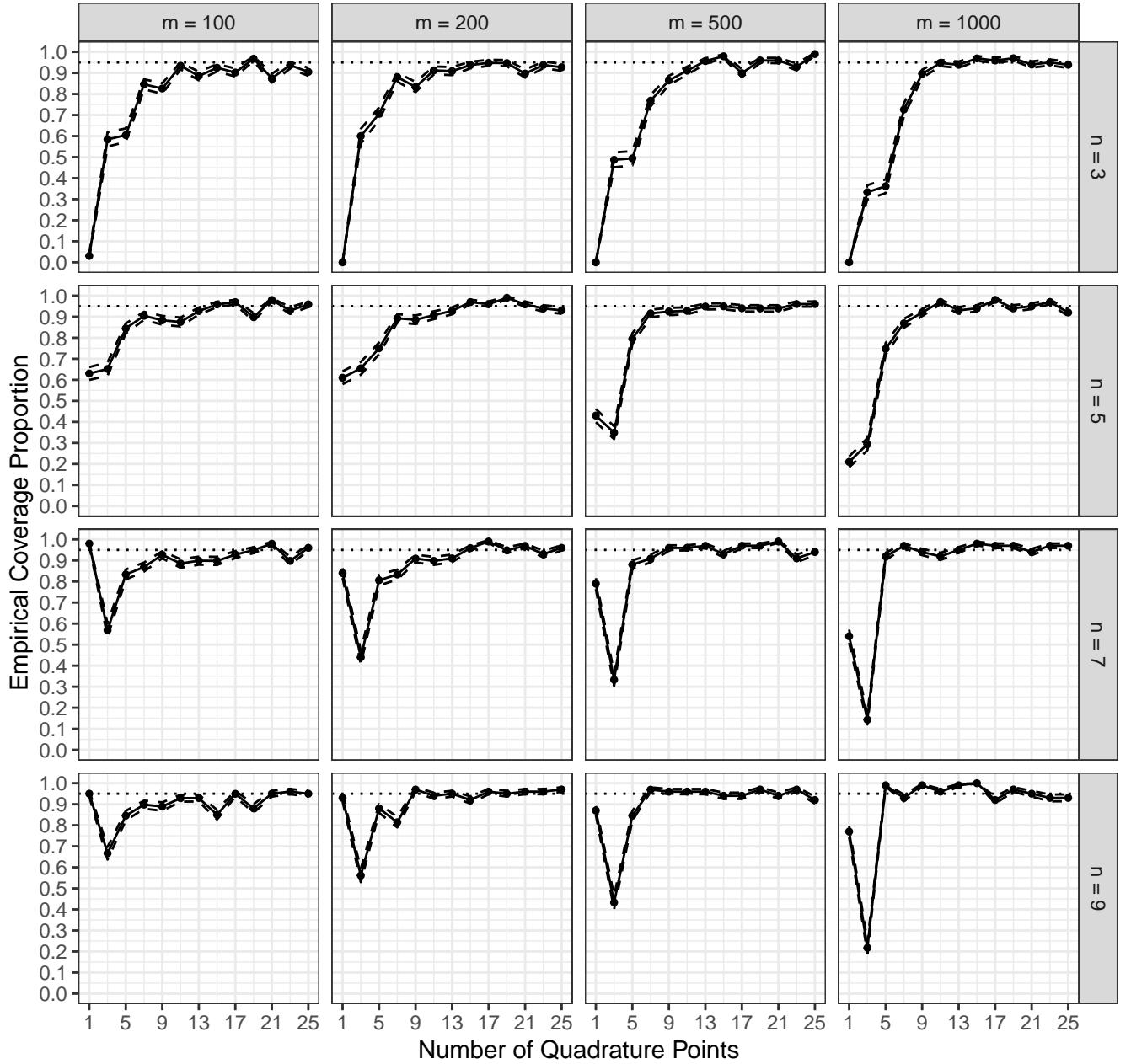


Figure 15: Empirical coverage proportion for $\hat{\beta}_0$ in the simulation study of Section 4.3 in the main manuscript, where 1000 sets of data were generated from the random-slopes model (14). The Laplace ($k = 1$) coverage is low for $n = 3, 5$ due to high bias and poor standard error estimation. Although the coverage appears nominal for $n \geq 7$, the intervals are also much wider than those for higher k (Figure 22). The $k = 3$ coverages are low due to strong negative bias. In all cases, taking k large enough leads to nominal empirical coverage, motivating the use of adaptive quadrature for fitting these models.

Empirical Coverage, β_1

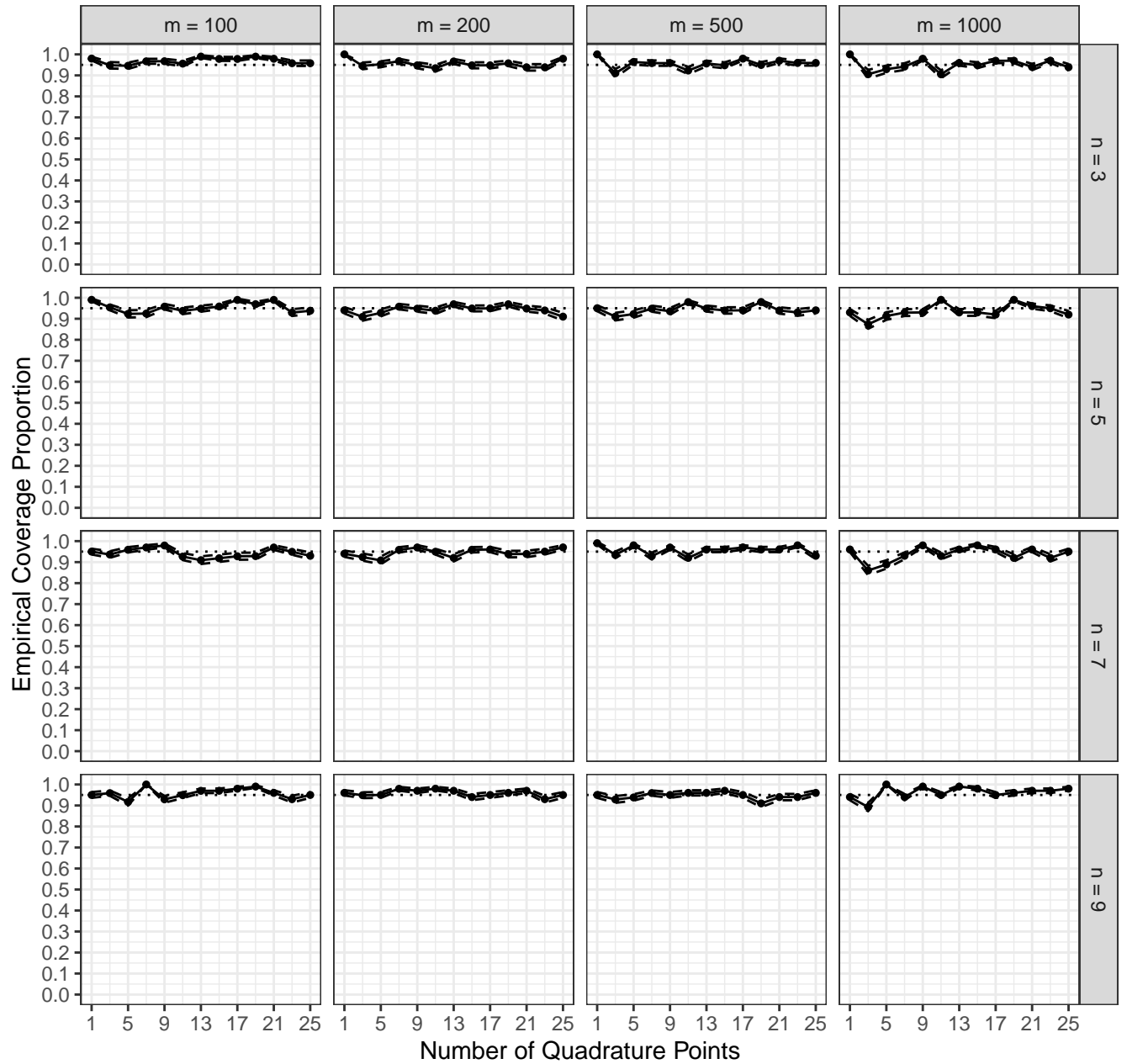


Figure 16: Empirical coverage proportion for $\hat{\beta}_1$ in the simulation study of Section 4.3 in the main manuscript, where 1000 sets of data were generated from the random-slopes model (14). The coverage is nominal across all values of m, n, k , which is expected for this parameter in this model.

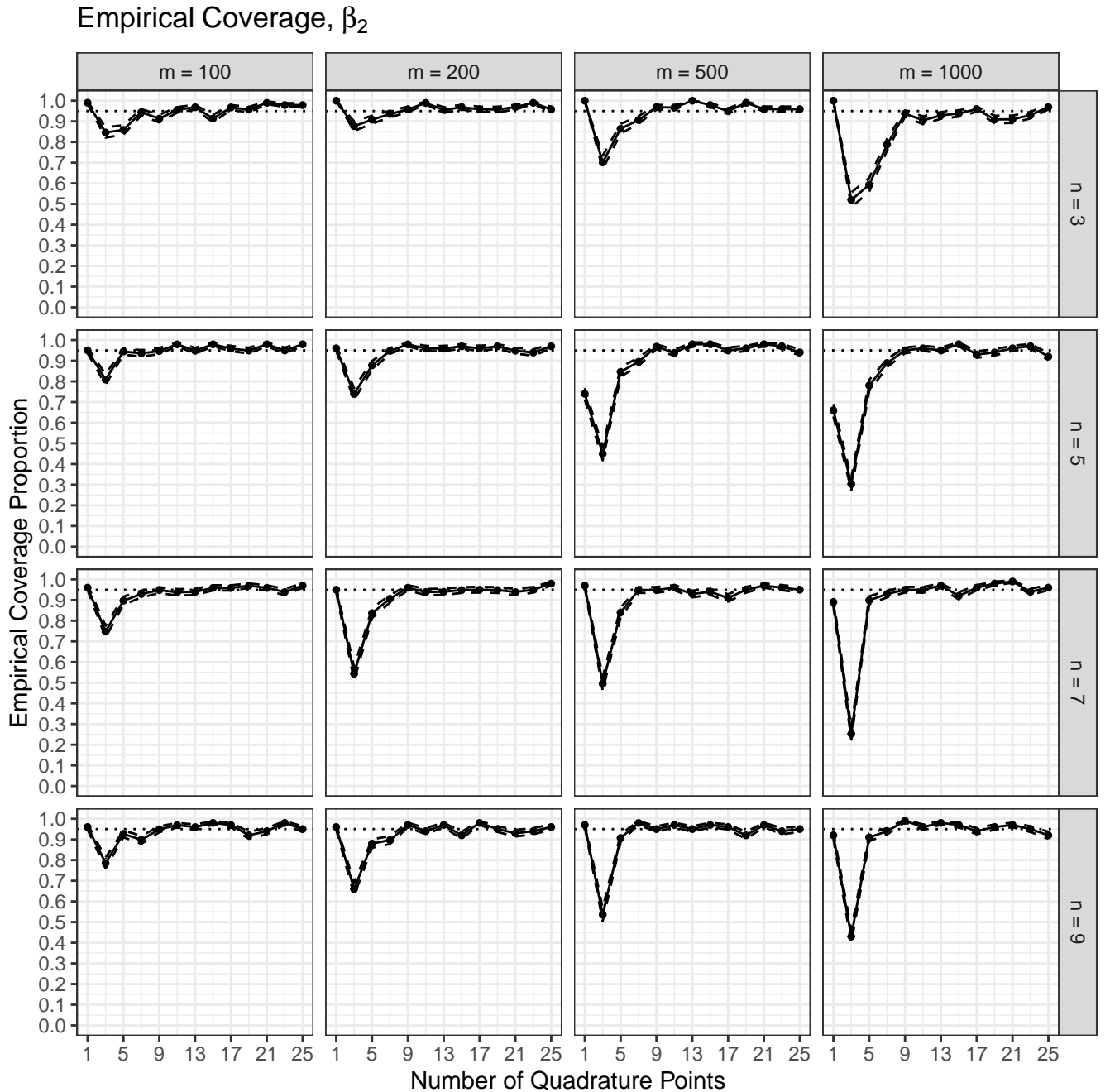


Figure 17: Empirical coverage proportion for $\hat{\beta}_2$ in the simulation study of Section 4.3 in the main manuscript, where 1000 sets of data were generated from the random-slopes model (14). The coverages are nominal except for $k = 3, 5$ for certain m, n . Examining the lengths of the intervals (Figure 24) shows that this is due to under-estimation of standard error; increasing k mitigates this and yields nominal coverage for all m, n .

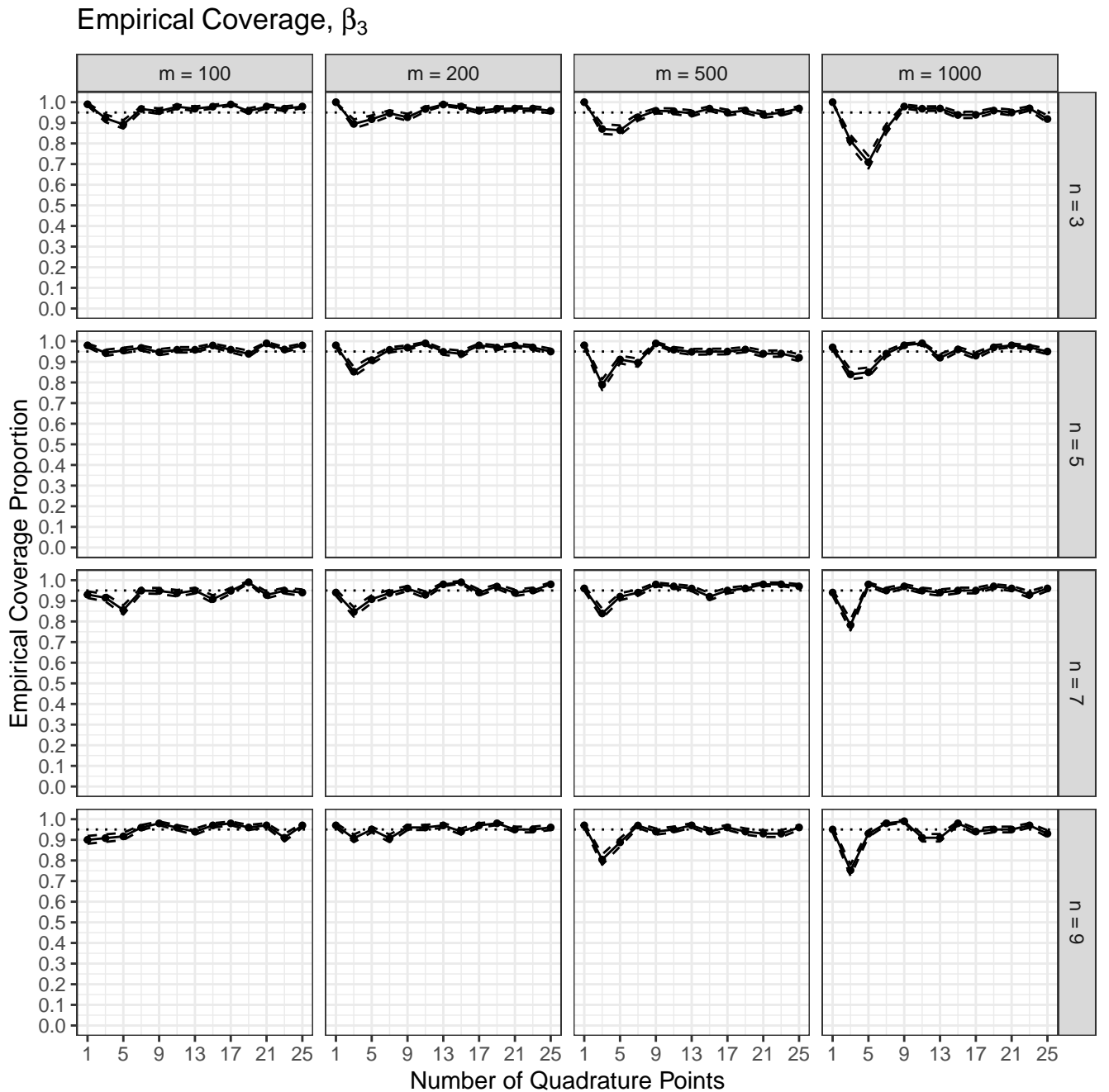


Figure 18: Empirical coverage proportion for $\hat{\beta}_3$ in the simulation study of Section 4.3 in the main manuscript, where 1000 sets of data were generated from the random-slopes model (14). The coverages are nominal except for $k = 3, 5$ for certain m, n . Examining the lengths of the intervals (Figure 25) shows that this is due to under-estimation of standard error; increasing k mitigates this and yields nominal coverage for all m, n .

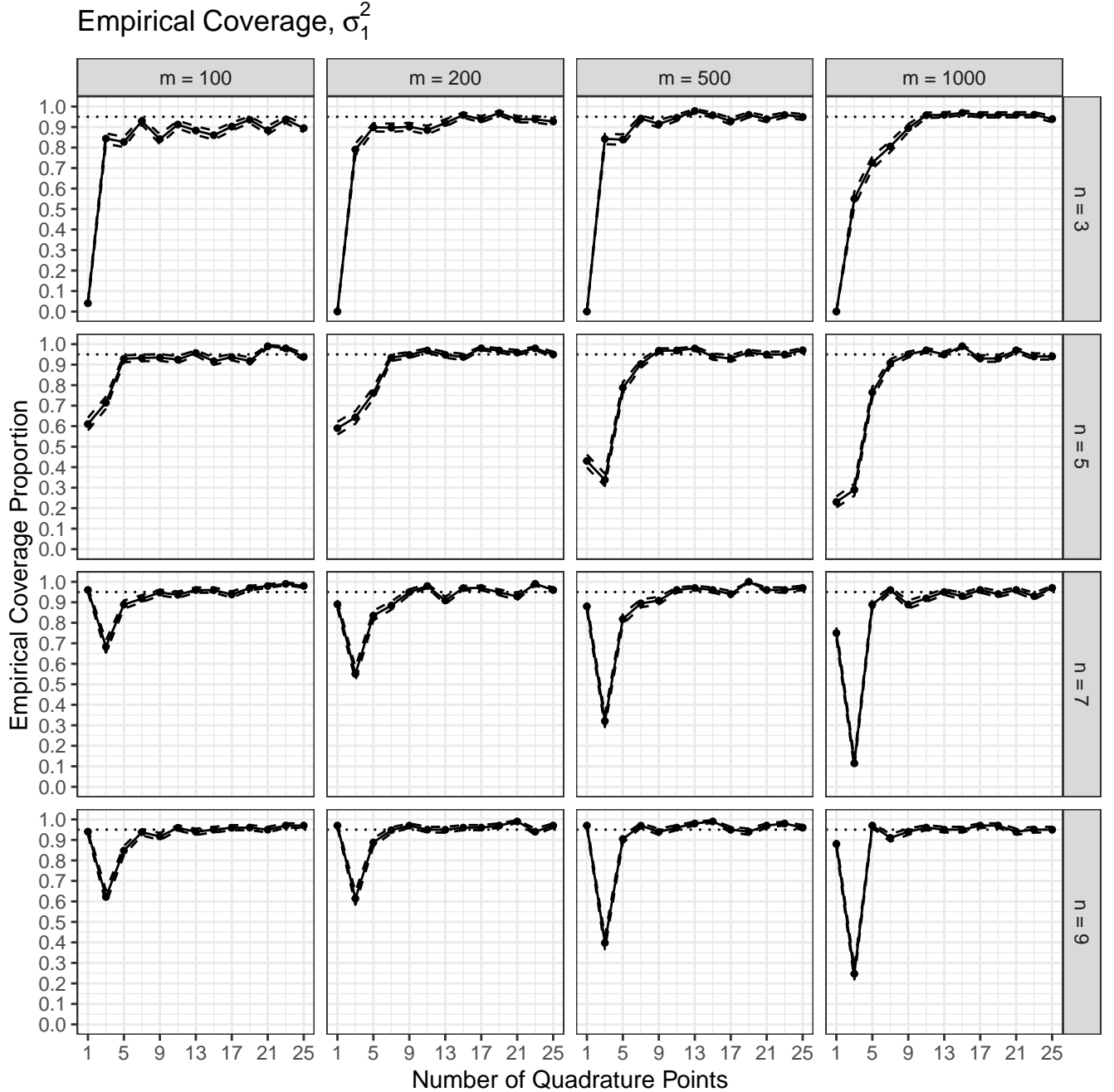


Figure 19: Empirical coverage proportion for $\widehat{\sigma}_1^2$ in the simulation study of Section 4.3 in the main manuscript, where 1000 sets of data were generated from the random-slopes model (14). The Laplace ($k = 1$) coverage is low for $n = 3, 5$ due to high bias and poor standard error estimation. Although the coverage appears nominal for $n \geq 7$, the intervals are also much wider than those for higher k (Figure 26). The $k = 3$ coverages are low due to strong negative bias. In all cases, taking k large enough leads to nominal empirical coverage, motivating the use of adaptive quadrature for fitting these models.

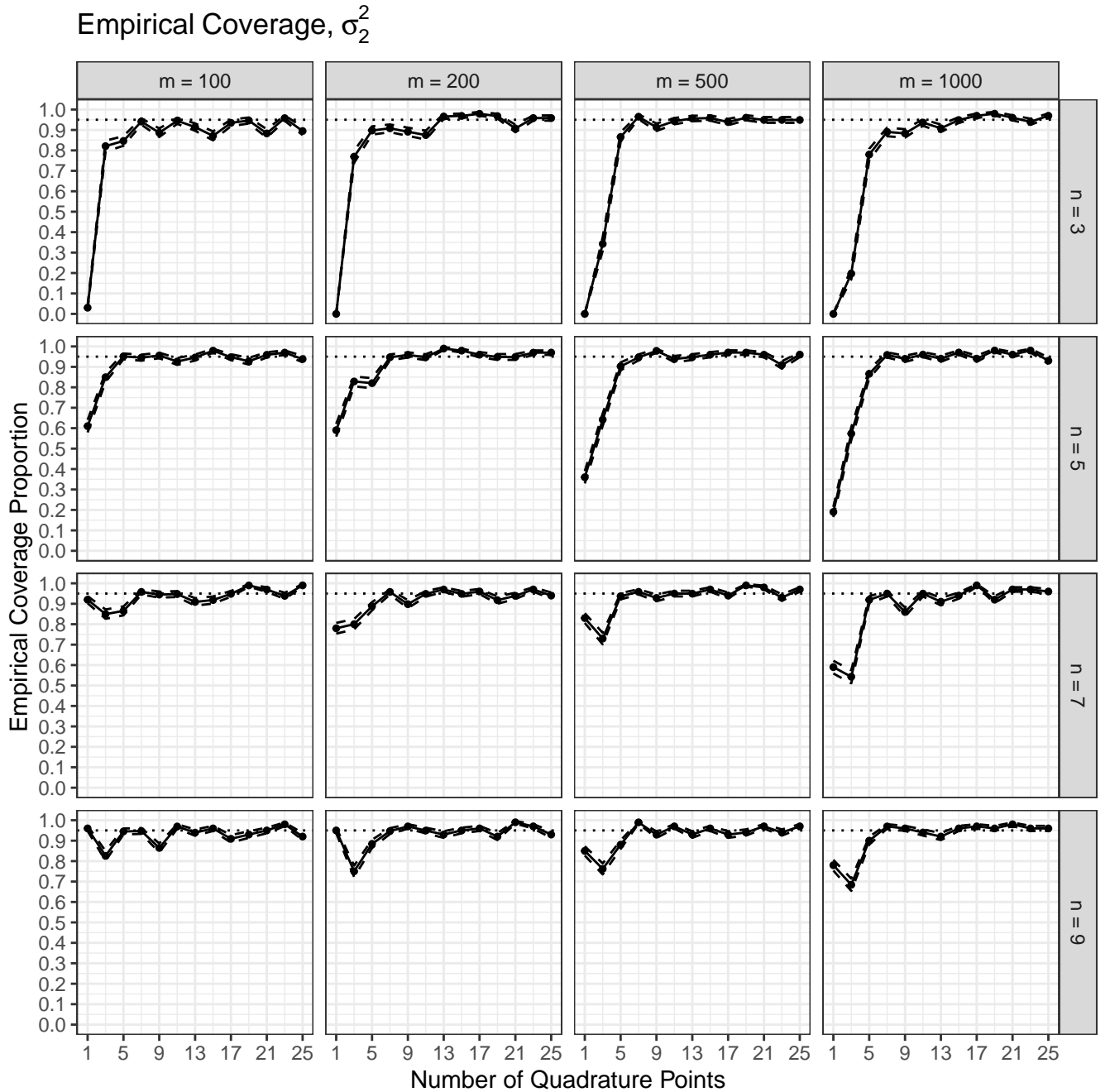


Figure 20: Empirical coverage proportion for $\widehat{\sigma}_2^2$ in the simulation study of Section 4.3 in the main manuscript, where 1000 sets of data were generated from the random-slopes model (14). The Laplace ($k = 1$) coverage is low for $n = 3, 5$ due to high bias and poor standard error estimation. Although the coverage appears nominal for $n \geq 7$, the intervals are also much wider than those for higher k (Figure 28). The $k = 3$ coverages are low due to strong negative bias. In all cases, taking k large enough leads to nominal empirical coverage, motivating the use of adaptive quadrature for fitting these models.

Empirical Coverage, σ_{12}

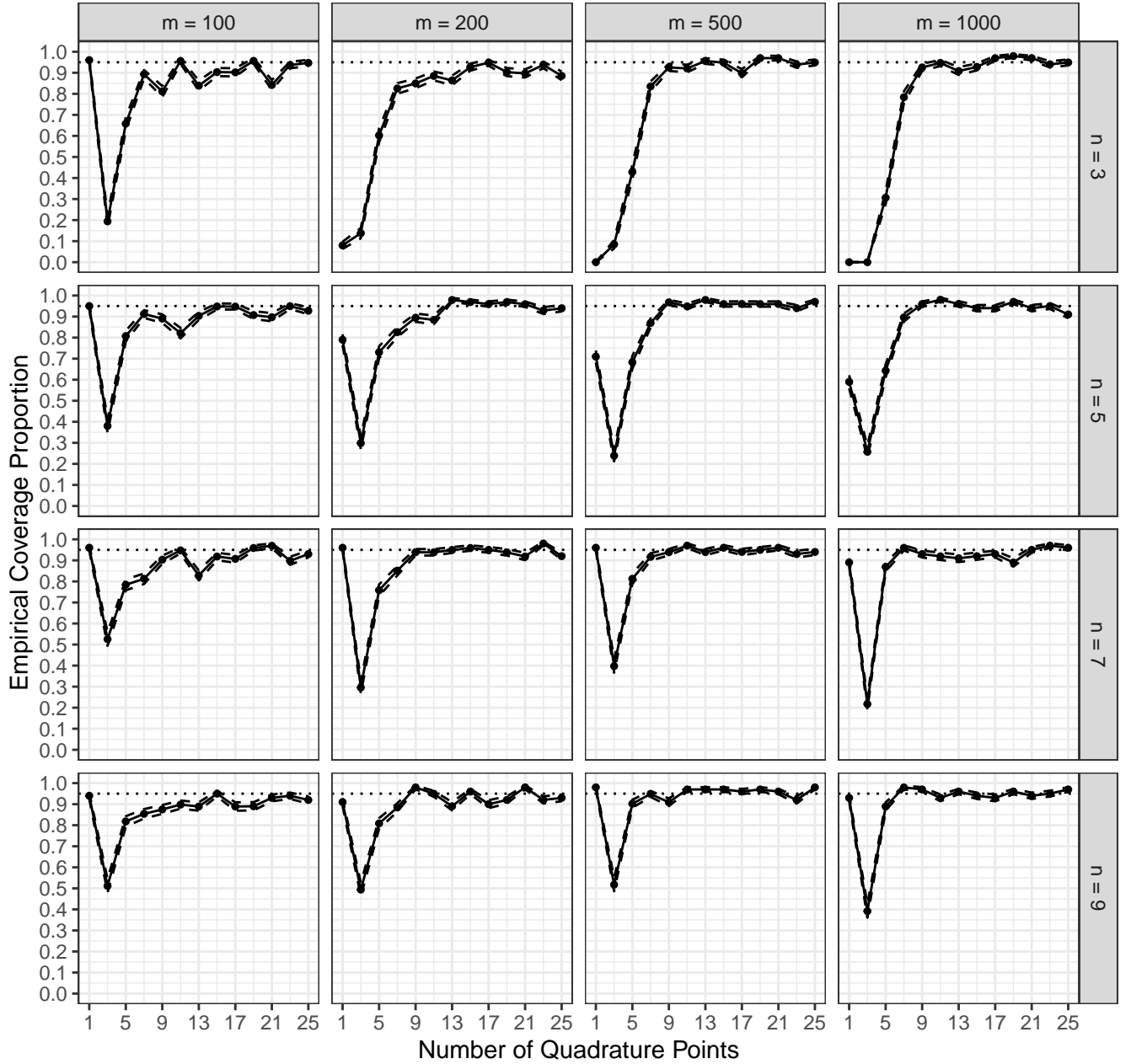


Figure 21: Empirical coverage proportion for $\widehat{\sigma}_{12}$ in the simulation study of Section 4.3 in the main manuscript, where 1000 sets of data were generated from the random-slopes model (14). The Laplace ($k = 1$) coverage is low for $n = 3, 5$ due to high bias and poor standard error estimation. Although the coverage appears nominal for $n \geq 7$, the intervals are also much wider than those for higher k (Figure 30). The $k = 3$ coverages are low due to strong negative bias. In all cases, taking k large enough leads to nominal empirical coverage, motivating the use of adaptive quadrature for fitting these models.

Length of Confidence Intervals, β_0

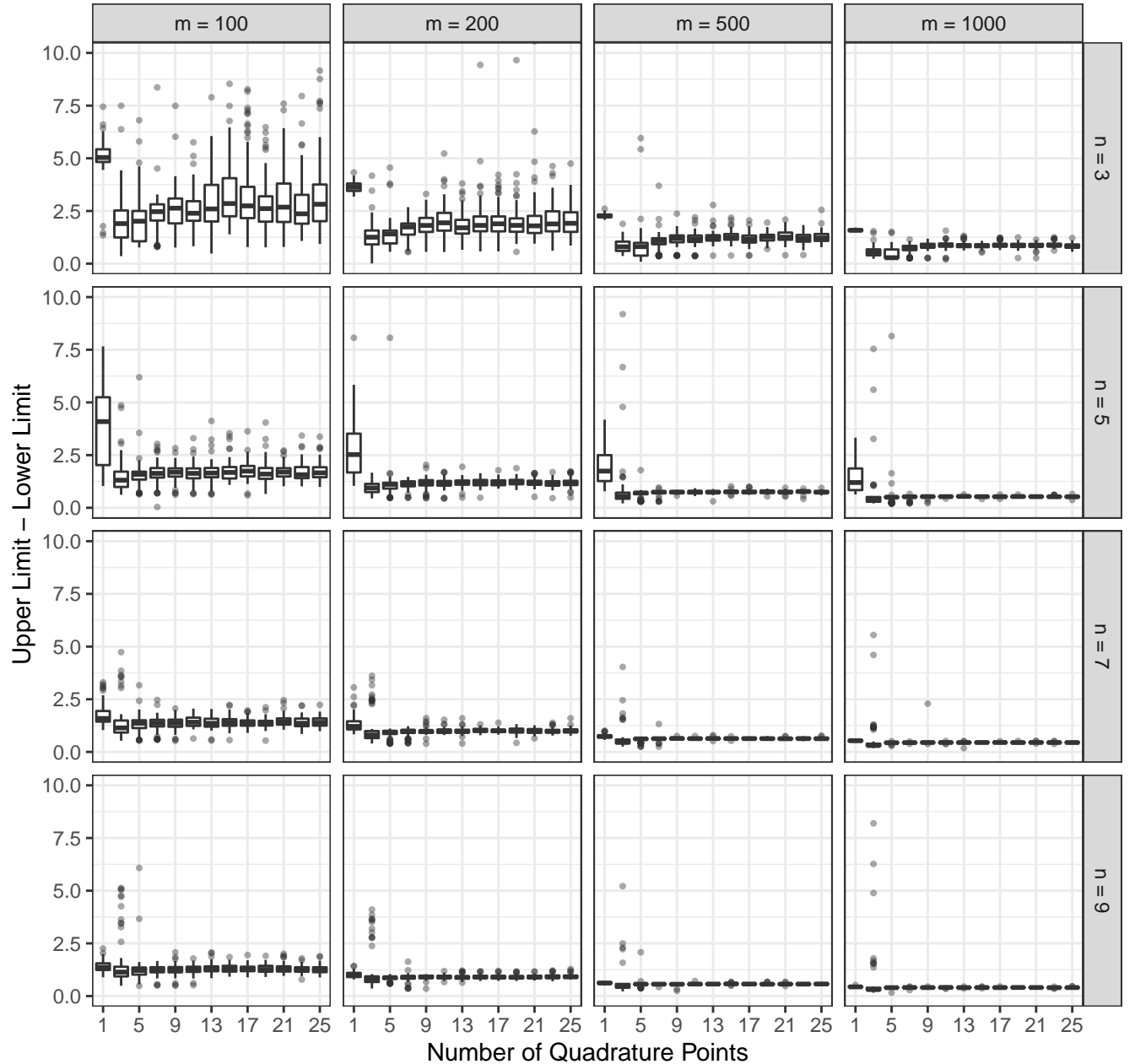


Figure 22: Length of the Wald intervals for $\widehat{\beta}_0$ in the simulation study of Section 4.3 in the main manuscript, where 1000 sets of data were generated from the random-slopes model (14). The Laplace ($k = 1$) intervals are substantially wider than those for larger k . Those for $k = 3, 5$ are narrower, and then the lengths level off for $k \geq 7$. This pattern coincides with coverages converging to nominal (Figure 15) as k increases, across values of m, n .

Length of Confidence Intervals, β_1

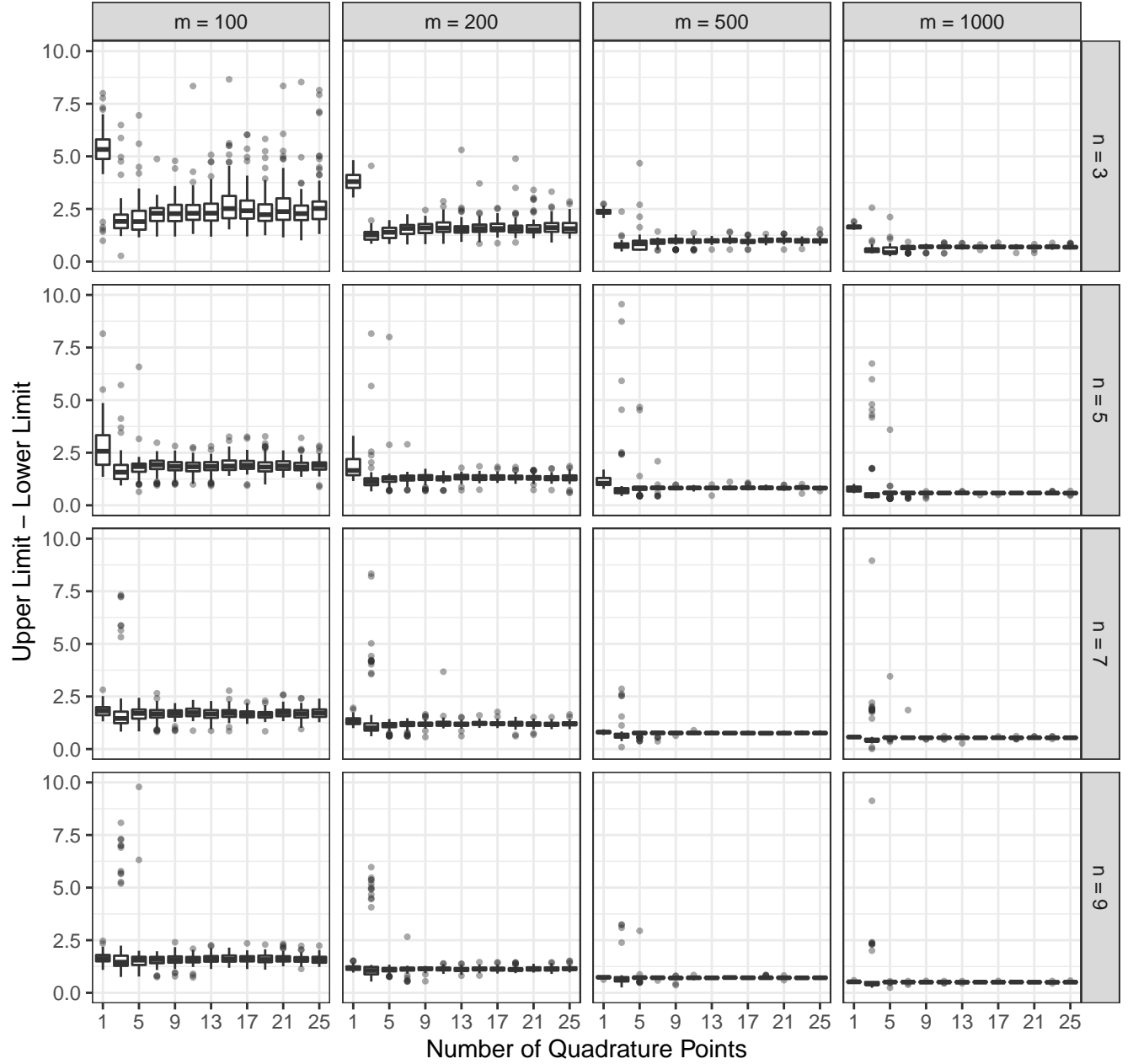


Figure 23: Length of the Wald intervals for $\widehat{\beta}_1$ in the simulation study of Section 4.3 in the main manuscript, where 1000 sets of data were generated from the random-slopes model (14). The Laplace ($k = 1$) intervals are substantially wider than those for larger k . Those for $k = 3, 5$ are narrower, and then the lengths level off for $k \geq 7$. This pattern coincides with coverages converging to nominal (Figure 16) as k increases, across values of m, n .

Length of Confidence Intervals, β_2

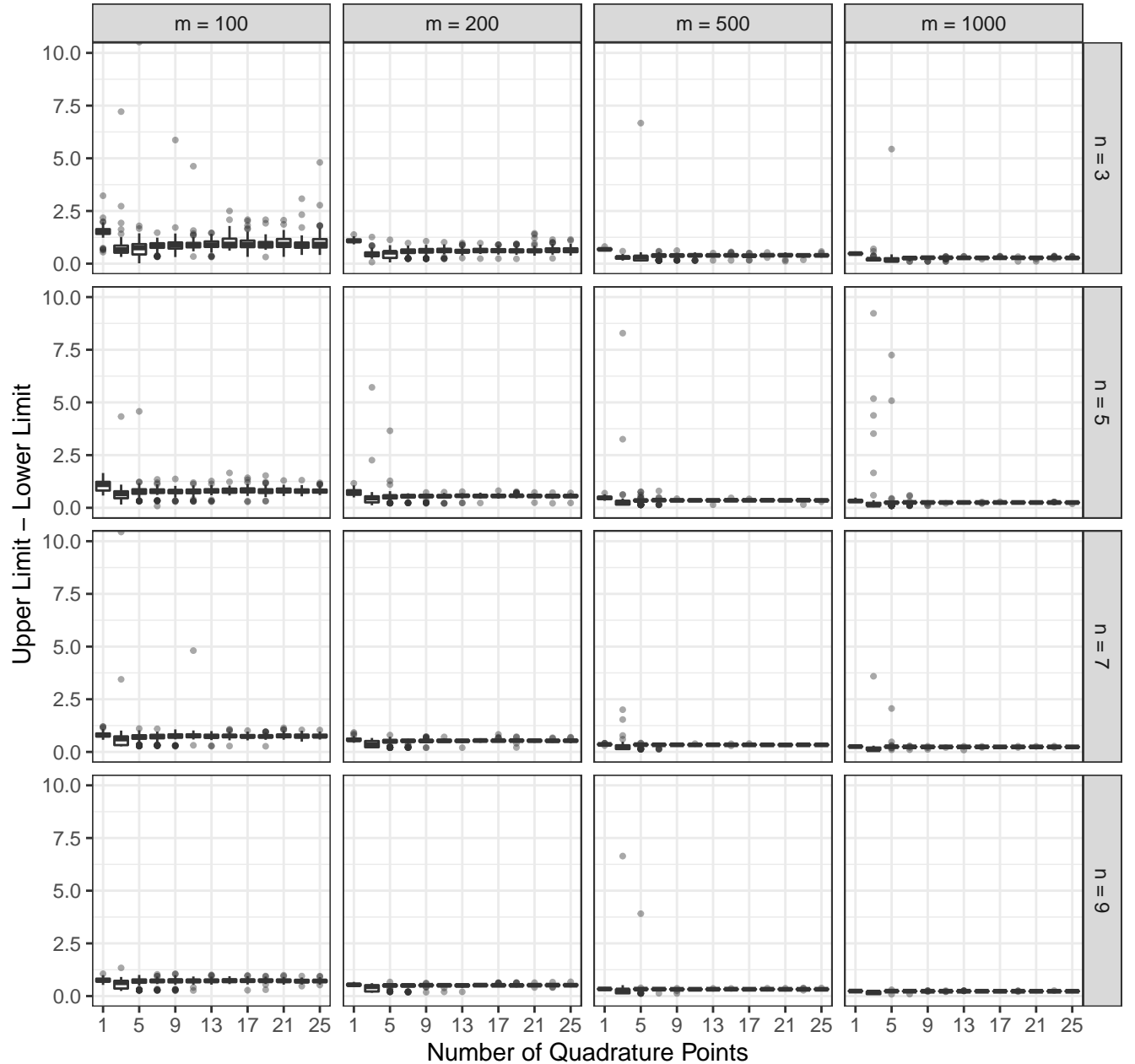


Figure 24: Length of the Wald intervals for $\widehat{\beta}_2$ in the simulation study of Section 4.3 in the main manuscript, where 1000 sets of data were generated from the random-slopes model (14). The Laplace ($k = 1$) intervals are somewhat wider than those for larger k . Those for $k = 3, 5$ are narrower, and then the lengths level off for $k \geq 7$. This pattern coincides with coverages converging to nominal (Figure 17) as k increases, across values of m, n .

Length of Confidence Intervals, β_3

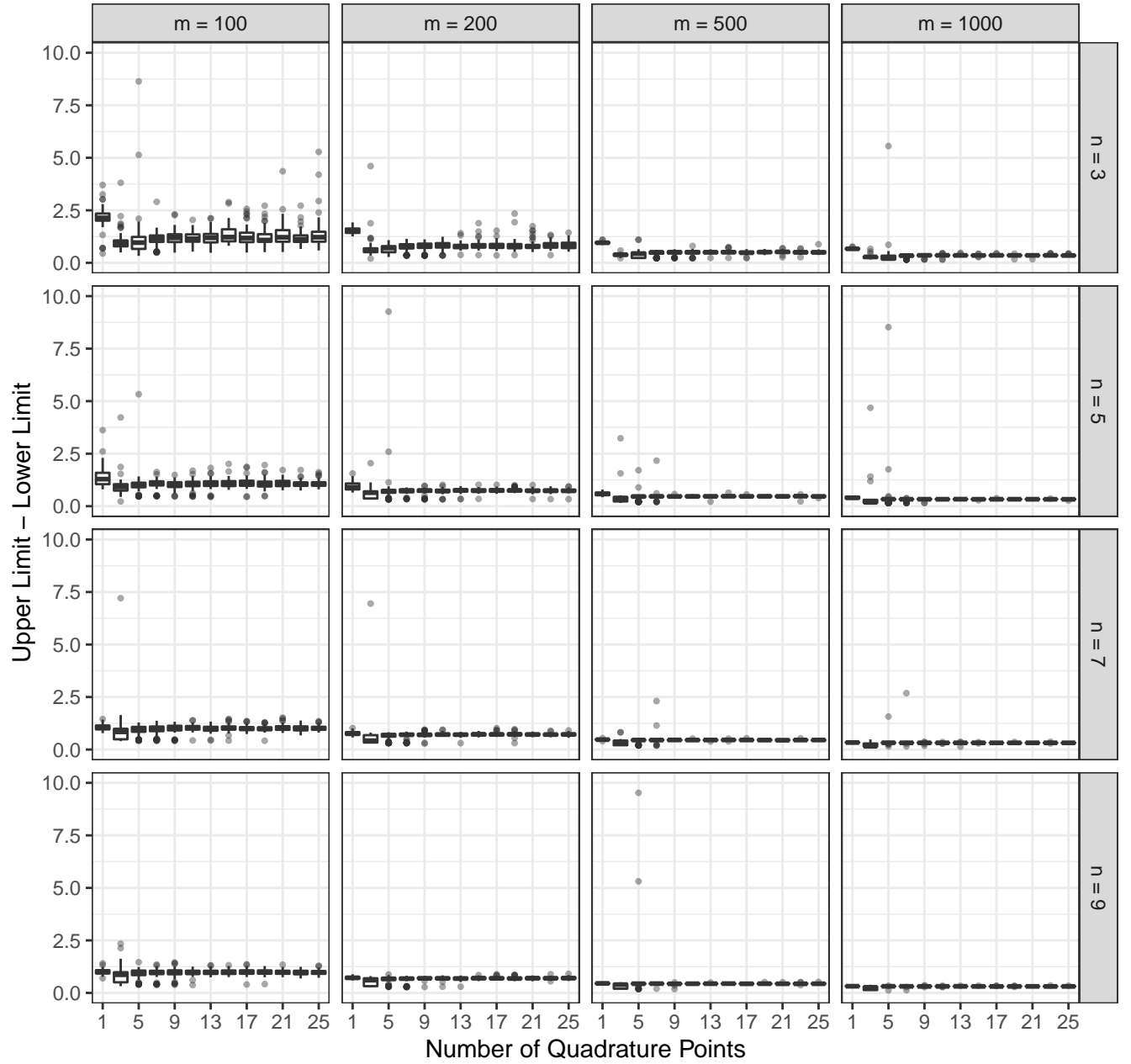


Figure 25: Length of the Wald intervals for $\widehat{\beta}_3$ in the simulation study of Section 4.3 in the main manuscript, where 1000 sets of data were generated from the random-slopes model (14). The Laplace ($k = 1$) intervals are somewhat wider than those for larger k . Those for $k = 3, 5$ are narrower, and then the lengths level off for $k \geq 7$. This pattern coincides with coverages converging to nominal (Figure 18) as k increases, across values of m, n .

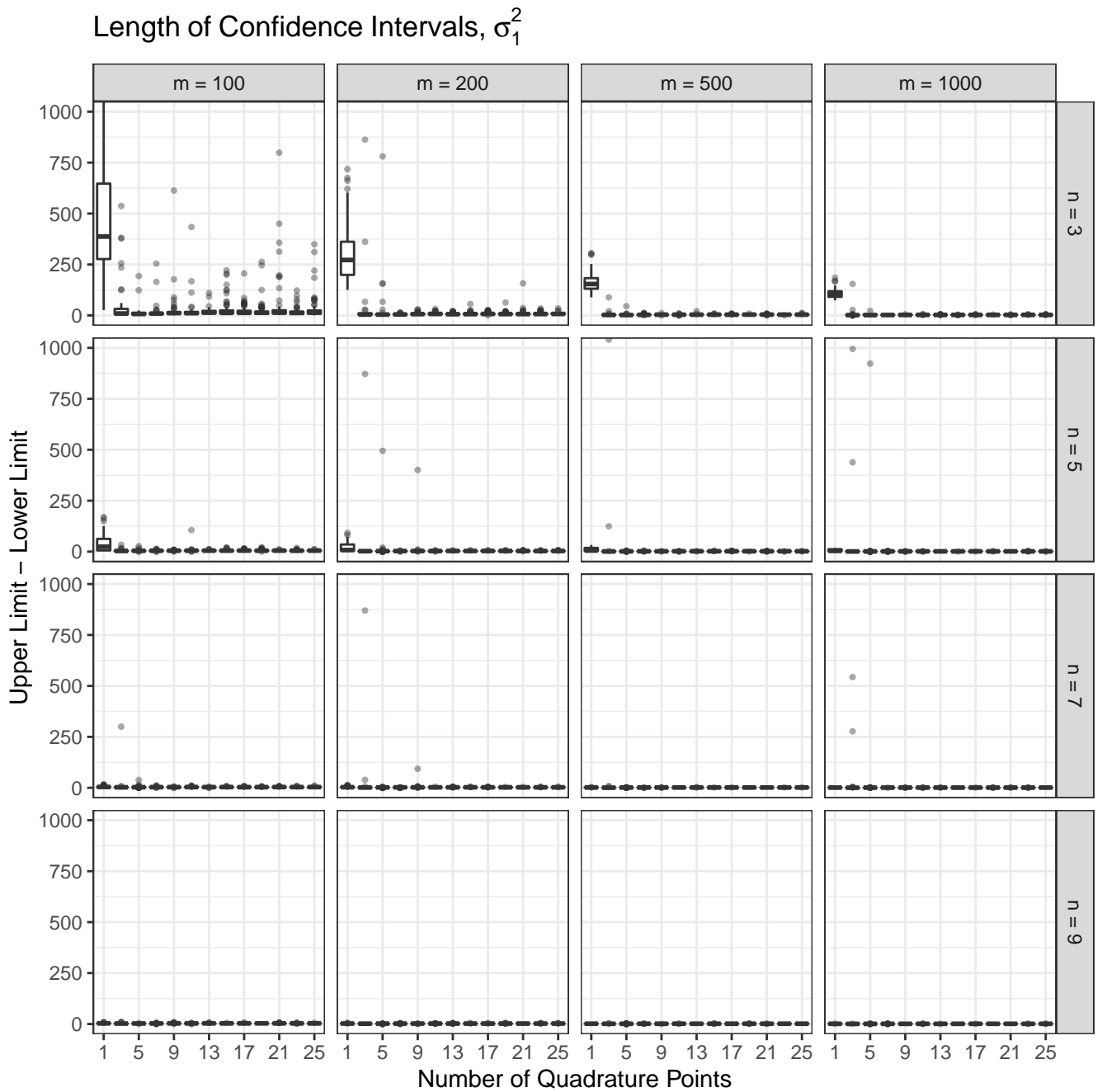


Figure 26: Length of the Wald intervals for $\hat{\sigma}_1^2$ in the simulation study of Section 4.3 in the main manuscript, where 1000 sets of data were generated from the random-slopes model (14). The Laplace ($k = 1$) intervals are orders of magnitude wider than those for larger k ; the y-axis is zoomed out to capture this.

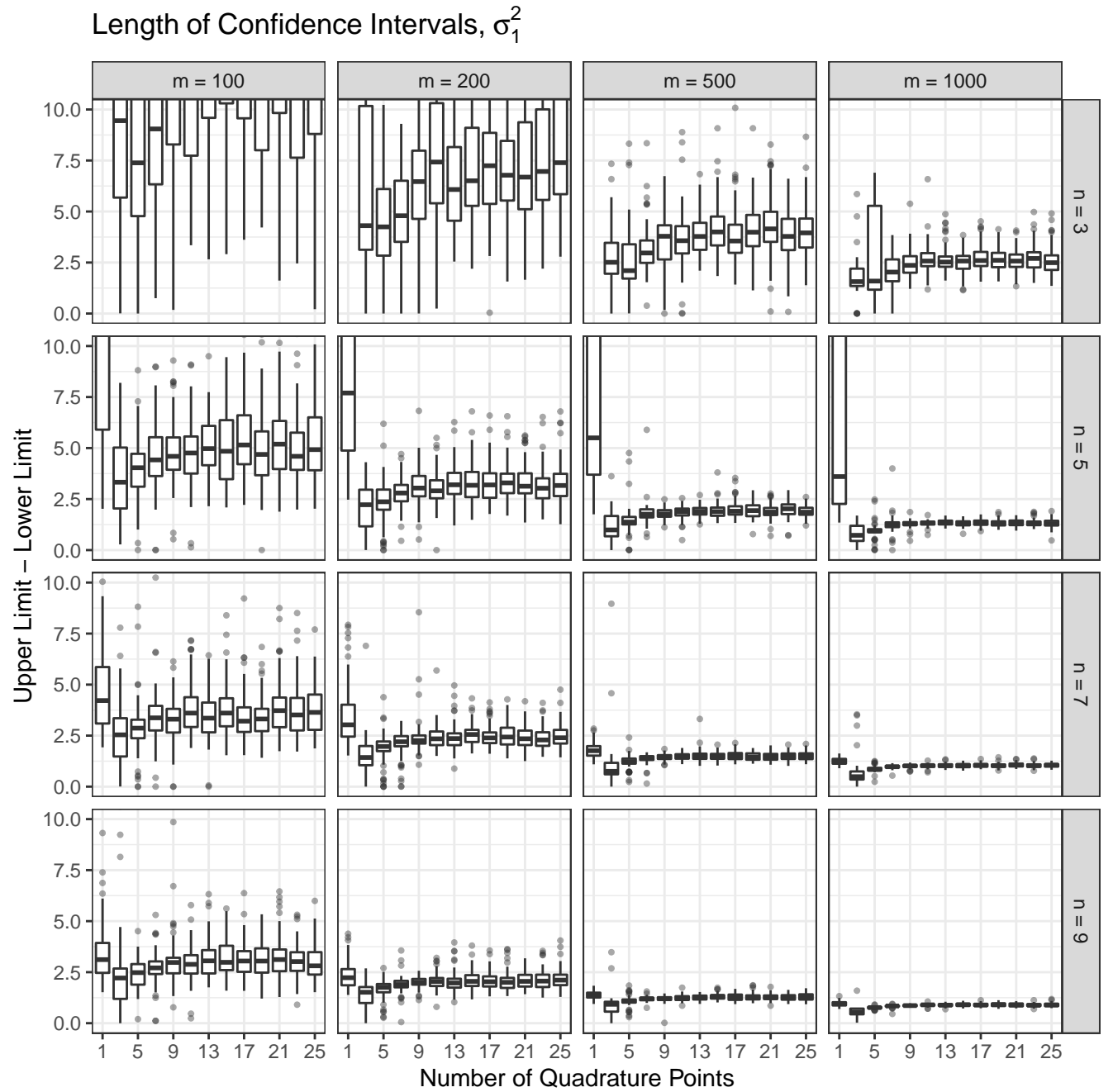


Figure 27: Length of the Wald intervals for $\hat{\sigma}_1^2$ in the simulation study of Section 4.3 in the main manuscript, where 1000 sets of data were generated from the random-slopes model (14). The y-axis is zoomed in, which obscures the massive length of the Laplace ($k = 1$) intervals. Those for $k = 3, 5$ are narrower, and then the lengths level off for $k \geq 7$. This pattern coincides with coverages converging to nominal (Figure 19) as k increases, across values of m, n .

Length of Confidence Intervals, σ_2^2

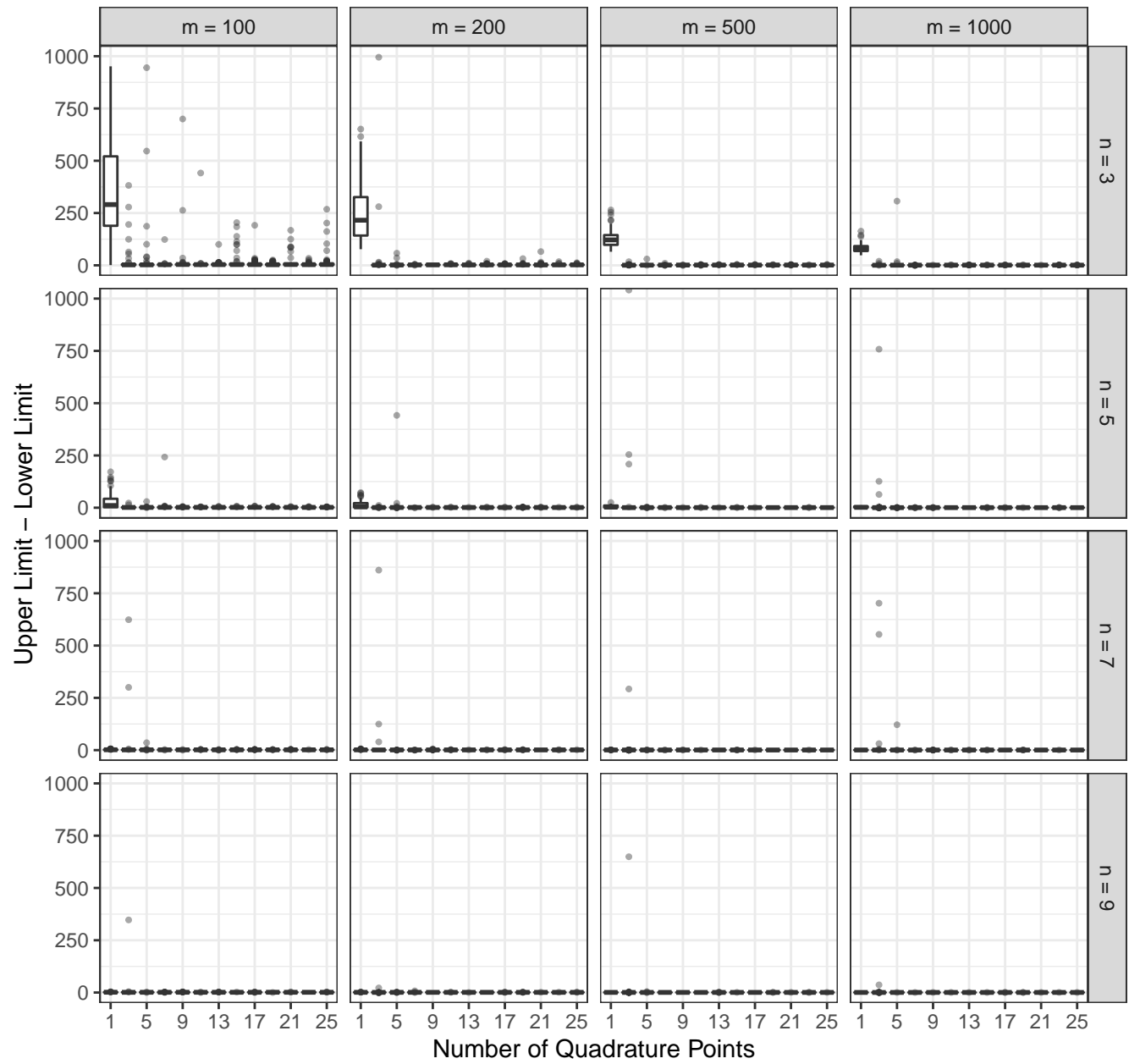


Figure 28: Length of the Wald intervals for $\hat{\sigma}_2^2$ in the simulation study of Section 4.3 in the main manuscript, where 1000 sets of data were generated from the random-slopes model (14). The Laplace ($k = 1$) intervals are orders of magnitude wider than those for larger k ; the y-axis is zoomed out to capture this.

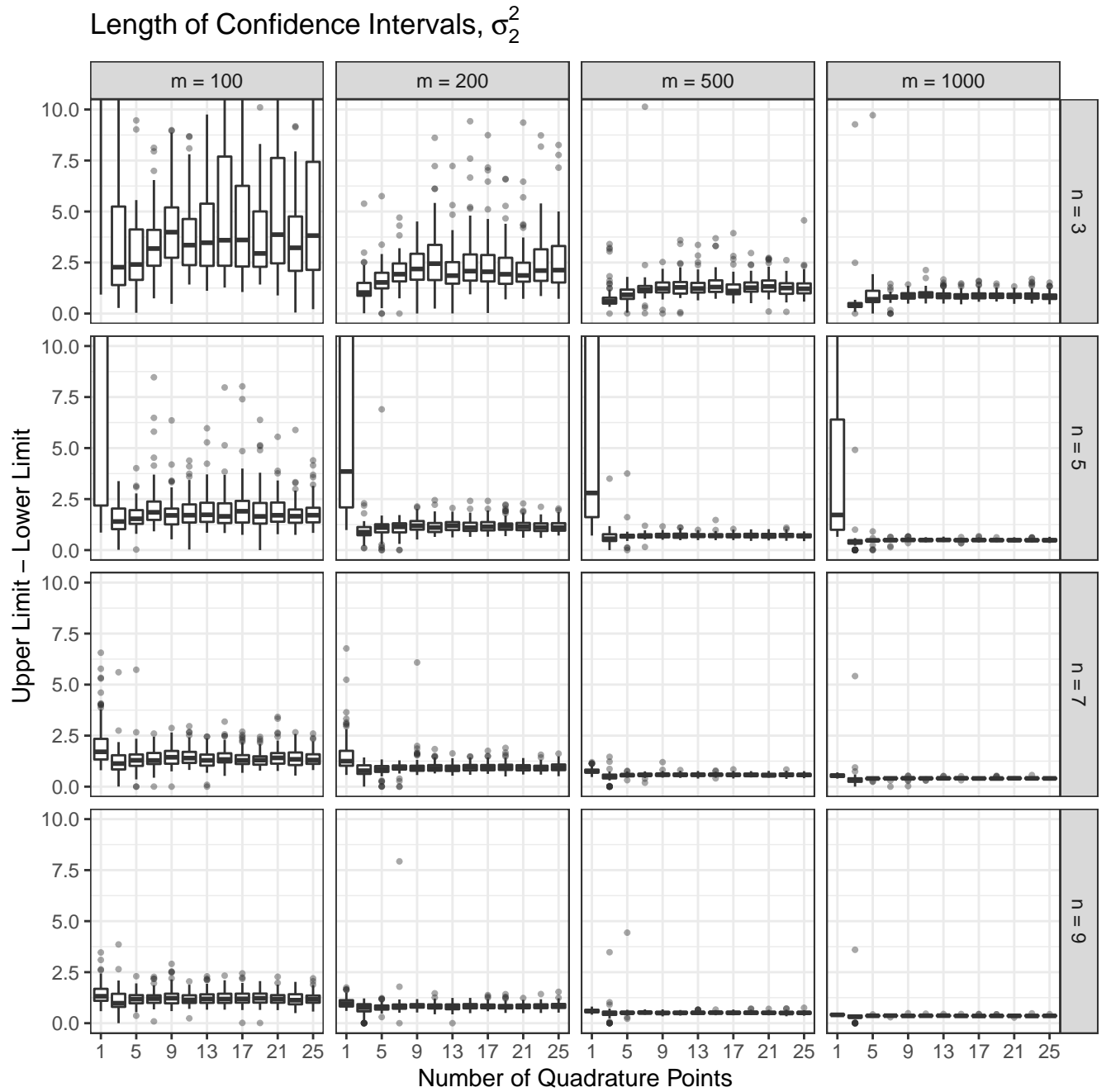


Figure 29: Length of the Wald intervals for $\hat{\sigma}_2^2$ in the simulation study of Section 4.3 in the main manuscript, where 1000 sets of data were generated from the random-slopes model (14). The y-axis is zoomed in, which obscures the massive length of the Laplace ($k = 1$) intervals. Those for $k = 3, 5$ are narrower, and then the lengths level off for $k \geq 7$. This pattern coincides with coverages converging to nominal (Figure 20) as k increases, across values of m, n .

Length of Confidence Intervals, σ_{12}

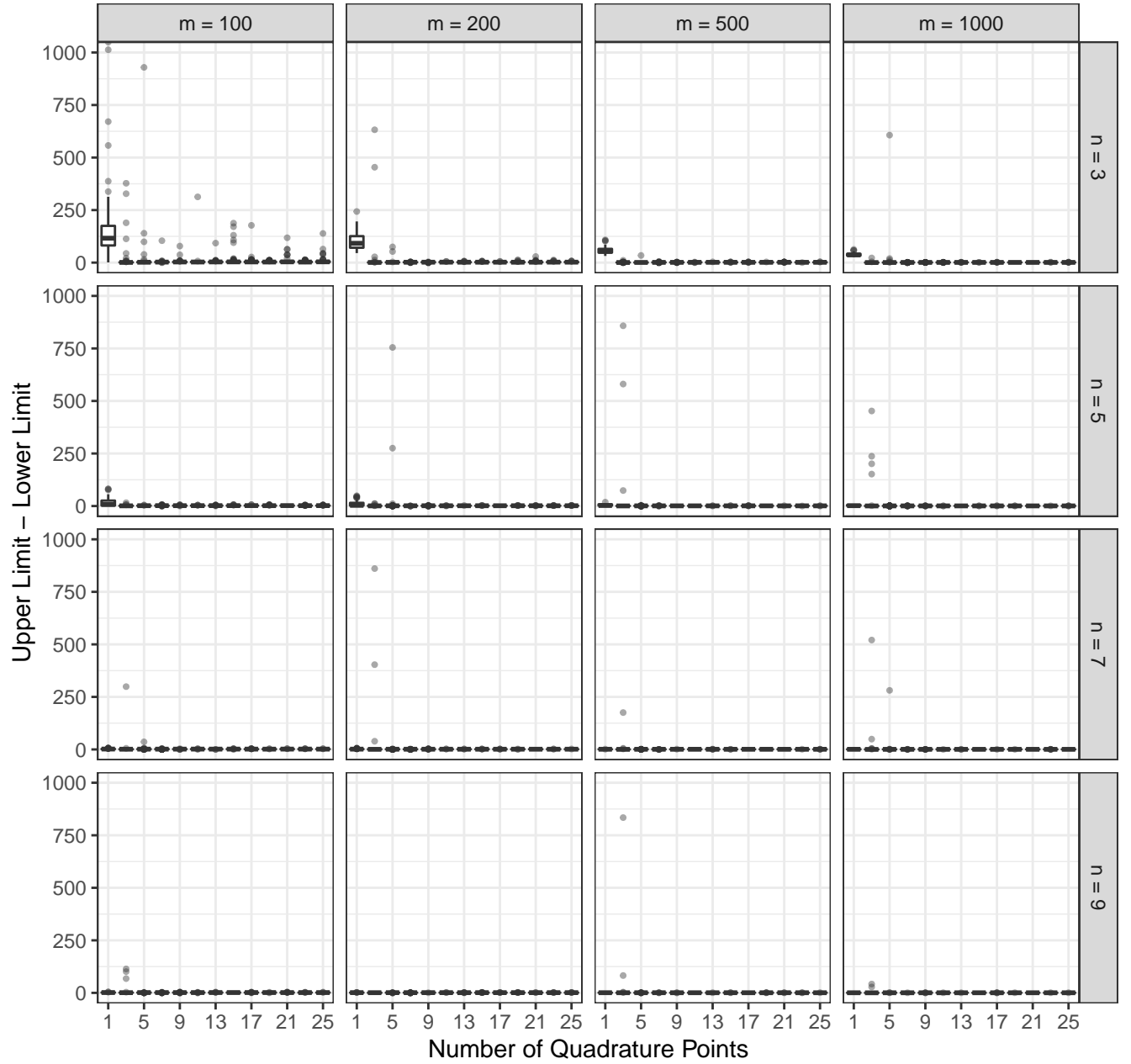


Figure 30: Length of the Wald intervals for $\hat{\sigma}_{12}$ in the simulation study of Section 4.3 in the main manuscript, where 1000 sets of data were generated from the random-slopes model (14). The Laplace ($k = 1$) intervals are orders of magnitude wider than those for larger k ; the y-axis is zoomed out to capture this.

Length of Confidence Intervals, σ_{12}

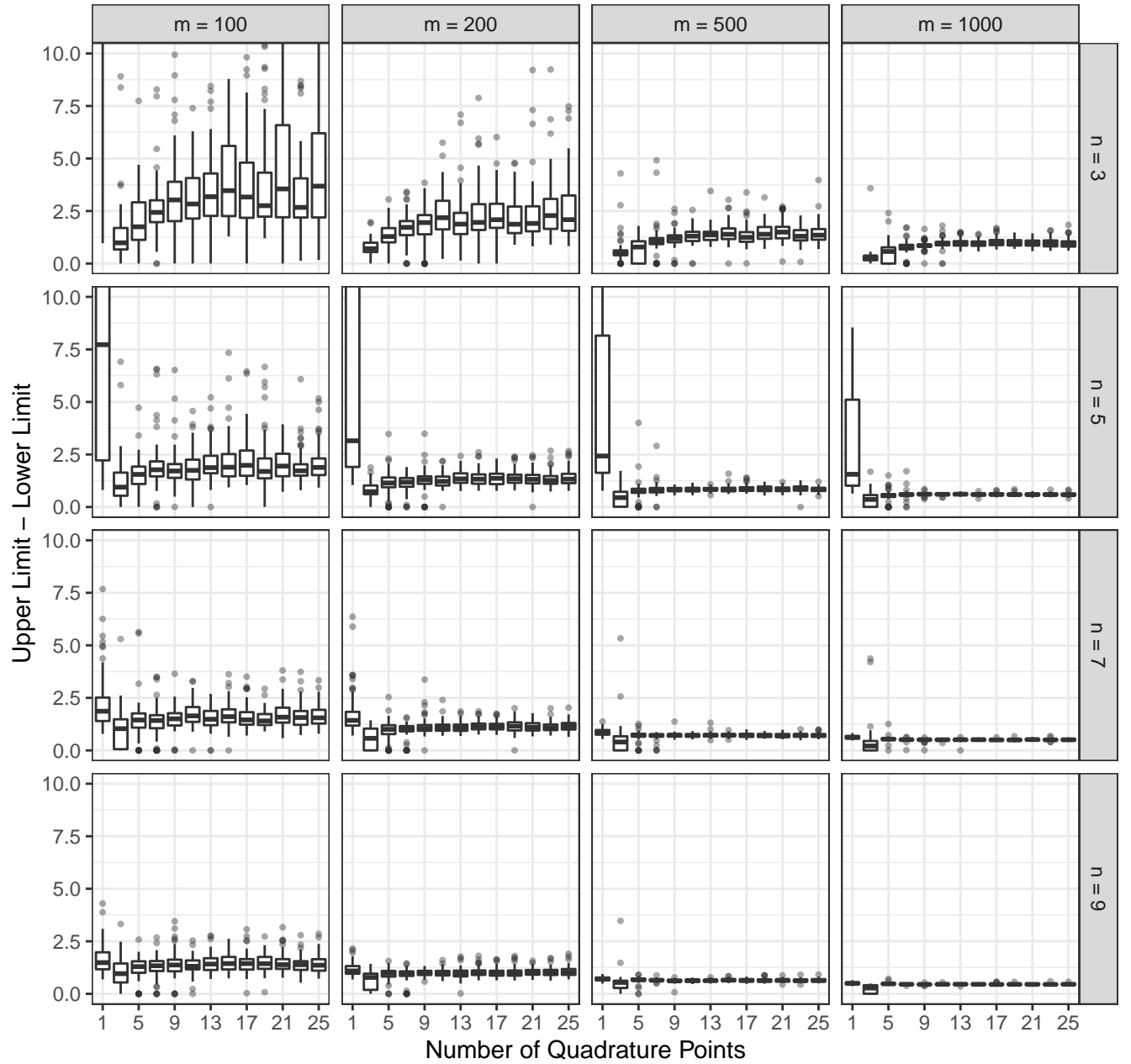


Figure 31: Length of the Wald intervals for $\hat{\sigma}_{12}$ in the simulation study of Section 4.3 in the main manuscript, where 1000 sets of data were generated from the random-slopes model (14). The y-axis is zoomed in, which obscures the massive length of the Laplace ($k = 1$) intervals. Those for $k = 3, 5$ are narrower, and then the lengths level off for $k \geq 7$. This pattern coincides with coverages converging to nominal (Figure 21) as k increases, across values of m, n .

C.2 Simulation 2: relative performance of the new method

We now assess the relative performance of the new method compared to the R packages `GLMMadaptive` and `lme4`. A method can be considered advantageous when compared to another method if it returns similar results in a faster time, and/or superior results in a similar amount of time. Accordingly, we compare computation times, proportion of successful model fits, computed minimized negative log-likelihood values, and computed gradient norms for each method. We broadly find that the new approach tends to return results at least as favourable or superior to other methods in terms of computed log-likelihood and gradient norm values in faster times, and has a higher empirical probability of providing a successful model fit. For all methods, computations at higher k take a longer amount of time but appear more stable.

C.2.1 Comparison with `GLMMadaptive`

We generated 500 datasets from model (14) and fit them using our procedure and `GLMMadaptive::mixed_model()` with the following non-default control options:

- `update_GH_every = 1`: update $\hat{\mathbf{u}}_i(\boldsymbol{\theta})$ for every new value of $\boldsymbol{\theta}$,
- `iter_EM = 0`: do not use the EM algorithm.

These options render `GLMMadaptive` as similar as possible to our approach, except for its use of finite-differenced gradients: it uses L-BFGS to directly minimize the AQ-approximate log-marginal likelihood, as does the new approach, which uses exact gradients.

We compute four summaries across simulations, shown in Figures 32 – 38:

1. **Computation times:** we report the absolute computation time of each method in seconds and the relative computation time of `GLMMadaptive`, which is defined as the absolute computation time of `GLMMadaptive` divided by the absolute computation time of the new method. Methods with lower absolute computation times for producing the same estimates are considered favourable. Values of relative computation time that are greater than 1 indicate that the new method produced a result in less time than `GLMMadaptive`.

2. **Successful runs:** a successful run is defined as a method returning finite numeric values for the point and interval estimates for all parameters. We report the proportion of successful runs for each method across simulations. It is favourable for a method to achieve a higher proportion of successful runs.
3. **Negative log-likelihood values:** the methods each terminate at a point estimate, $\hat{\theta}_k^{\text{AQ}}$, which corresponds to the smallest computed value for the negative log-likelihood, $-\tilde{\ell}_k^{\text{AQ}}(\hat{\theta}_k^{\text{AQ}})$. We report the average base-10 log-likelihood, $-\tilde{\ell}_k^{\text{AQ}}(\hat{\theta}_k^{\text{AQ}})/(N \log 10)$ where $N = mn$, for each simulation and each method, as well as the difference in these values for `GLMMadaptive` minus that from the new method. Methods returning smaller such values are favourable. A positive value of the difference indicates that the new method performed favourably on this metric. We use our own implementation to compute $\tilde{\ell}_k^{\text{AQ}}(\hat{\theta}_k^{\text{AQ}})$ for all methods.
4. **Gradient norm values:** the optimization procedures all attempt to find $\hat{\theta}_k^{\text{AQ}}$ such that $\|\nabla \tilde{\ell}_k^{\text{AQ}}(\hat{\theta}_k^{\text{AQ}})\|_2 = 0$. We report the average base-10 log of the norm of the gradient at the computed maximum, $\log_{10} \|\nabla \tilde{\ell}_k^{\text{AQ}}(\hat{\theta}_k^{\text{AQ}})\|_2/N$, for each simulation and each method. It is favourable for a method to return a smaller value of this metric. We also compute the difference in these values for `GLMMadaptive` minus that from the new method. A positive value of this difference indicates that the new method performed favourably on this metric. We use our own implementation to compute $\nabla \tilde{\ell}_k^{\text{AQ}}(\hat{\theta}_k^{\text{AQ}})$ for all methods.

Relative computation times are more relevant to comparison of methods because they are less sensitive to hardware, and their interpretation generalizes more readily to data and models other than the specific one(s) considered in a particular simulation study. Absolute computation times are of passing interest only, and should not be considered representative of how each method would perform using different hardware and data. We report only relative computation times in the manuscript, but report both relative and absolute computation times in this supplement. All computations were performed on a 2021 M1 Mac Book Pro with 64 Gb of RAM, with individual simulations run in parallel across 10 CPU cores.

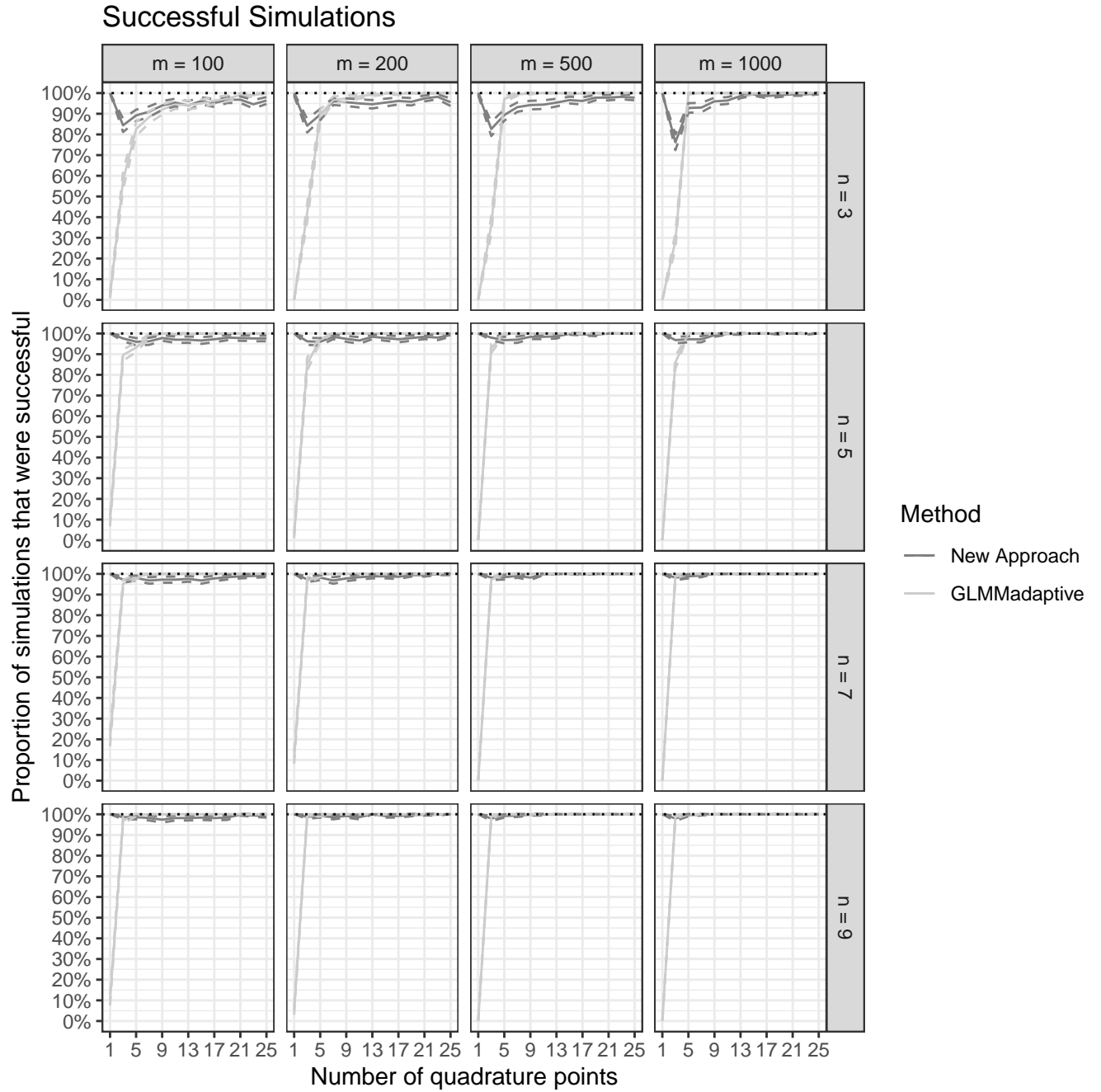


Figure 32: Proportion of successful simulation runs for the new method and `GLMMadaptive` out of 500 simulated data sets. Both methods achieve nearly 100% success for larger k at all combinations of m and n . For low n , moderate k , and all values of m , the new method achieves slightly fewer successful runs, however inspection of Figures 36 and 38 indicate that the runs that were successful tended to yield superior estimates. For the Laplace approximation ($k = 1$), `GLMMadaptive` achieves a low success rate for every m, n .

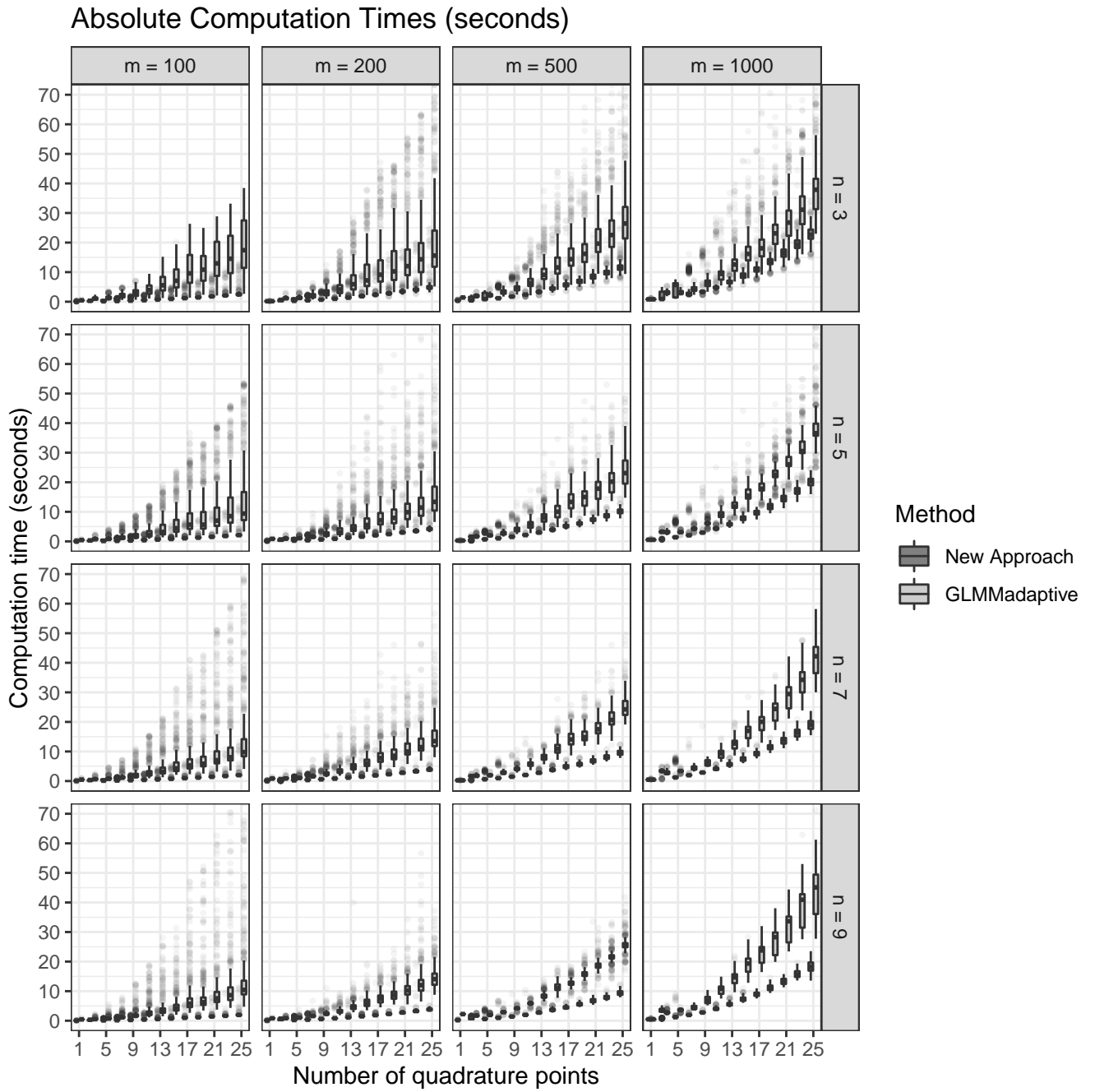


Figure 33: Absolute computation times in seconds for the new method and **GLMMadaptive**. The latter takes more computation time at all values of m , n , and k . The new method appears more stable than **GLMMadaptive** in the sense that the distributions of its run times appear more concentrated and have fewer outlying run times.

Relative Computation Times, GLMMadaptive / New Approach

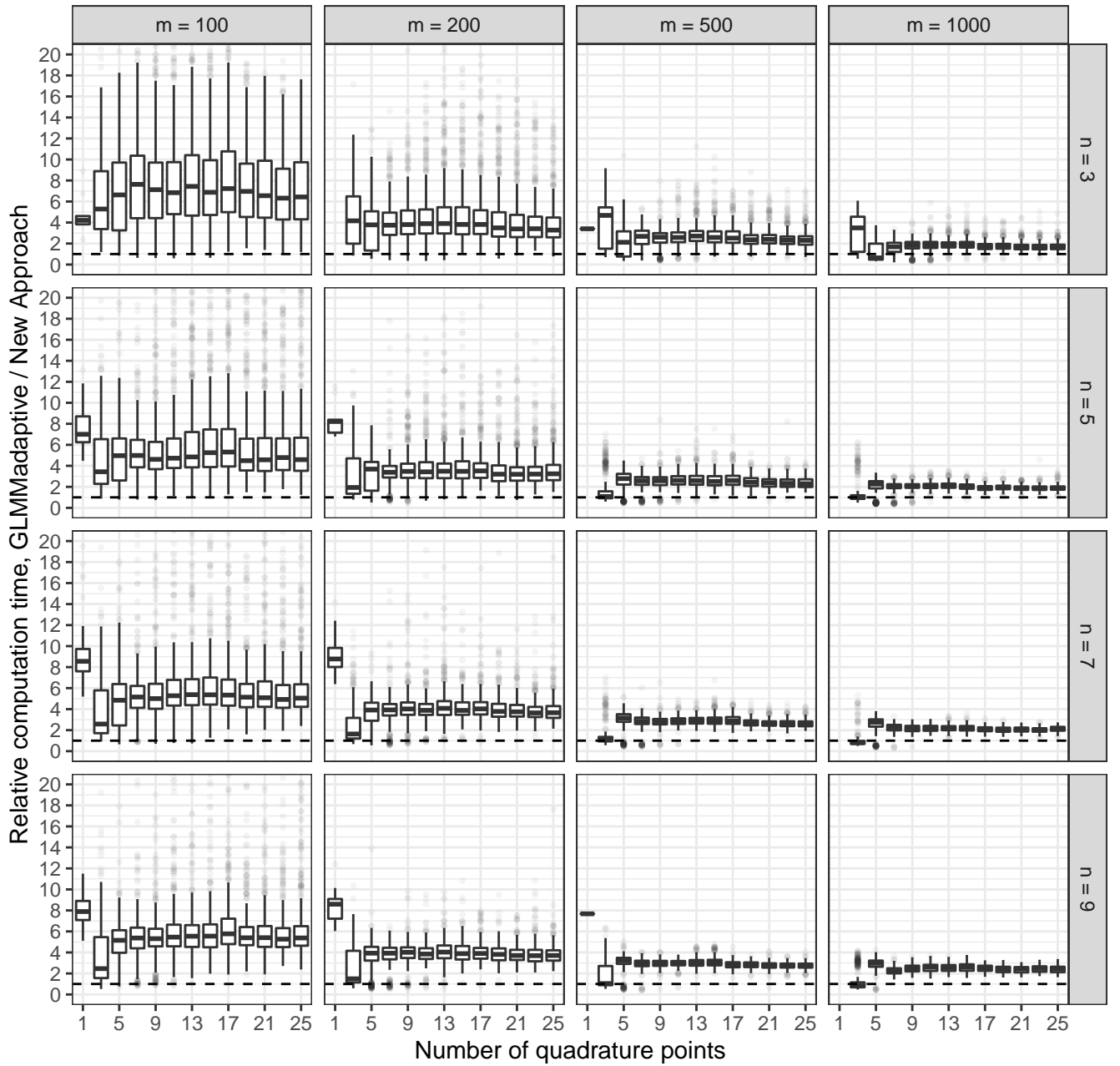


Figure 34: Relative computation times for `GLMMadaptive` compared to the new method; for example, a value of 2 indicates that `GLMMadaptive` ran in twice as much time as the new method. The new method appears to run much faster than `GLMMadaptive` for lower m , and then settles at about 3 times faster for large values of m and k . The total run time should be affected by data size, but also by accuracy of the approximation, with less accurate likelihood and gradient approximations leading to slower optimization, even while smaller data size leads to faster evaluation; this may partly explain why the relative computation times appear to settle around a common value at all of m , n , and k increase.

Average negative log-likelihood values by method

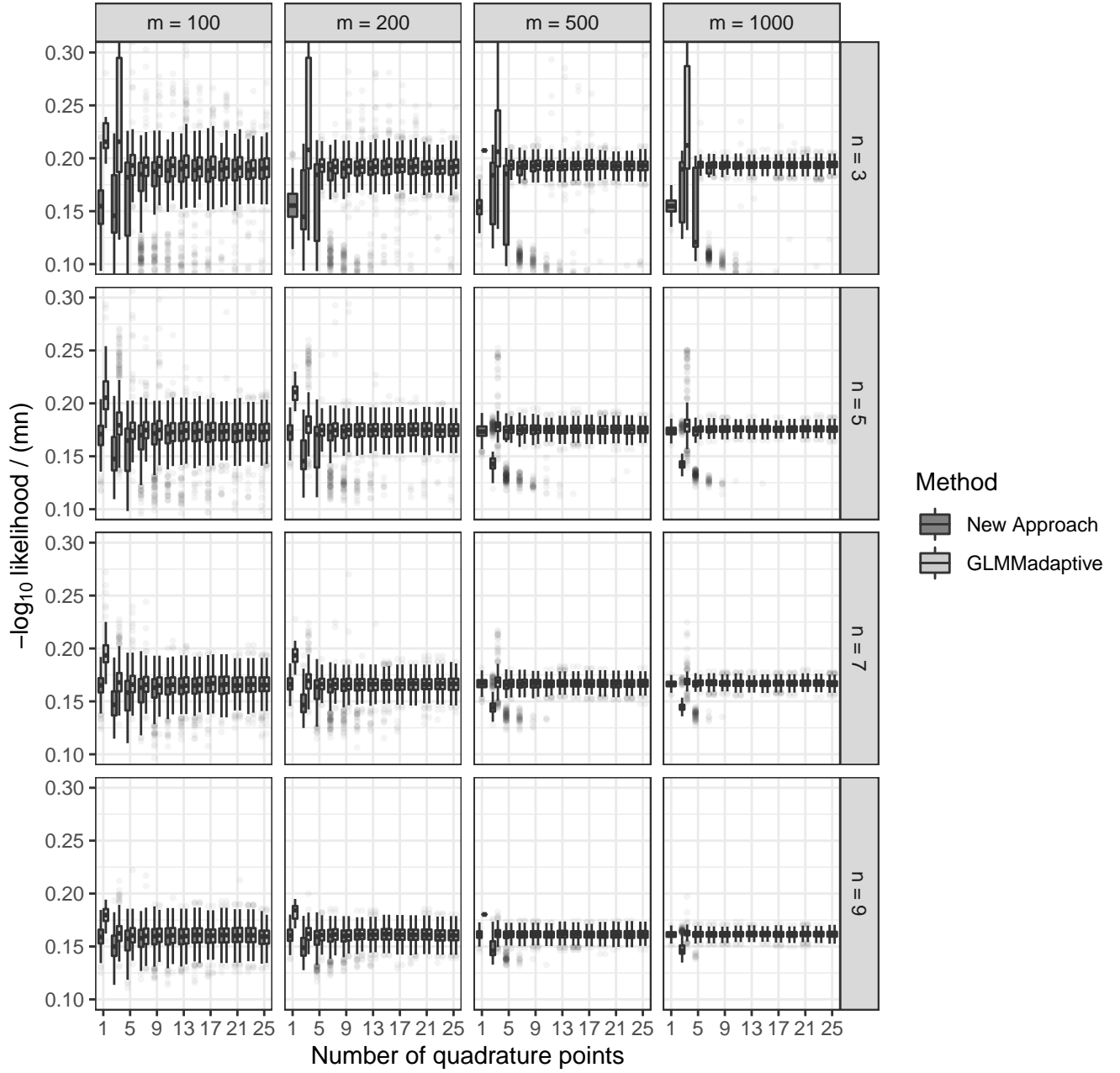


Figure 35: Values of $-\tilde{\ell}_k^{\text{AQ}}(\hat{\boldsymbol{\theta}}_k^{\text{AQ}})/(N \log 10)$ for each method. Lower values are more desirable.

The two methods return broadly the same values for moderate k and higher. While the new method appears to return lower values for lower k , this is not a substantial practical advantage since the practical recommendation is to increase k until these values stop changing, which will yield similar results from both methods. However, we point out that as substantiated in Figure 34, the new method returns these results several times faster.

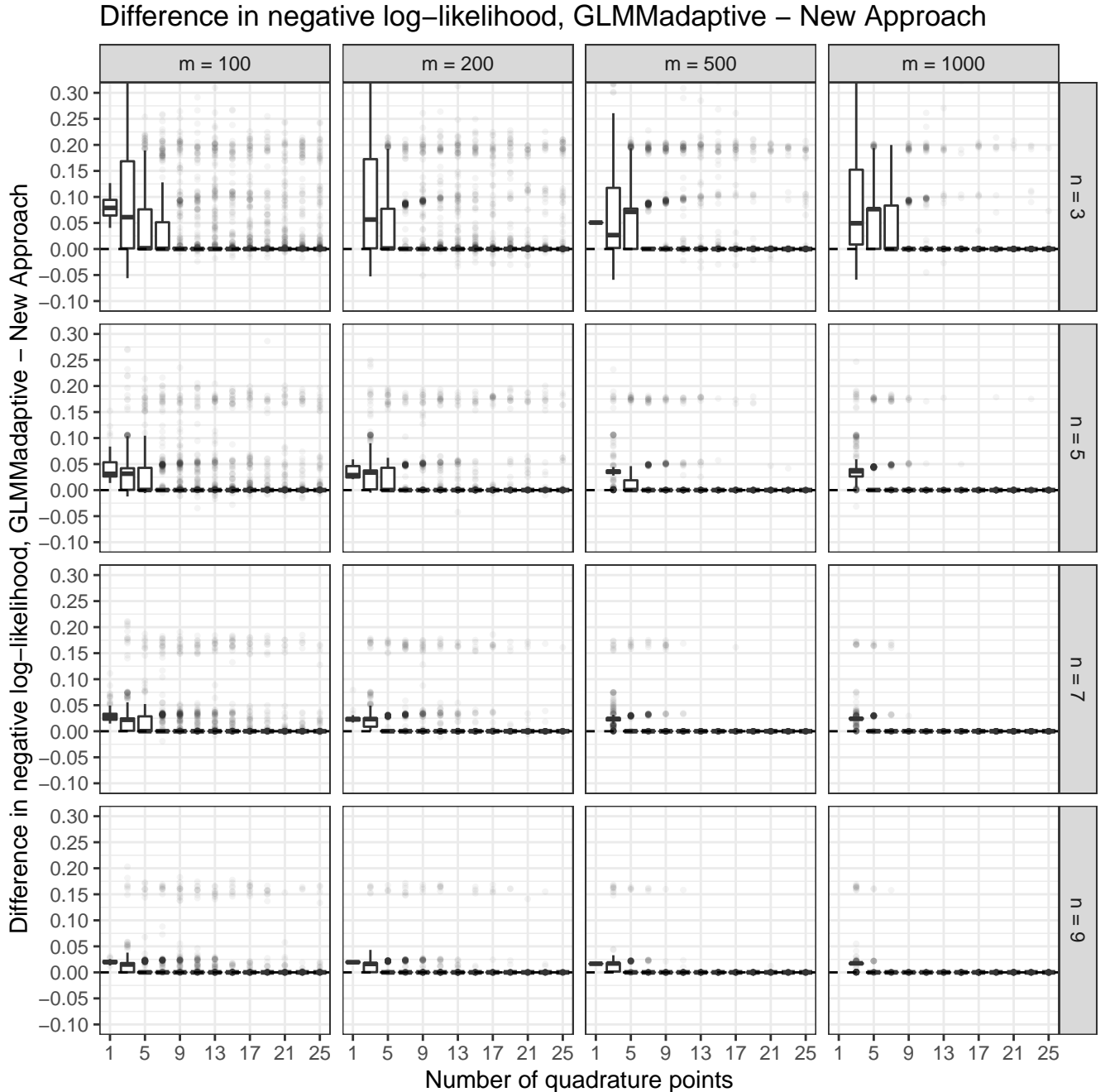


Figure 36: Difference of $-\tilde{\ell}_k^{\text{AQ}}(\hat{\theta}_k^{\text{AQ}})/(N \log 10)$ for GLMMadaptive minus the new method. A positive value indicates that the new method achieved a lower value of $-\tilde{\ell}_k^{\text{AQ}}(\hat{\theta}_k^{\text{AQ}})$ than GLMMadaptive, and hence superior performance. The two methods return broadly the same values for moderate k and higher, with GLMMadaptive returning higher values in a small number of simulations. While the new method appears to return lower values for lower k , this is not a substantial practical advantage since the practical recommendation is to increase k until these values stop changing, which will yield similar results from both methods. However, we point out that as substantiated in Figure 34, the new method returns these results several times faster.

Average log–norm of gradient by method

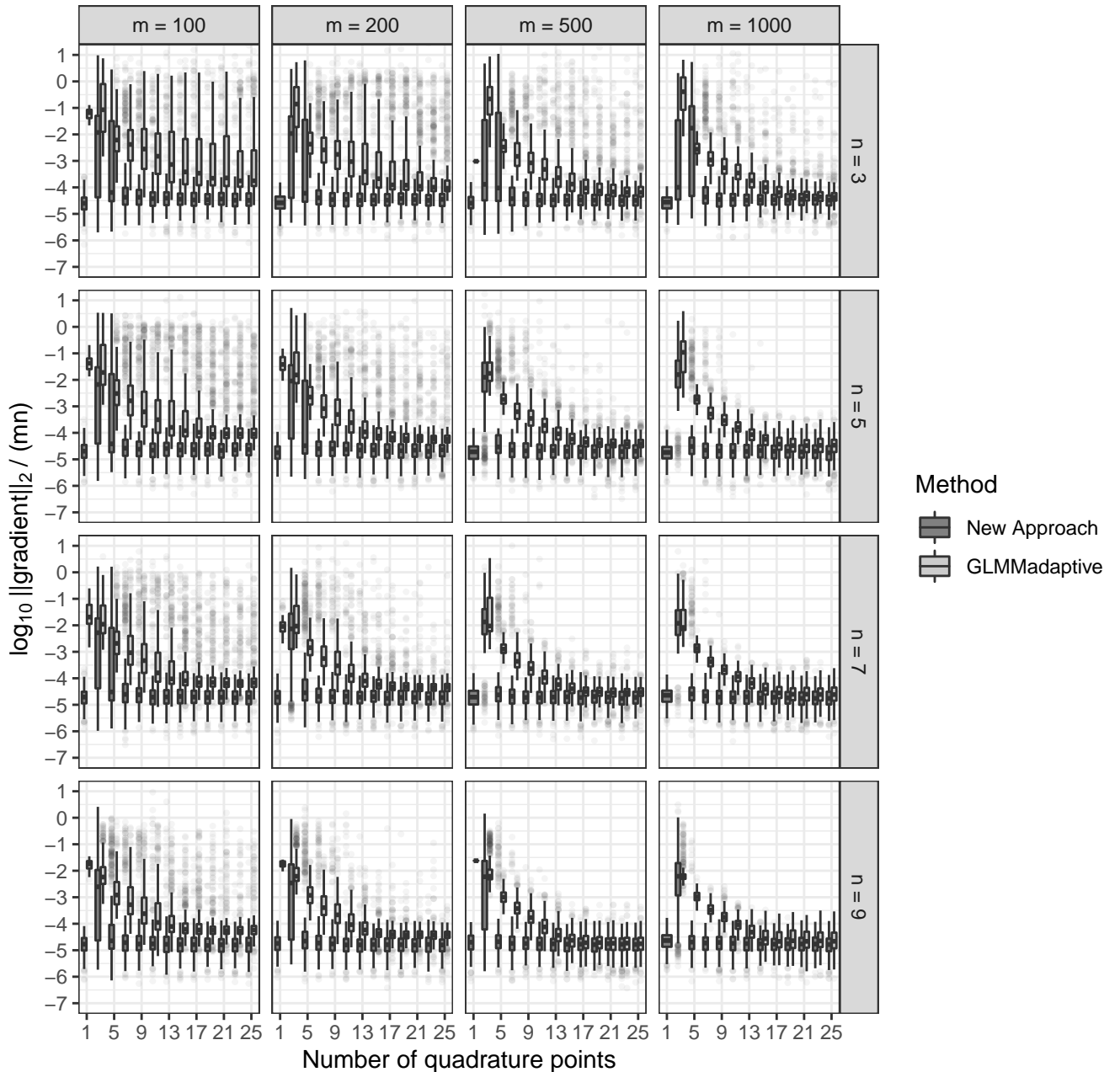


Figure 37: Values of $\log_{10} \|\tilde{\nabla \ell}_k^{\text{AQ}}(\hat{\boldsymbol{\theta}}_k^{\text{AQ}})\|/N$ for each method. Lower values are more desirable. The new method appears very stable, achieving approximately the same values for all m , n , and k with concentrated distributions across simulations; the exception to the last point is for either small m and/or small n combined with lower k , where the distribution across simulations is right-skewed. In contrast, **GLMMadaptive** achieves results that clearly improve with increasing k , and stabilize at just slightly higher than the new method. Because **GLMMadaptive** minimizes the norm of a finite-differenced gradient, it is not surprising that it would not achieve as favourable a result on this metric as the new approach, which uses exact gradients. In practice, because the recommendation is to increase k until results stop changing, both approaches would end up giving similar results on this metric; however,

Difference in log-norm of gradient, GLMMadaptive – New Approach

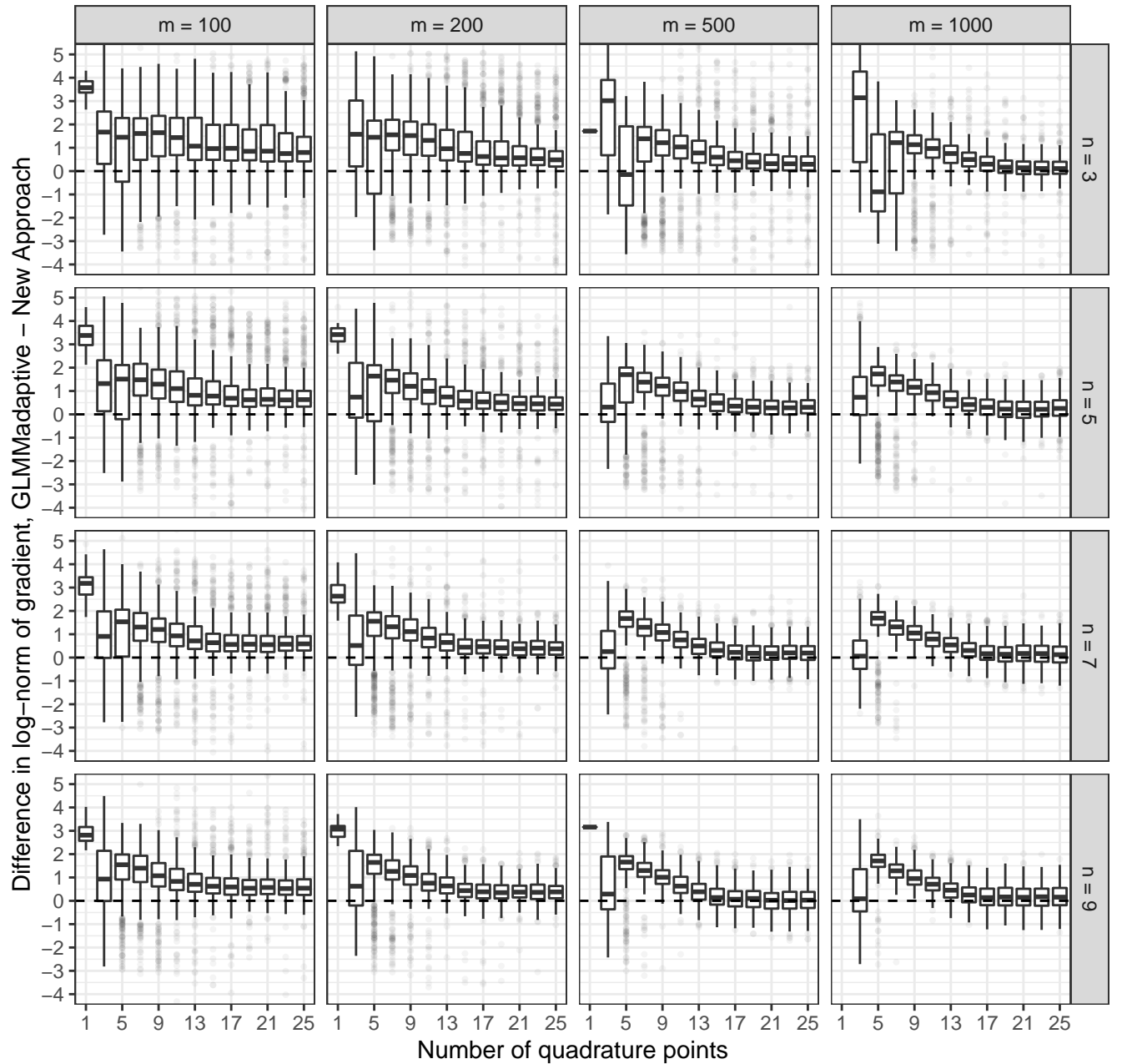


Figure 38: Difference of $\log_{10} \|\nabla \tilde{\ell}_k^{\text{AQ}}(\hat{\boldsymbol{\theta}}_k)\|$ for GLMMadaptive minus the new method. A positive value indicates that the new method achieved a lower value of $-\tilde{\ell}_k^{\text{AQ}}(\hat{\boldsymbol{\theta}}_k)$ than GLMMadaptive and hence performed favourably. The distribution of this difference is concentrated on positive values for nearly all combinations of m , n , and k , indicating broadly superior performance. For all m and n , the difference appears to settle around 0–1 as k is increased; since the practical recommendation is to increase k until results stop changing, this indicates that both approaches will end up yielding similar results, with the new approach often slightly favourable. Figure 34 shows that the new method returns these favourable results several times faster.

C.2.2 Comparison with `lme4`

Because `lme4` cannot fit model (14) with $k > 1$, we instead simulate from the following model:

$$Y_{ij} \mid u_i \stackrel{\text{ind}}{\sim} \text{Bern}(p_{ij}), \quad u_i \stackrel{\text{iid}}{\sim} \text{N}(0, \sigma^2), \quad \log \frac{p_{ij}}{1 - p_{ij}} = \beta_0 + \beta_1 x_i + u_i. \quad (15)$$

We simulate 1000 sets of data from model (15) with $\beta = (-2.5, -0.15)$ and $\sigma^2 = 2$. We compute and report the same statistics with the same interpretations as for the comparison to `GLMMadaptive` in Section C.2.

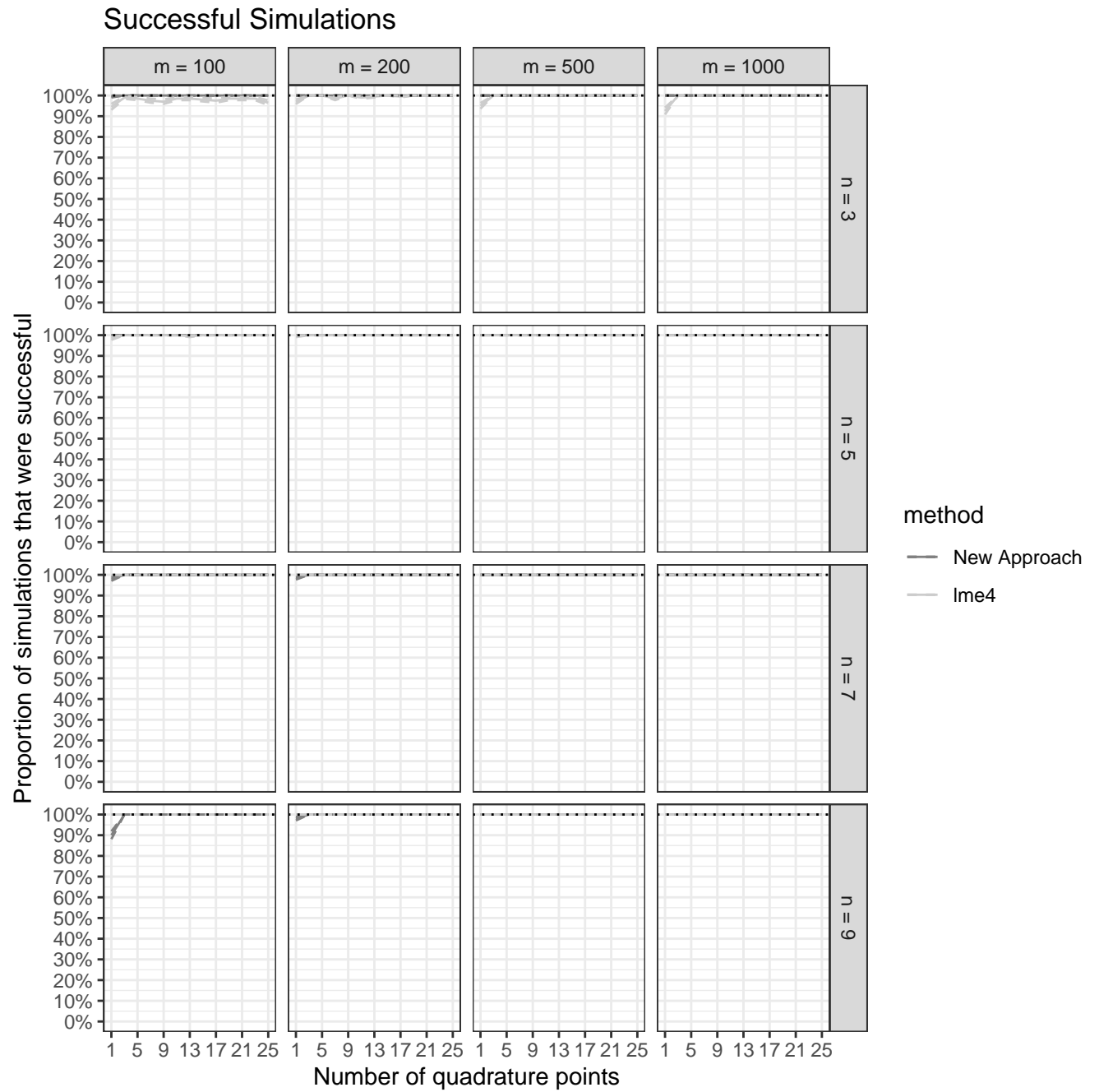


Figure 39: Proportion of successful simulation runs for the new method and `lme4`. Both methods appear highly stable at all values of m , n , and k , with `lme4` achieving a very slightly lower proportion of successful runs in the very difficult $m = 100$, $n = 3$ case.

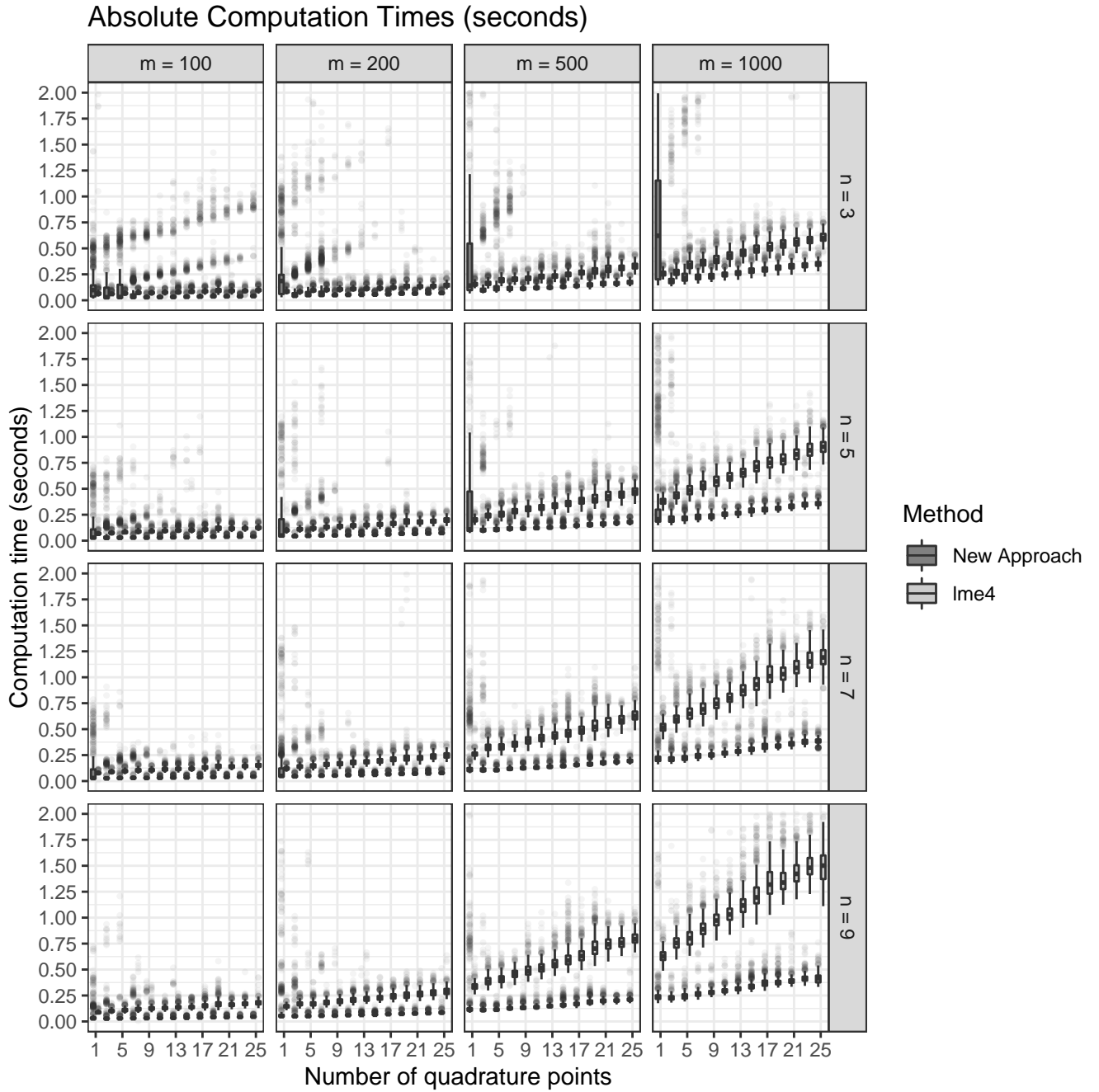


Figure 40: Absolute computation times in seconds for the new method and `lme4`. The new approach appears broadly faster and more stable than `lme4`, defined as having a distribution of run times across simulations centred at a lower value and exhibiting less variability. The $k = 1$ case appears challenging for the new approach, while `lme4` performs well in this case; however, the new approach appears much faster and less variable at higher m . We point out that the practitioner can choose k , but often cannot choose m .

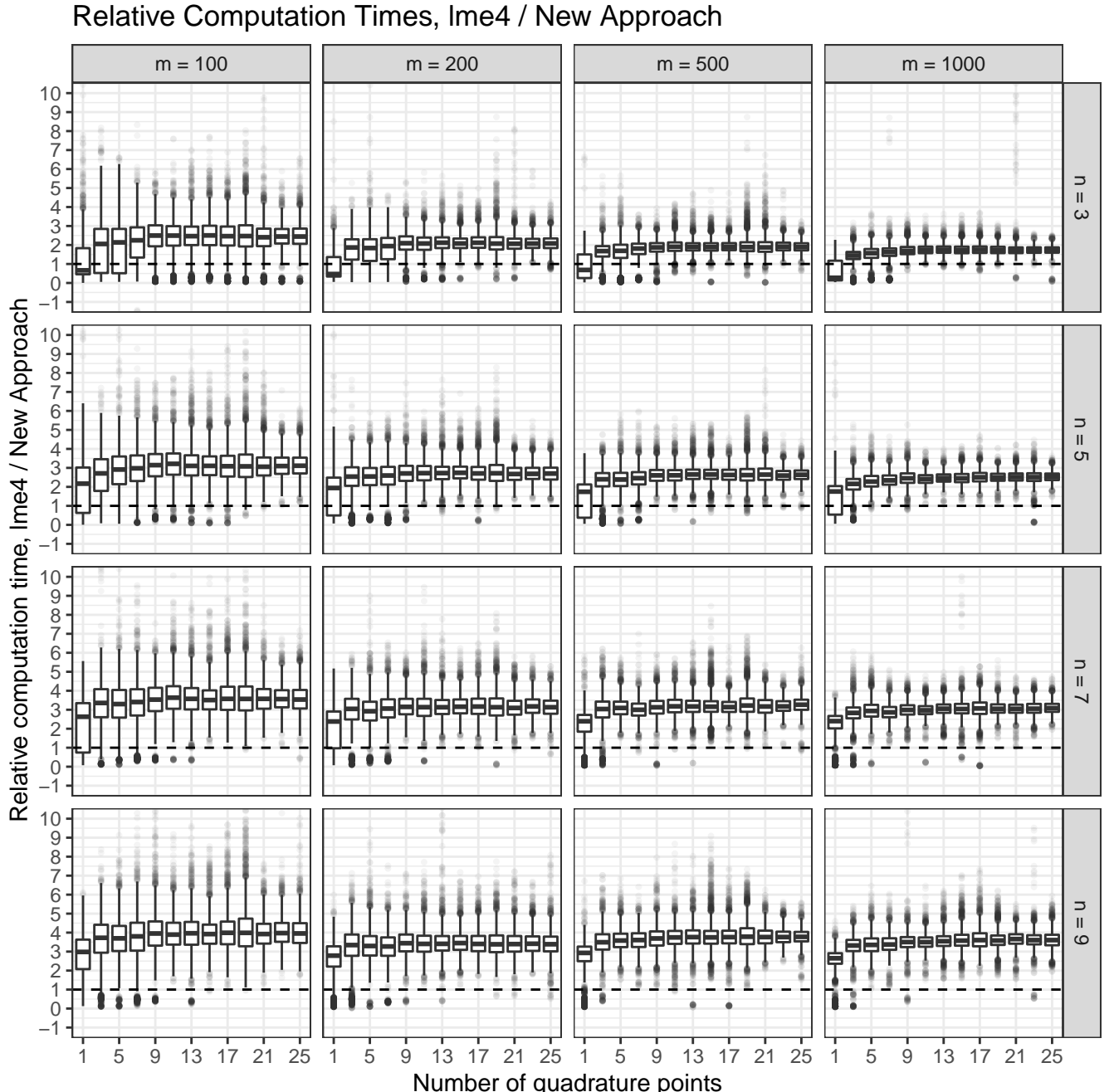


Figure 41: Relative computation times for `lme4` compared to the new method; for example, a value of 2 indicates that `lme4` ran in twice as much time as the new method. The new method appears to be about 2 – 4 times faster than `lme4`, with concentrated, symmetric distributions of run times, for almost all m , n , and k . For $k = 1$, `lme4` is sometimes faster for lower n , and the $k = 1, n = 3$ case is the only case for which `lme4` appears superior overall in terms of relative computation time. The practical implications of this are limited, as the method is not expected to be accurate for low k combined with low n . Further, Figures 42 – 45 show that the computed results from both methods change as k is increased beyond 1, and hence the practical advice to increase k until results stop changing would yield faster run times from the new method.

Average negative log-likelihood values by method

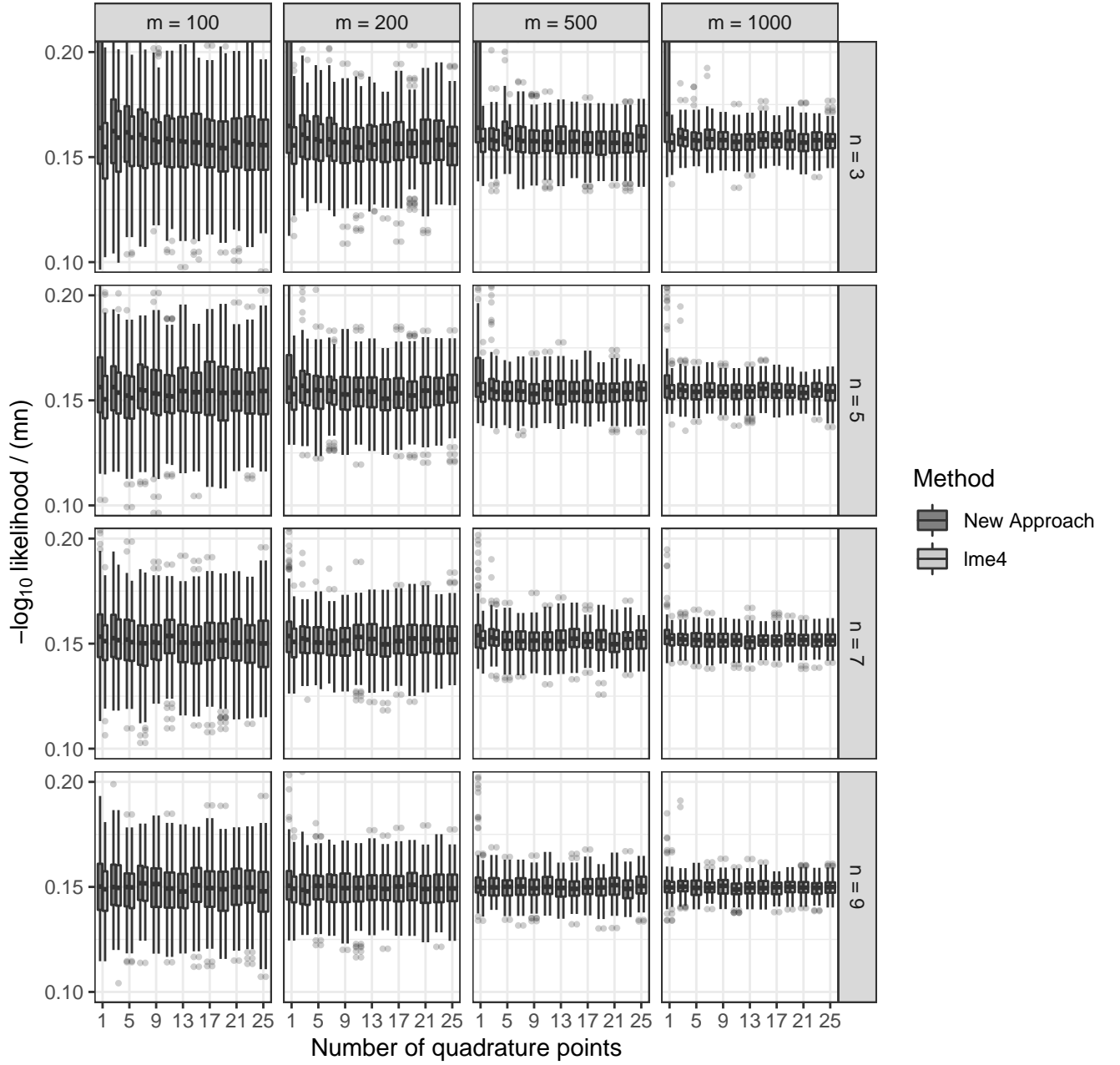


Figure 42: Values of $-\tilde{\ell}_k^{\text{AQ}}(\hat{\theta}_k^{\text{AQ}})/(N \log 10)$ for each method. The methods broadly return comparable results. The $k = 1$ case is better handled by `lm4` when n is low. The practical implications of this are limited, as the method is not expected to be accurate for low k combined with low n . The practical advice is to k until results stop changing, and it is clear that this would yield similar results from both methods; Figure 41 shows that these results are obtained several times faster using the new method.

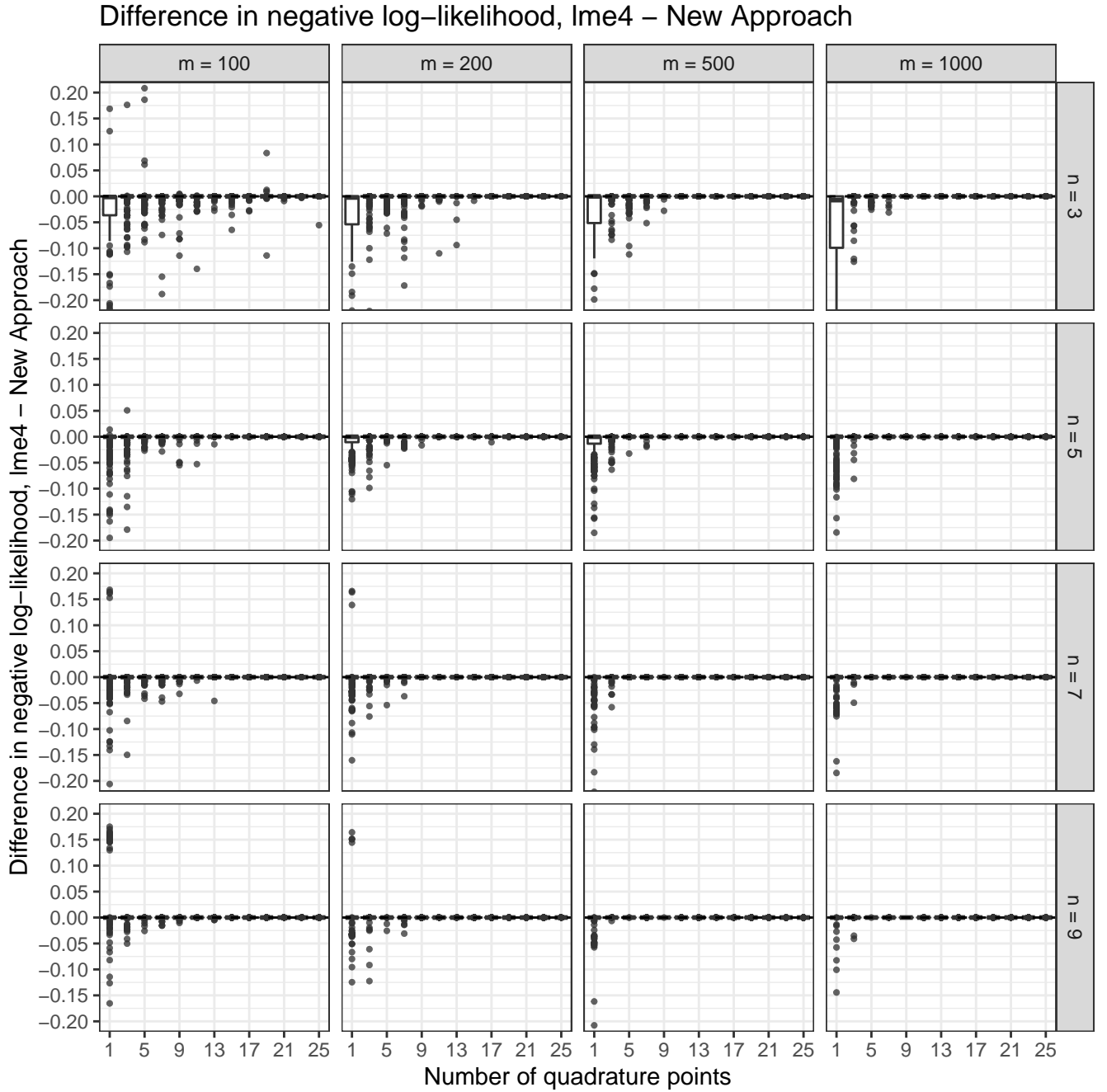


Figure 43: Difference of $-\tilde{\ell}_k^{\text{AQ}}(\hat{\boldsymbol{\theta}}_k^{\text{AQ}})/N$ for `lme4` minus the new method. A positive value indicates that the new method achieved a lower value of $-\tilde{\ell}_k^{\text{AQ}}(\hat{\boldsymbol{\theta}}_k^{\text{AQ}})$ than `lme4`. The methods broadly return similar results, with `lme4` achieving superior results in a small number of the 1000 simulated data sets, for smaller values of k . The practical implications of this are limited, as the advice is to k until results stop changing, and it is clear that this would yield similar results from both methods; Figure 41 shows that these results are obtained several times faster using the new method.

Average log–norm of gradient by method

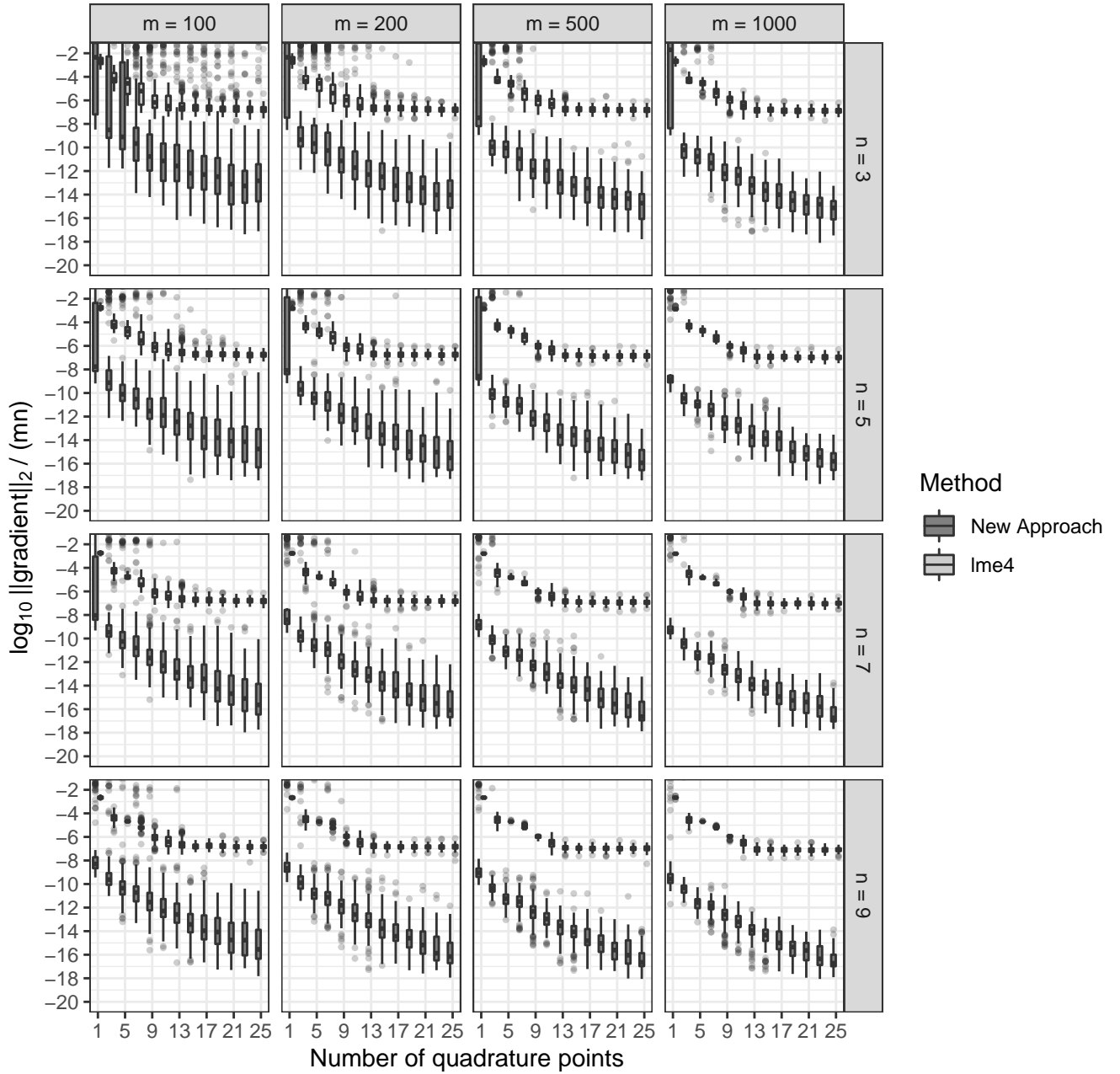


Figure 44: Values of $\log_{10} \|\nabla \tilde{\ell}_k^{\text{AQ}}(\hat{\boldsymbol{\theta}}_k^{\text{AQ}})\|/N$ for each method. The new method appears to return smaller gradient norms than `lme4` overall, and hence achieves superior performance on this metric. We emphasize that the performance of `lme4` is also quite satisfactory, and when combined with Figure 41, the conclusion is that the two methods performed similarly with the new approach returning results several times faster; this figure serves to confirm that the new approach does not achieve these higher run times at the expense of satisfactory performance.

Difference in log-norm of gradient, lme4 – New Approach

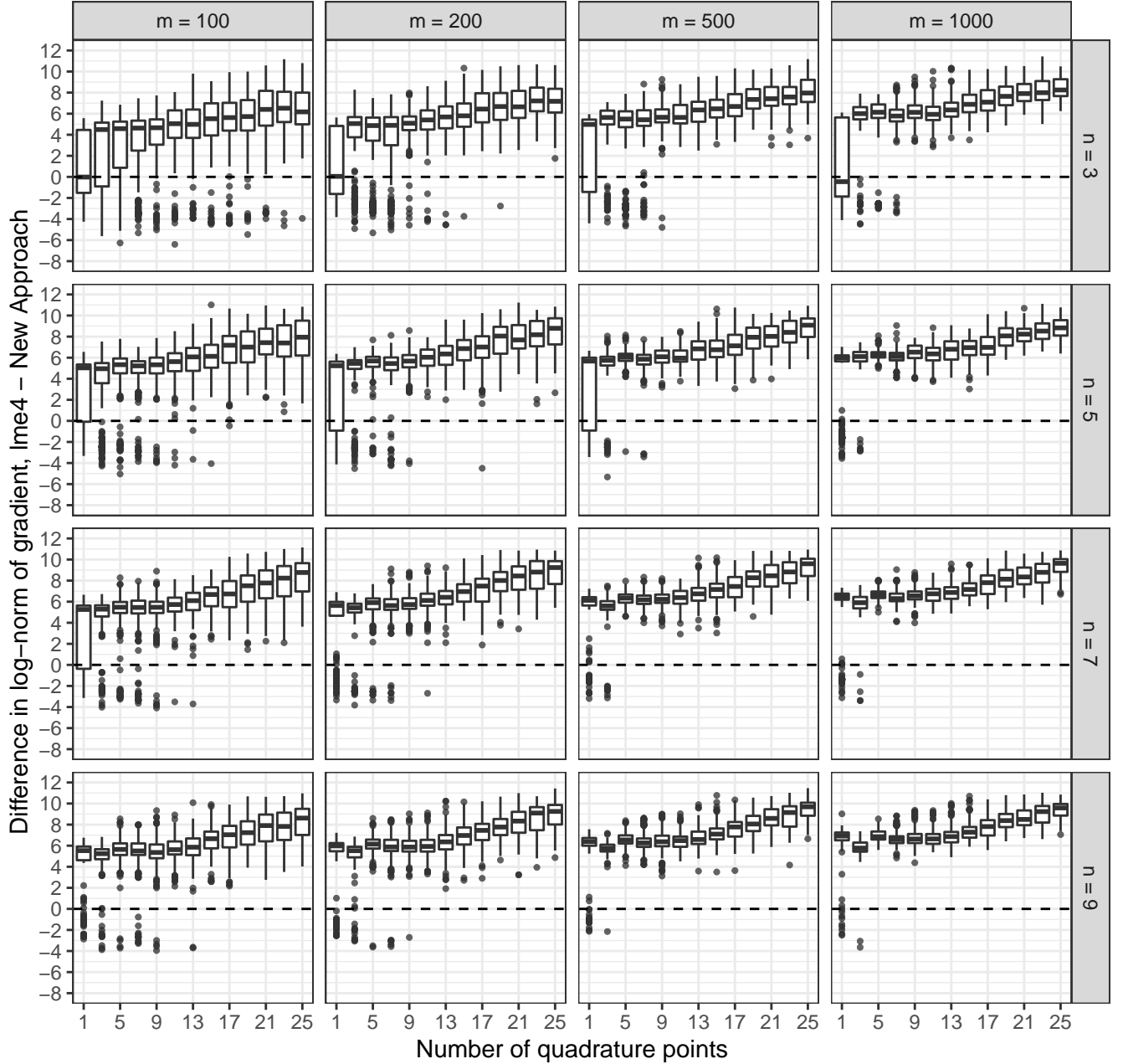


Figure 45: Difference of $\log_{10} \|\nabla \tilde{\ell}_k^{\text{AQ}}(\hat{\theta}_k^{\text{AQ}})\|$ for `lme4` minus the new method. A positive value indicates that the new method achieved a lower value of $-\tilde{\ell}_k^{\text{AQ}}(\hat{\theta}_k^{\text{AQ}})$ than `lme4`. The new method appears to return smaller gradient norms than `lme4` overall, and hence achieves superior performance on this metric. Combined with Figure 41, we conclude that the new approach achieves faster computation times than `lme4` without sacrificing performance.

C.2.3 Comparison with `glmmTMB`

The `glmmTMB` package implements the Laplace approximation via automatic differentiation using the `TMB` package. While we do not advocate the use of the Laplace approximation to fit the mixed models discussed in this paper, it is of interest to compare how a partial implementation of the gradient-based methods we investigate here via automatic differentiation compares to our present implementation. We find that our implementation is slightly faster except for the case of a large number of small groups (m large and n small). Care should be taken to not over-interpret these results, as the efficiency of both the new method and any method based on automatic differentiation will be sensitive to implementation details.

C.3 Additional simulation: scalar random effects

In this supplement only, we repeat Simulation 1 for the less interesting case of the scalar random effects model (15). Figures 47 – 57 show the results. The only interesting point is that the coverage for the Laplace approximation appears to get worse as n increases for β_0 and σ , despite the bias decreasing. This can be explained by looking at the plots of confidence interval lengths; for $k = 1$, the lengths of the intervals for β_0 and σ get much smaller for larger n , leading to worse coverage even with slightly less bias. As with all such scenarios in all of the simulations here, the solution is to increase k .

Relative Computation Times, glmmTMB / New Approach

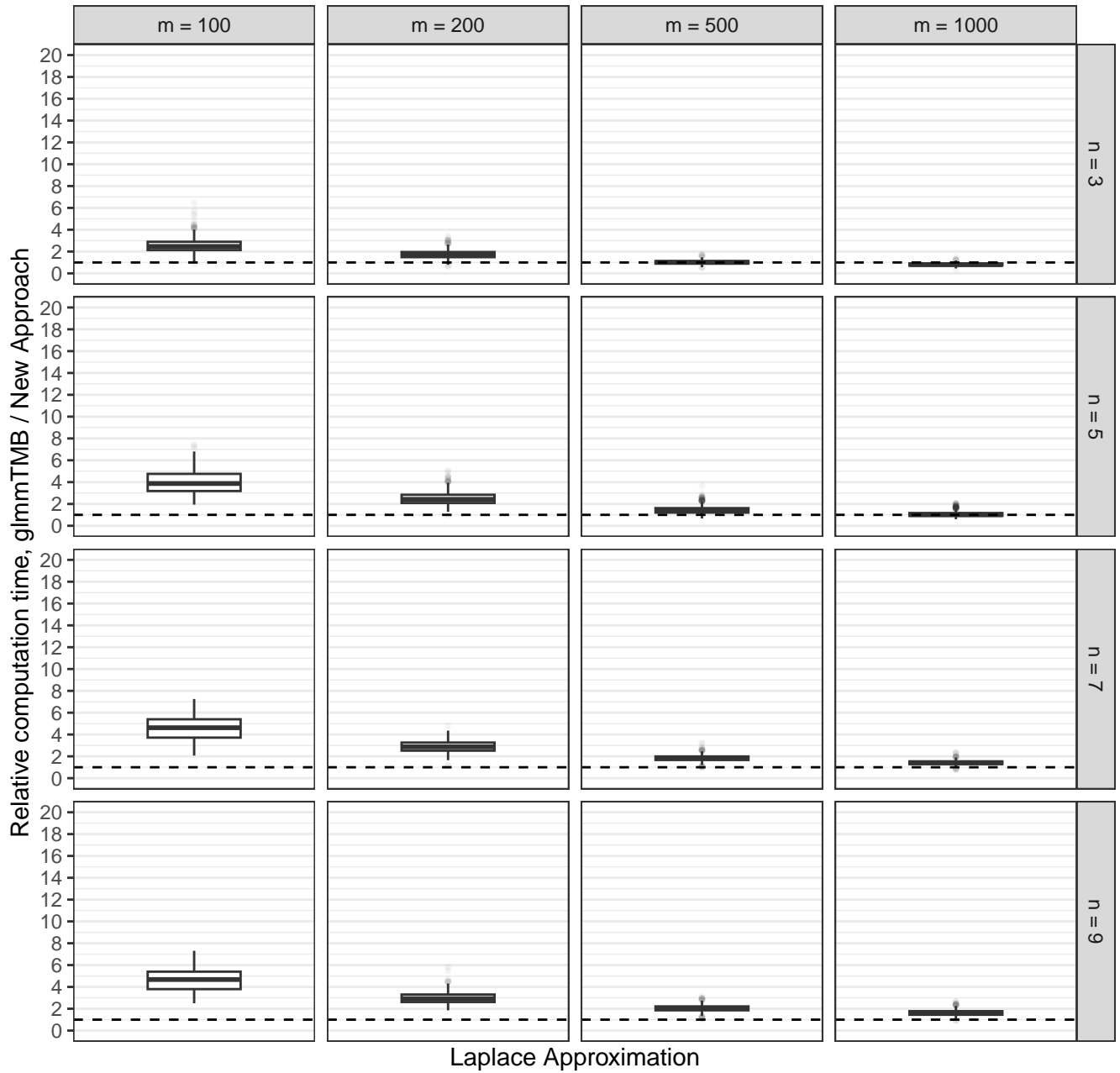


Figure 46: Relative computation times for `glmmTMB` compared to the new method; for example, a value of 2 indicates that `glmmTMB` ran in twice as much time as the new method. Only the Laplace approximation ($k = 1$) is shown because this is what `glmmTMB` computes.

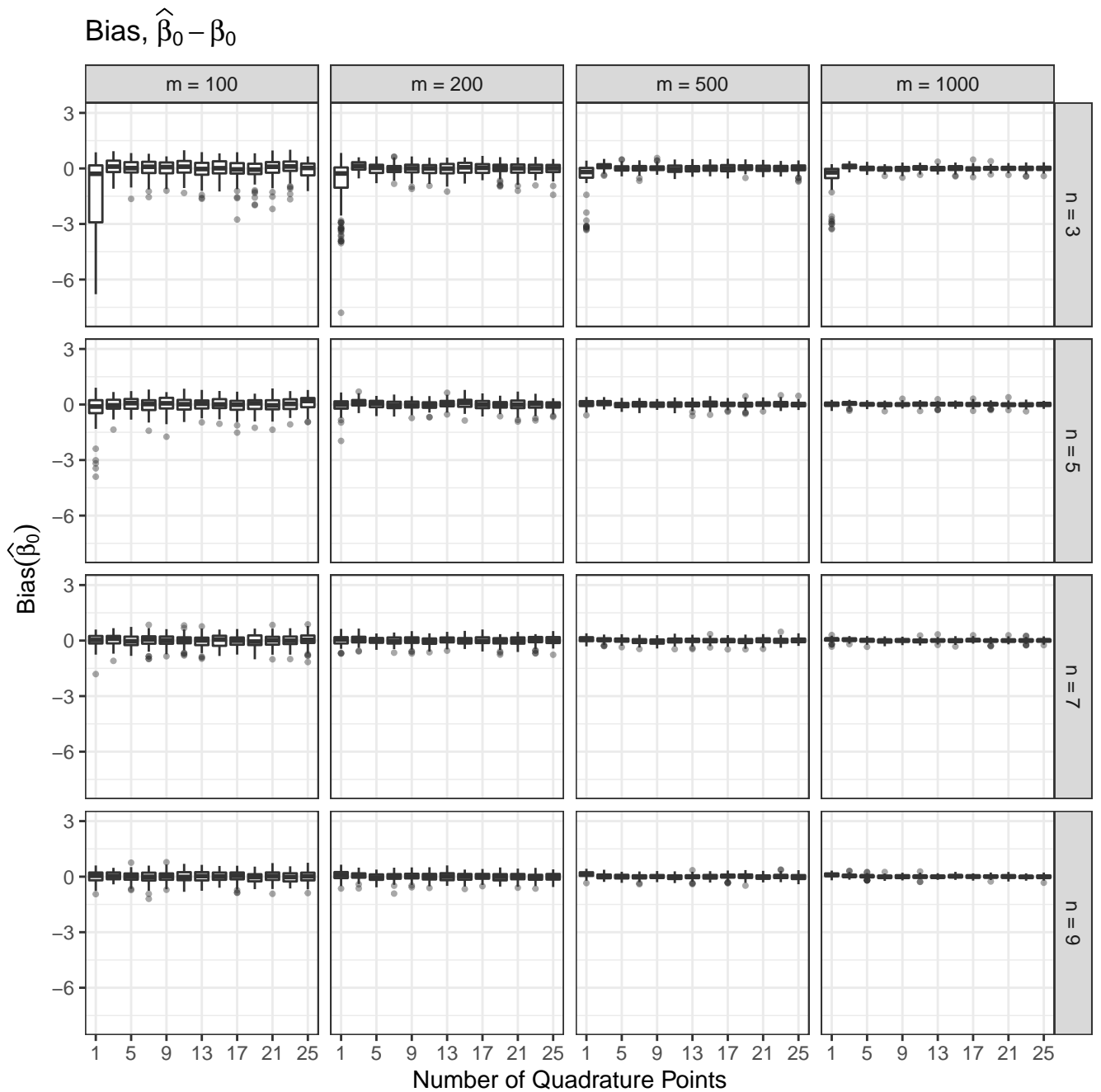


Figure 47: Empirical bias, $\hat{\beta}_0 - \beta_0$, for β_0 from the random intercepts model (15), based on 1000 sets of simulated data. The Laplace approximation exhibits high bias for low to moderate n . This is mitigated by increasing k .

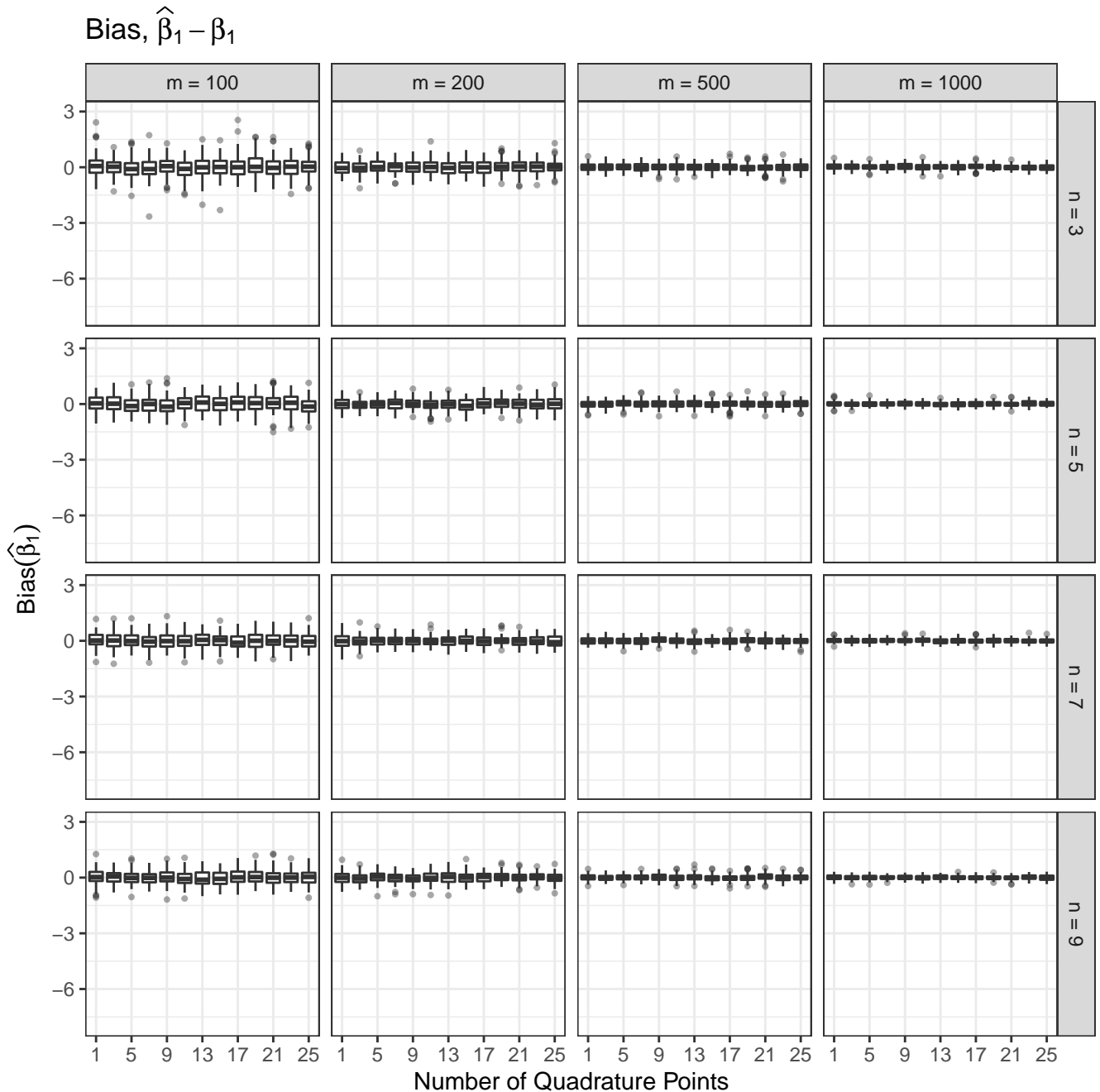


Figure 48: Empirical bias, $\hat{\beta}_1 - \beta_1$, for β_1 from the random intercepts model (15), based on 1000 sets of simulated data. All values of k appear to yield low bias estimates.

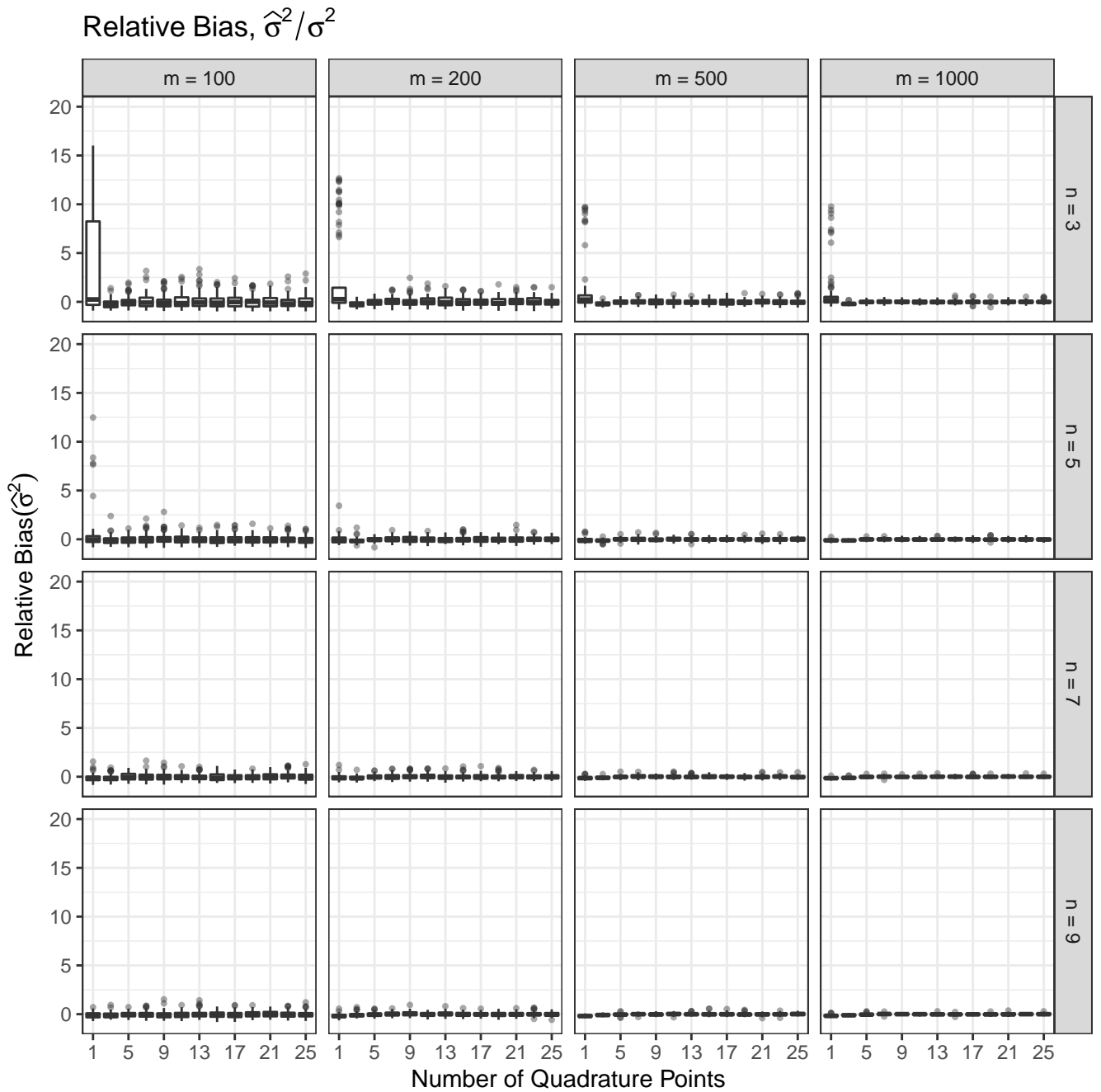


Figure 49: Empirical relative bias, $\hat{\sigma}^2/\sigma^2$, for σ^2 from the random intercepts model (15), based on 1000 sets of simulated data. The y-axis range is very large so that the scale of the relative bias for the Laplace approximation with low n is visible. For $k > 1$, taking k larger leads to somewhat reduced bias across values of m and n .

Relative Bias, $\hat{\sigma}^2/\sigma^2$

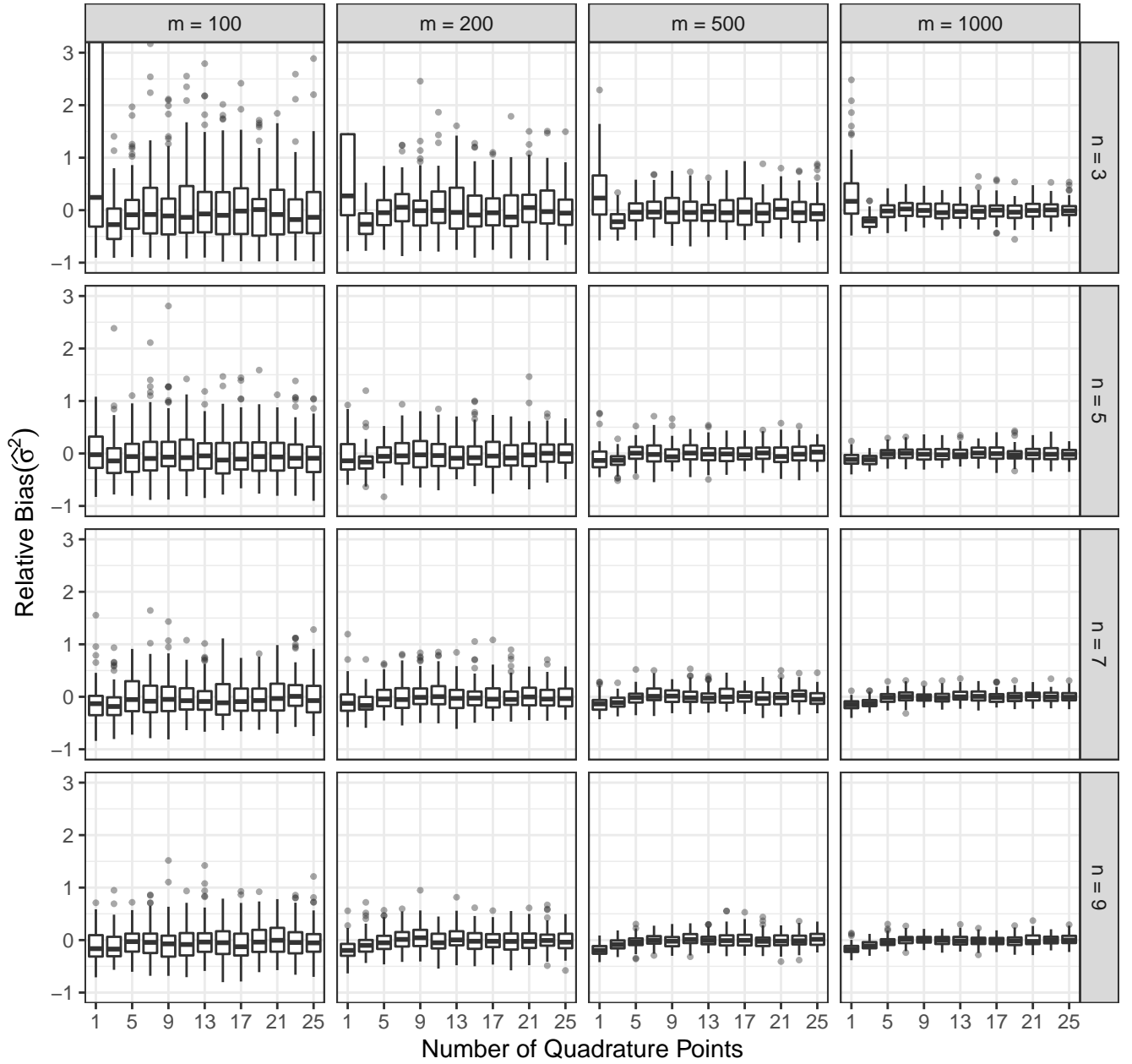


Figure 50: Empirical relative bias, $\hat{\sigma}^2/\sigma^2$, for σ^2 from the random intercepts model (15), based on 1000 sets of simulated data. The y-axis range is zoomed in so that results are visible for all except the Laplace approximation. For $k > 1$, taking k larger leads to somewhat reduced bias across values of m and n .

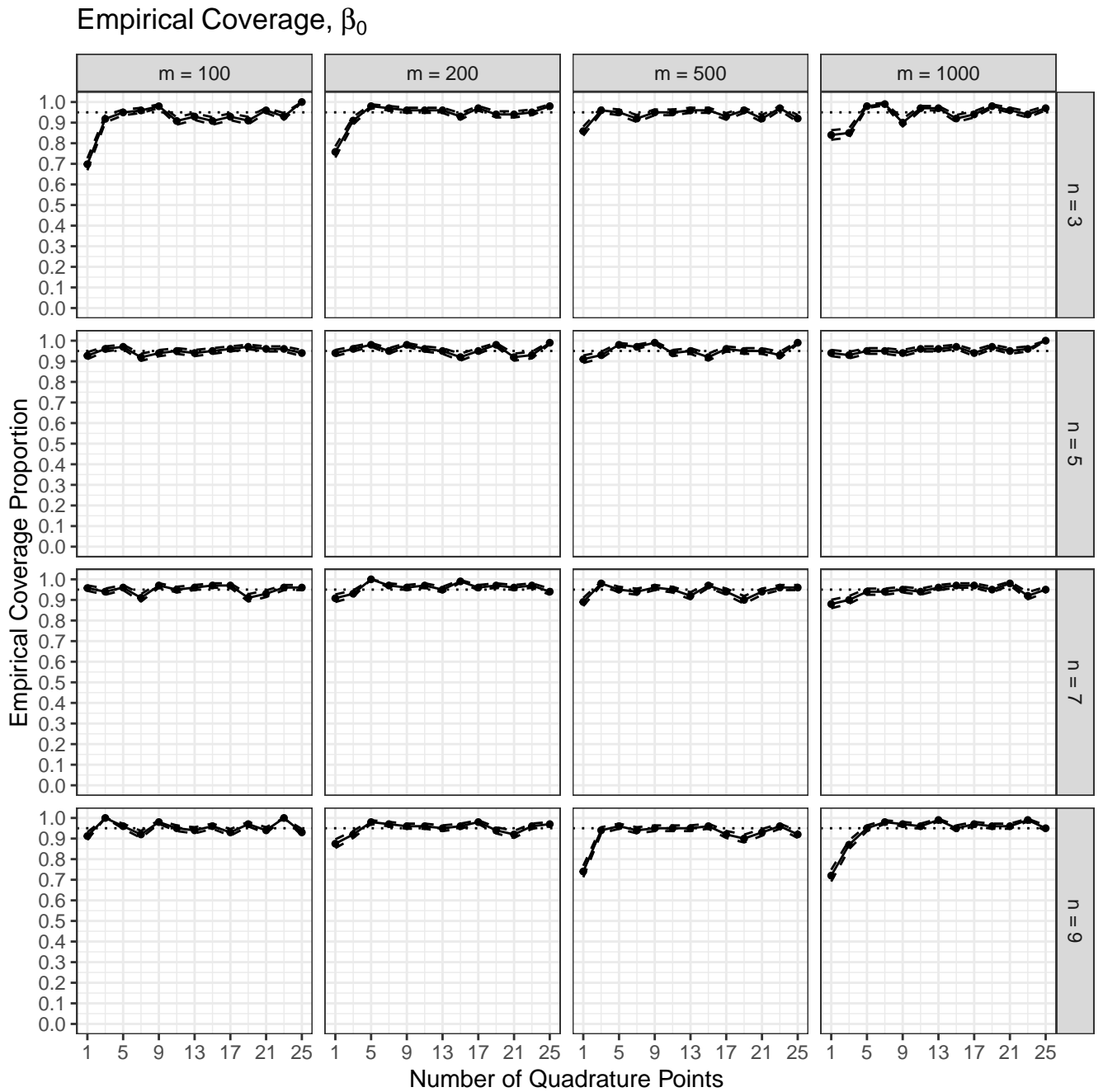


Figure 51: Empirical coverage proportion for $\hat{\beta}_0$ from the random intercepts model (15), based on 1000 sets of simulated data. The Laplace ($k = 1$) coverage is low for $n = 3$ due to high bias and poor standard error estimation. In all cases, taking k large enough leads to nominal empirical coverage, motivating the use of adaptive quadrature for fitting these models.

Empirical Coverage, β_1

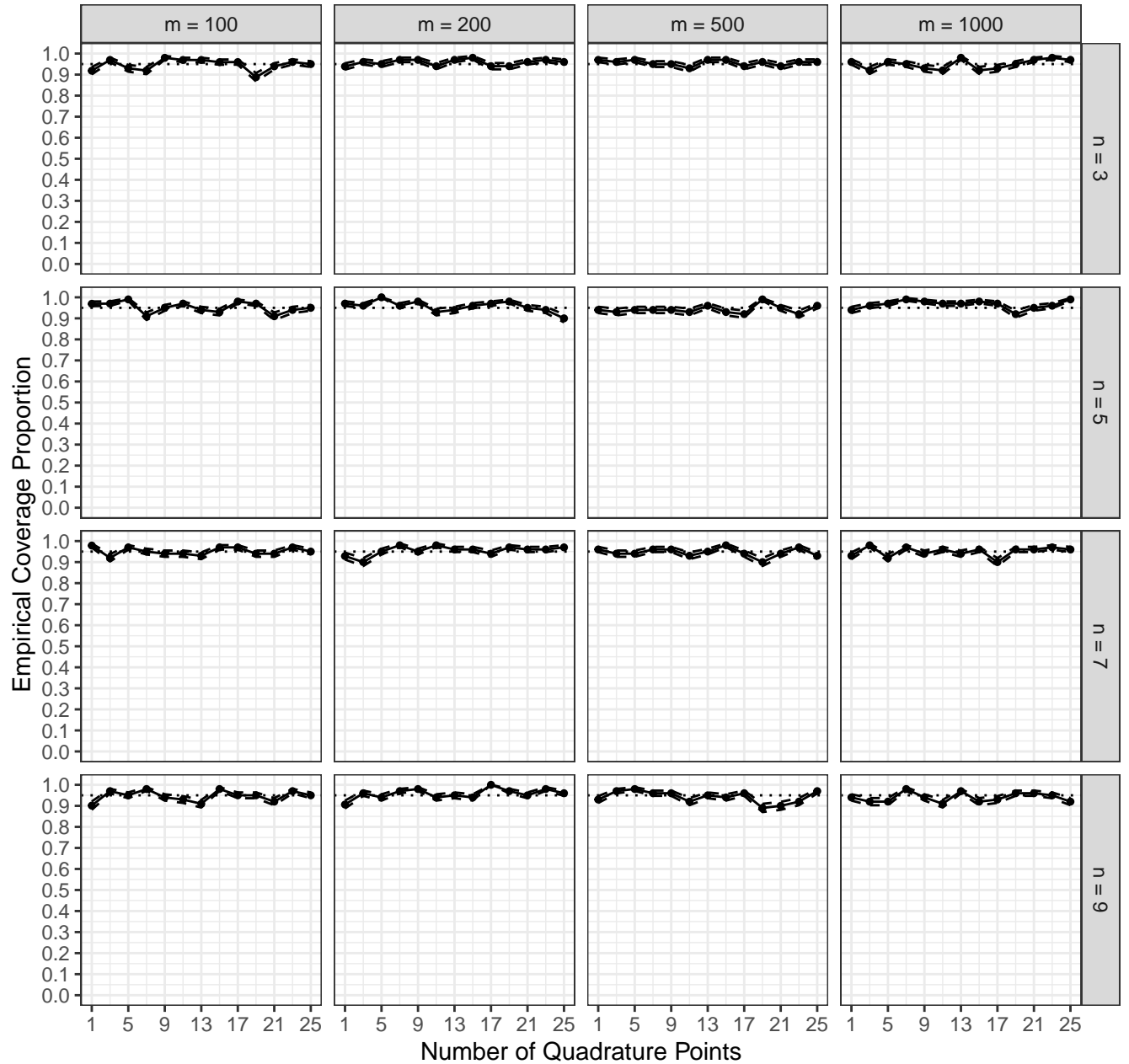


Figure 52: Empirical coverage proportion for $\hat{\beta}_1$ from the random intercepts model (15), based on 1000 sets of simulated data. The coverage is nominal across all values of m, n, k , which is expected for this parameter in this model.

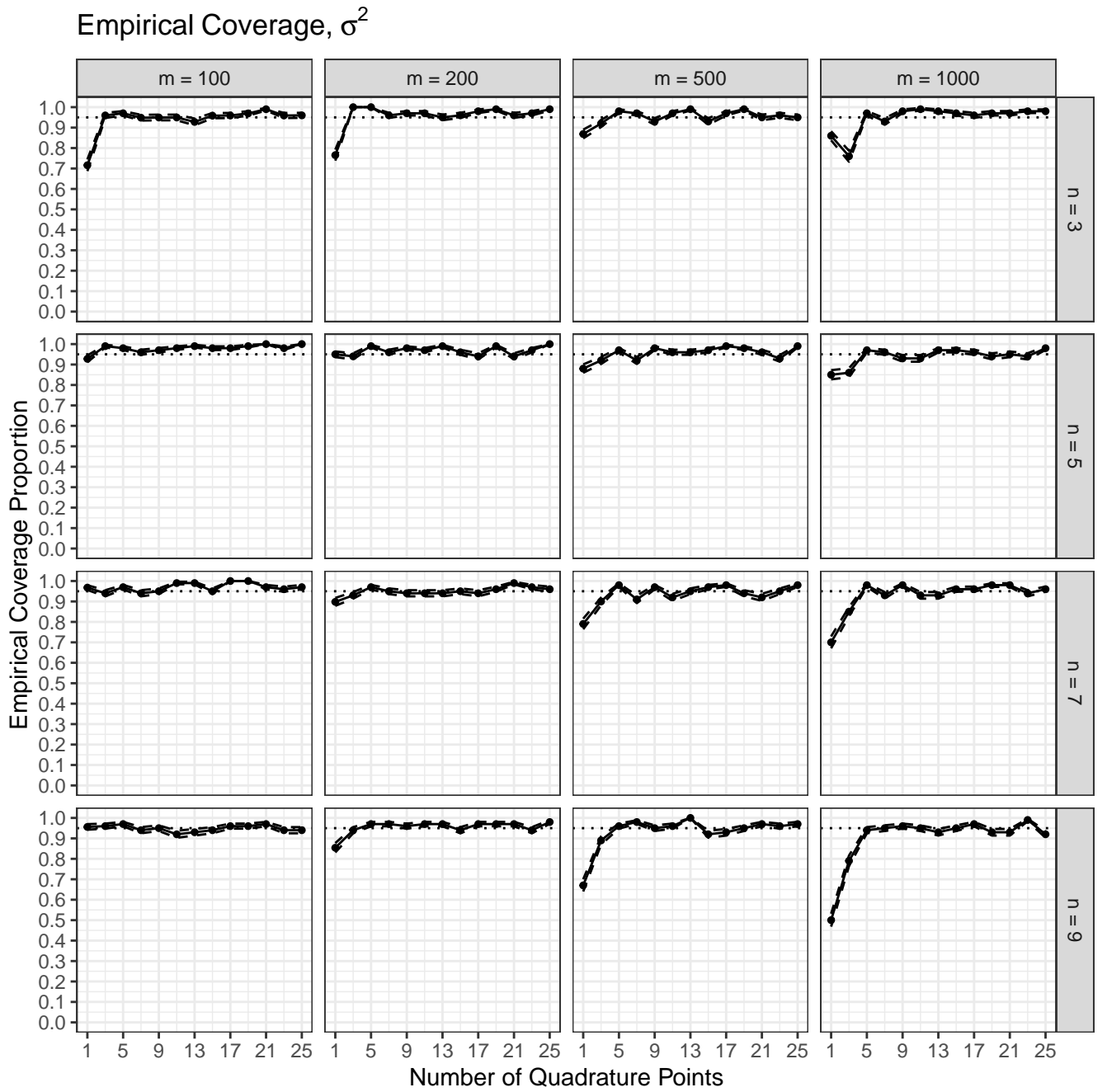


Figure 53: Empirical coverage proportion for $\hat{\sigma}^2$ from the random intercepts model (15), based on 1000 sets of simulated data. The Laplace ($k = 1$) coverage is low for $n = 3, 5$ due to high bias and poor standard error estimation. As n increases, the bias decreases but the standard error also decreases, leading to worsening coverage. Again, the solution is to simply use a larger k .

Length of Confidence Intervals, β_0

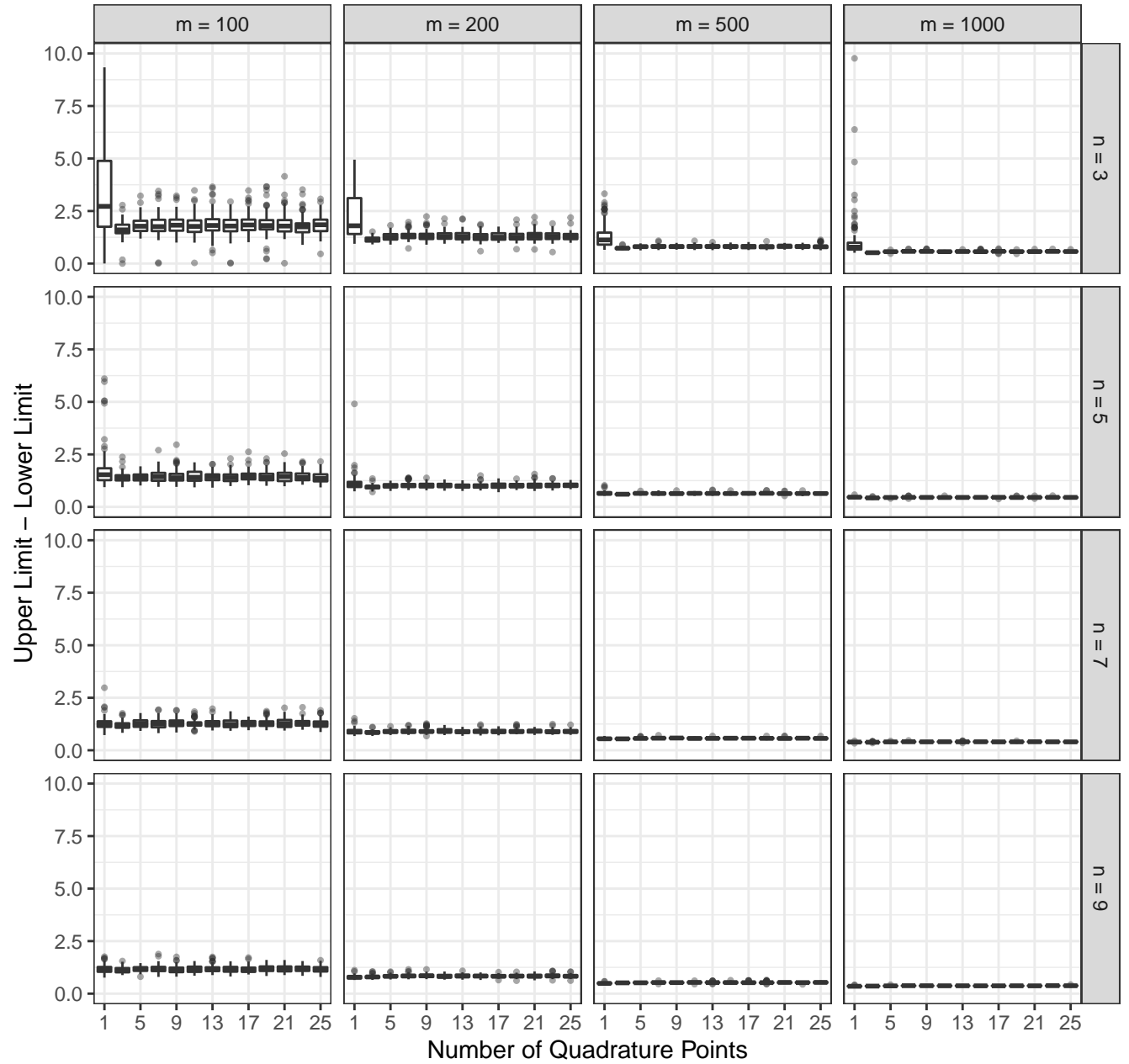


Figure 54: Length of the Wald intervals for $\hat{\beta}_0$ from the random intercepts model (15), based on 1000 sets of simulated data. The Laplace ($k = 1$) intervals are substantially wider than those for larger k .

Length of Confidence Intervals, β_1

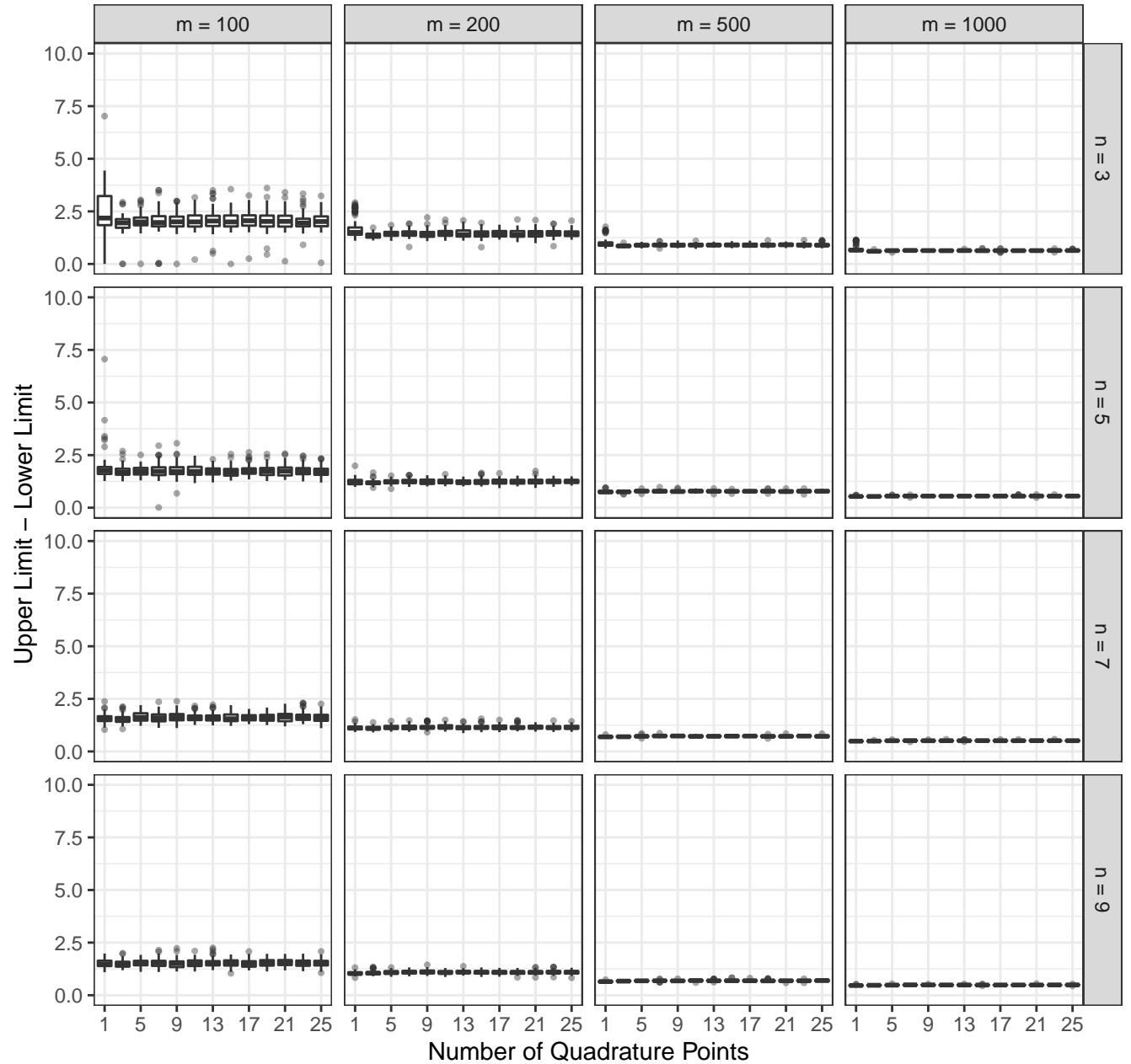


Figure 55: Length of the Wald intervals for $\hat{\beta}_1$ from the random intercepts model (15), based on 1000 sets of simulated data. The Laplace ($k = 1$) intervals are somewhat wider than those for larger k .

Length of Confidence Intervals, σ_1^2

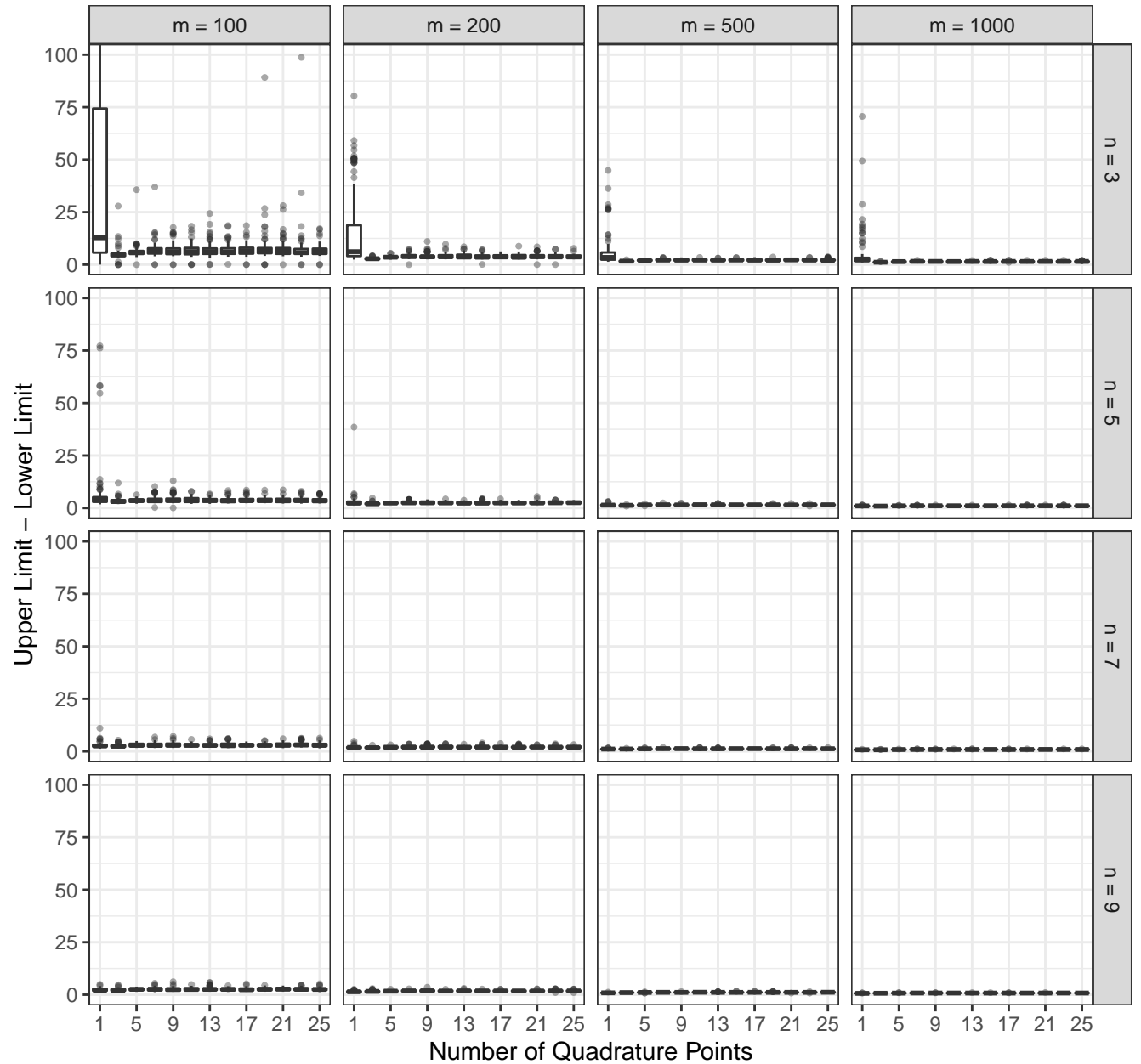


Figure 56: Length of the Wald intervals for $\hat{\sigma}_1^2$ from the random intercepts model (15), based on 1000 sets of simulated data. The Laplace ($k = 1$) intervals are orders of magnitude wider than those for larger k ; the y-axis is zoomed out to capture this.

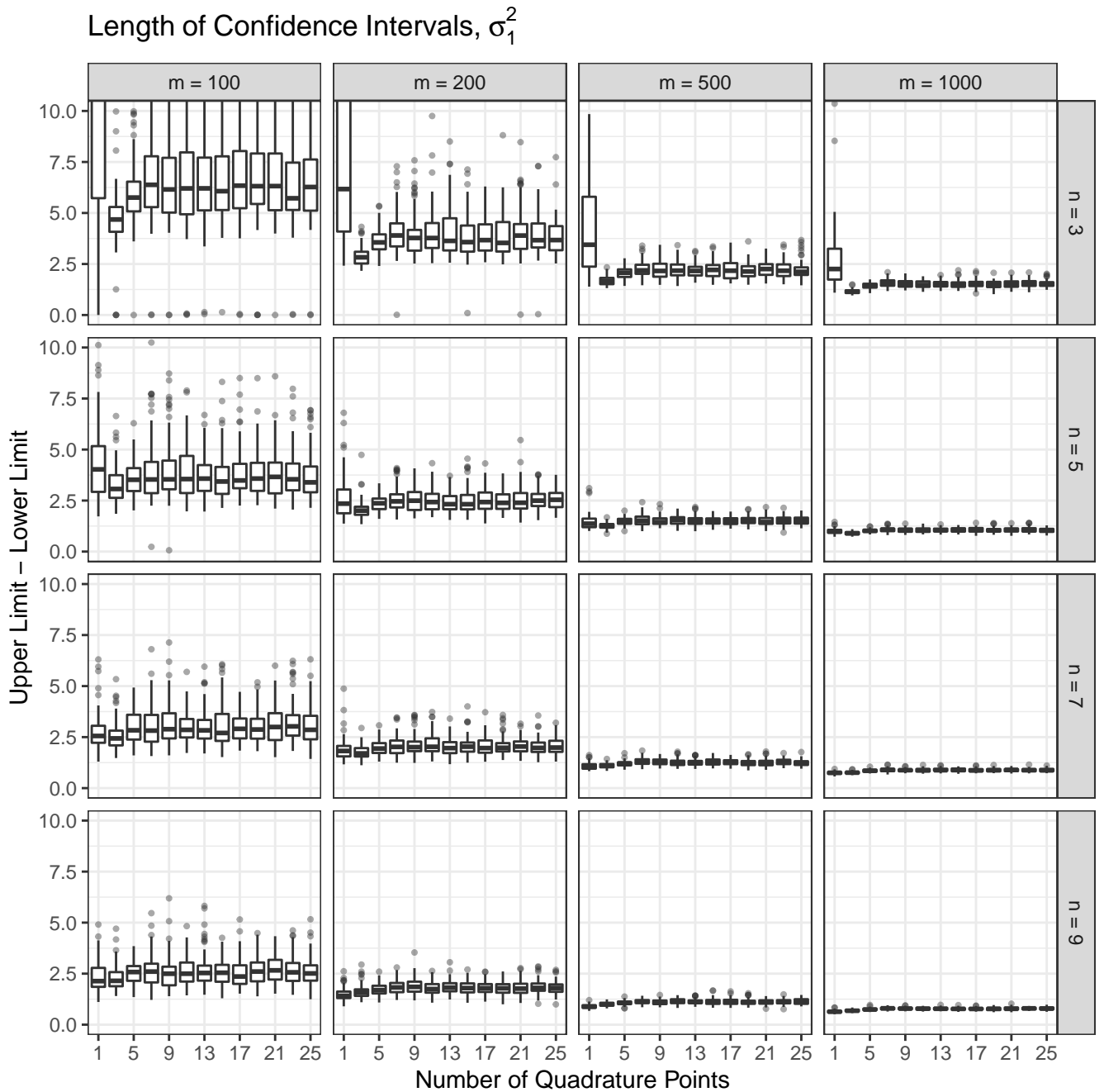


Figure 57: Length of the Wald intervals for $\hat{\sigma}_1^2$ from the random intercepts model (15), based on 1000 sets of simulated data. The y-axis is zoomed in, which obscures some of the lengths of the Laplace ($k = 1$) intervals.

D Additional details for data analyses

D.1 Smoking cessation

We report parameter estimates and both absolute and relative run times for the smoking cessation data from Section 5.1. The following model was fit with both the new procedure as well as **GLMMadaptive**:

$$Y_{ij} \mid \mathbf{u}_i \stackrel{\text{ind}}{\sim} \text{Bern}(p_{ij}), \quad \mathbf{u}_i \stackrel{\text{iid}}{\sim} \mathcal{N}\{\mathbf{0}, \boldsymbol{\Sigma}(\boldsymbol{\sigma})\}, \quad \log \frac{p_{ij}}{1 - p_{ij}} = \beta_0 + \beta_1 x_i + \beta_2 t_j + \beta_3 x_i t_j + u_{i1} + u_{i2} t_j. \quad (16)$$

Here Y_{ij} is a binary indicator where value 1 indicates smoking cessation for subject i at time j . The covariate x_i is a binary group indicator with value 0 corresponding to no social support and value 1 to the subject receiving a type of social support. The covariate t_j is a normalized time value representing follow-up at 0, 6, 12, and 24 months post-intervention. Some subjects had missing follow-ups. There are hence $n_i \in \{1, \dots, 4\}$ measurements on each of the $m = 489$ subjects. Note that this overall setup is nearly identical to model (14) used in the simulations, save for the varying number of measurements per subject.

Figures 58 – 61 show the parameter estimates and computation times for the new approach and **GLMMadaptive**. Selected such results are shown in the manuscript. In all cases, inferences stop changing after k is increased large enough. The new approach yields comparable inferences to **GLMMadaptive** with the latter taking 3 – 10 times as long as the new method. For σ_{12} , the Wald intervals (Figure 59) produced by the new method are narrower than those from **GLMMadaptive**; combined with the nominal coverage for these intervals for this parameter shown in simulations (Figure 21), this may be regarded as an advantage of the new approach.

Point and interval estimates for β parameters

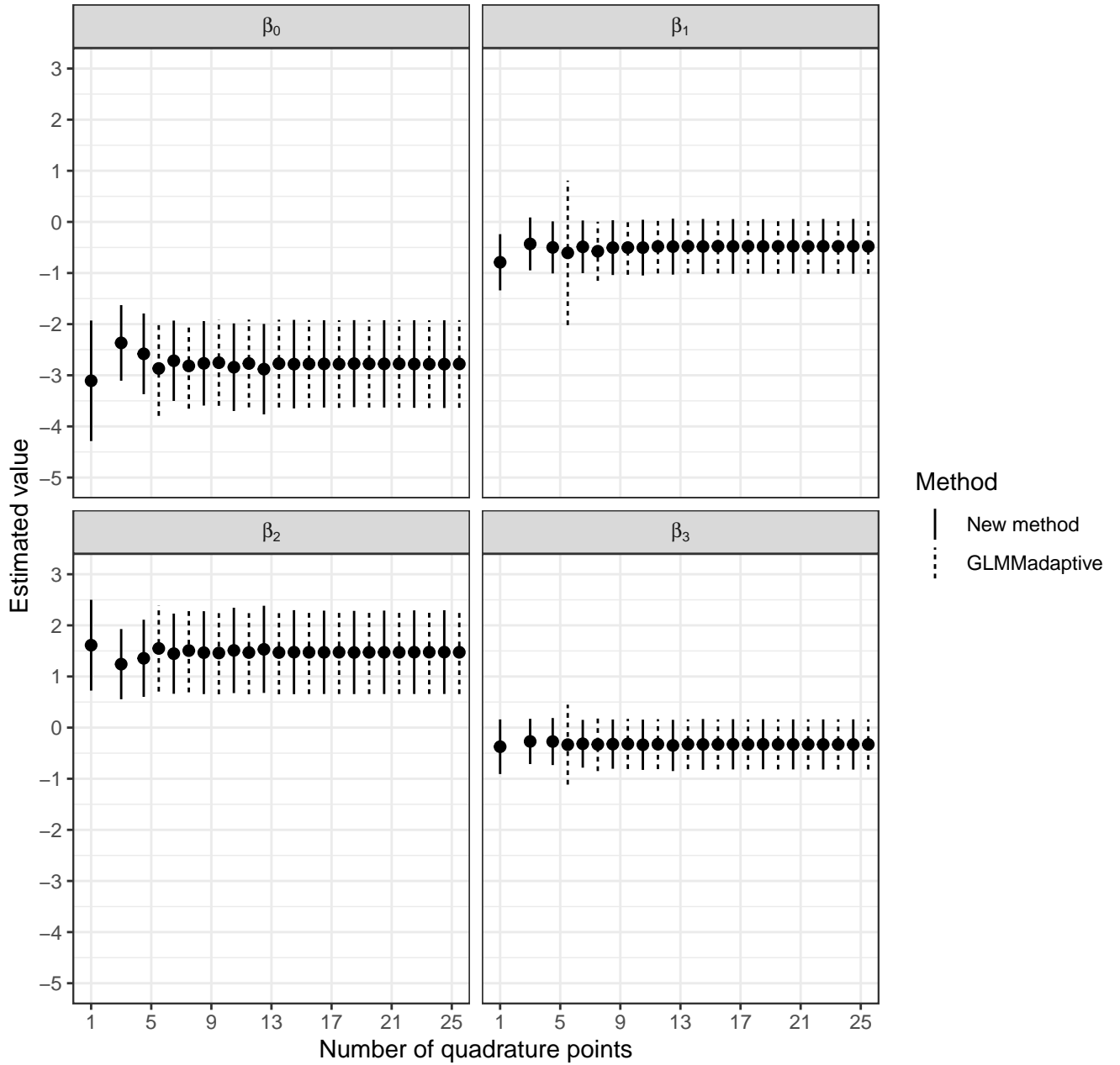


Figure 58: Point and interval estimates for regression coefficients in the smoking cessation data, for the new method and `GLMMadaptive`. The new method successfully returns a positive-definite Hessian matrix for all values of k ; `GLMMadaptive` does so only for $k \geq 7$ or so. The two methods return comparable inferences at high enough values of k . For all parameters, there is a clear point at which increasing k stops changing the point and interval estimates.

Point and interval estimates for σ parameters

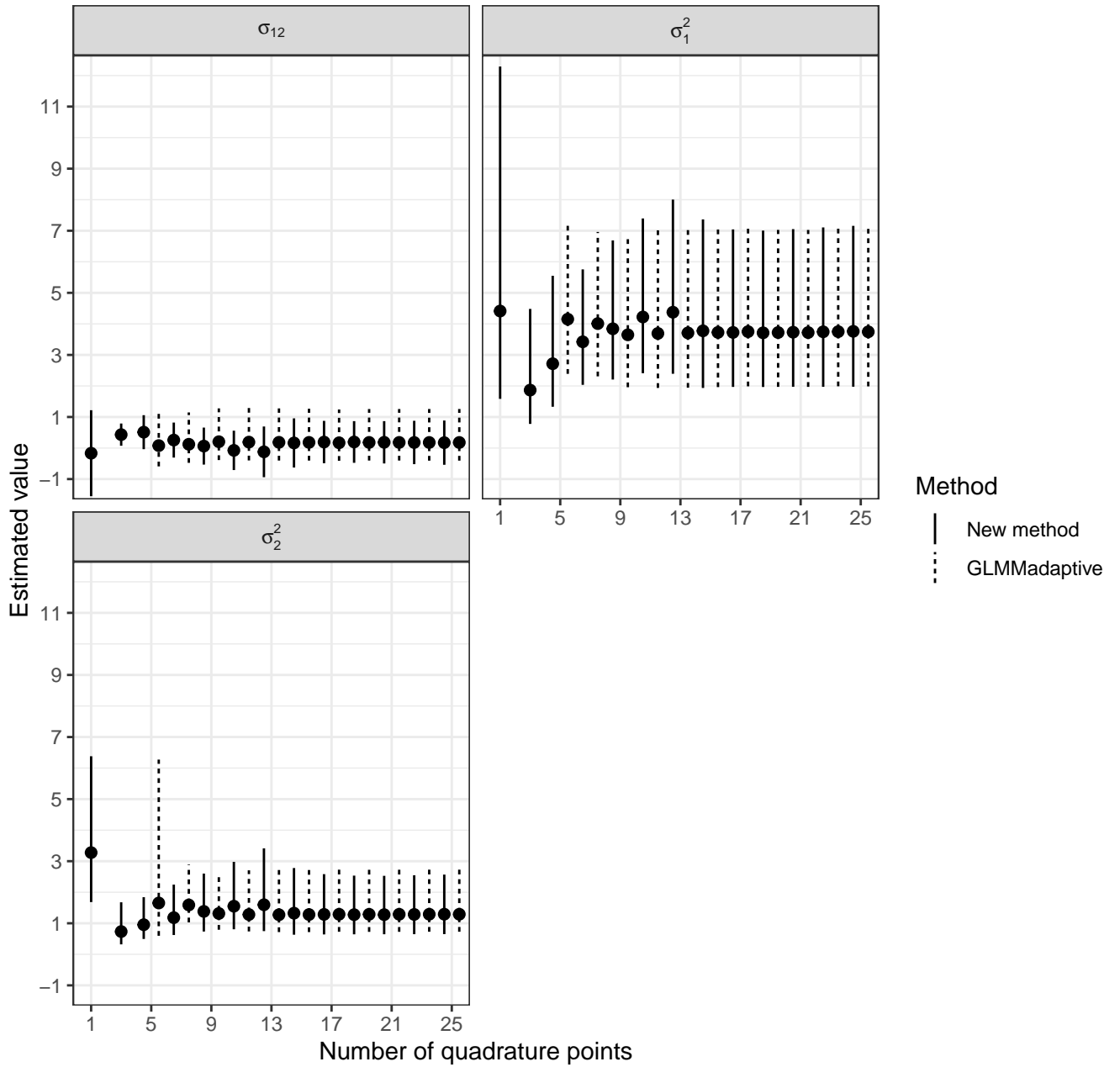


Figure 59: Point and interval estimates for variance components in the smoking cessation data, for the new method and `GLMMadaptive`. The new method successfully returns a positive-definite Hessian matrix for all values of k ; `GLMMadaptive` does so only for $k \geq 5$ or so. The two methods return comparable inferences at high enough values of k . For all parameters, there is a clear point at which increasing k stops changing the point and interval estimates. For σ_2^2 and σ_{12} , the final, stable intervals from the new method are narrower than those from `GLMMadaptive`.

Relative computation times

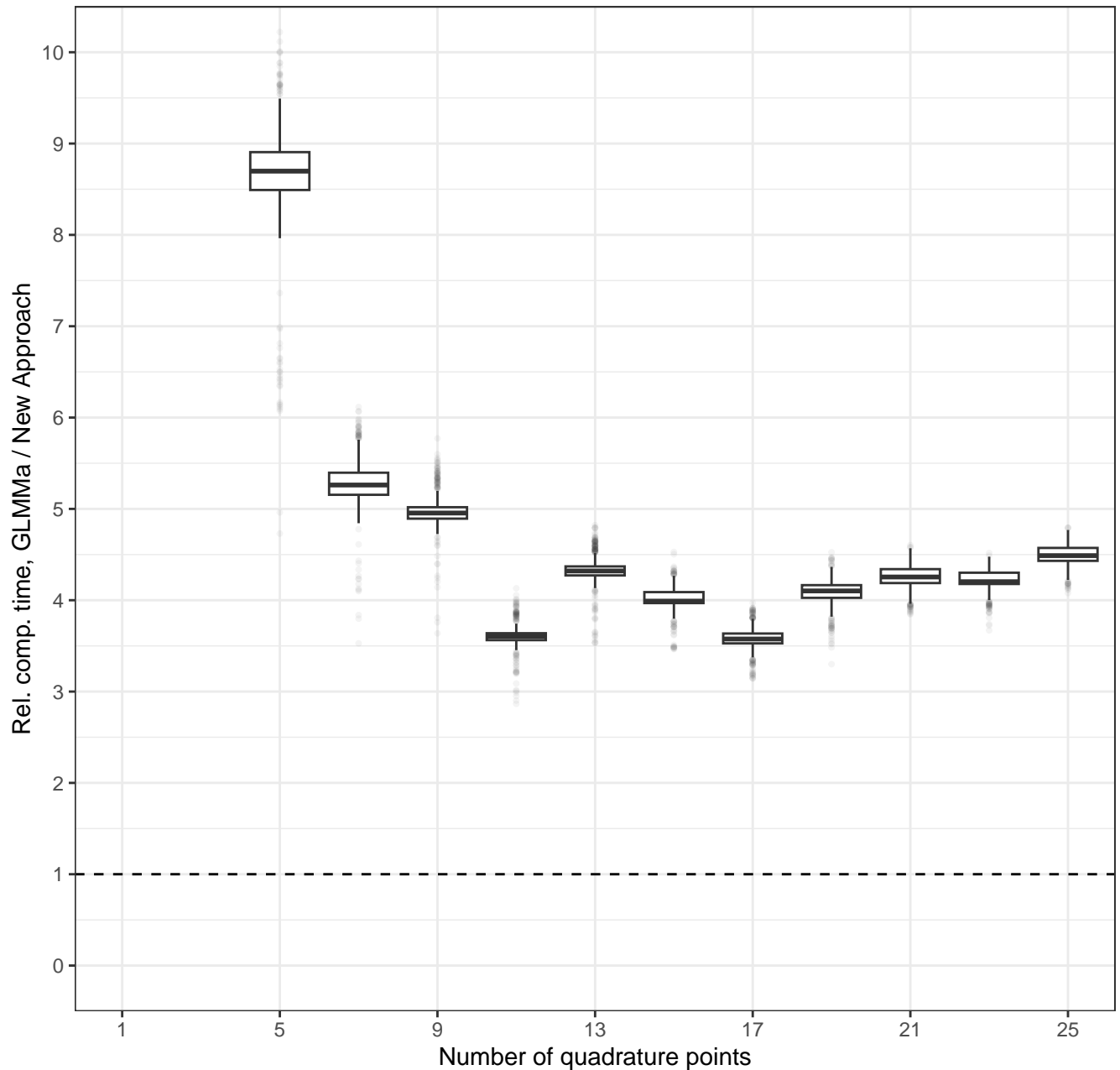


Figure 60: Relative computation times for the smoking cessation data, for the new method and `GLMMadaptive`, over 500 repeated runs. The new method achieves a speedup of between 3 and 10 times, which varies with k , and is never slower than `GLMMadaptive`. The times for $k = 1, 3, 5$ are not shown because `GLMMadaptive` did not return a usable inferential result in these cases.

Absolute computation times (seconds), smoking cessation data

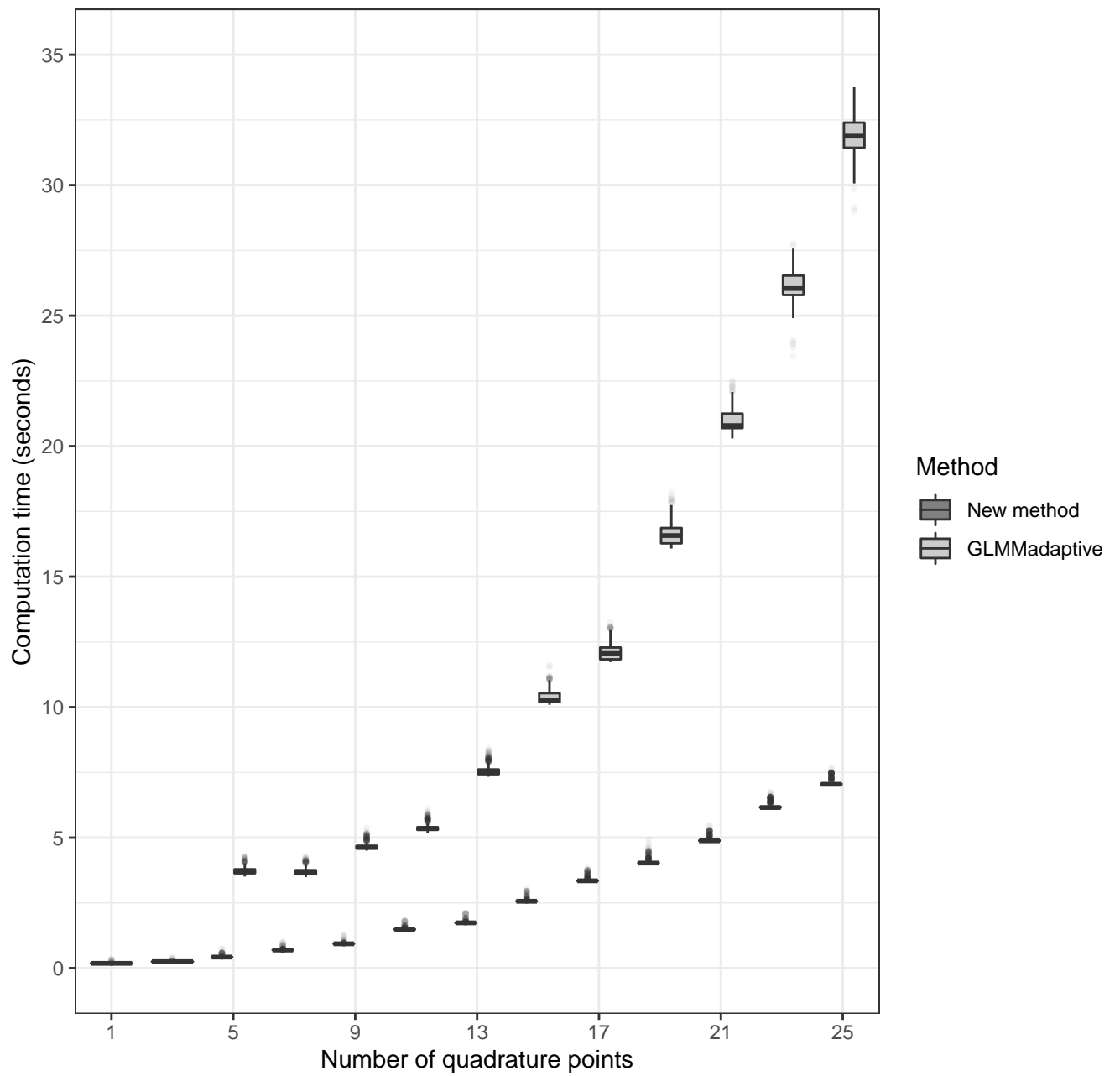


Figure 61: Absolute computation times in seconds for the smoking cessation data, for the new method and `GLMMadaptive`, over 500 repeated runs. Both methods generally take more time for larger k , which is expected. All computations were performed on an M1 Mac book Pro laptop with 10 cores and 64Gb of RAM.

D.2 Toenail fungus treatment

We report parameter estimates and both absolute and relative run times for the toenail fungus treatment data from Section 5.2. The following model was fit with the new procedure as well as **GLMMadaptive** and **lme4**:

$$Y_{ij} \mid u_i \stackrel{\text{ind}}{\sim} \text{Bern}(p_{ij}), \quad u_i \stackrel{\text{iid}}{\sim} N(0, \sigma^2), \quad \log \frac{p_{ij}}{1 - p_{ij}} = \beta_0 + \beta_1 x_i + \beta_2 t_j + \beta_3 x_i t_j + u_{i1}. \quad (17)$$

Here Y_{ij} is a binary indicator with $Y_{ij} = 1$ indicating the absence of toenail infection. There are $i = 1, \dots, m = 294$ subjects who were given an oral treatment for toenail infection, $x_i = 1$, or not, $x_i = 0$. The subjects were followed up at $j = 1, \dots, n_j \in \{1, \dots, 7\}$ times, $t_j = -3, \dots, 3$.

Figures 62 – 65 show the parameter estimates and computation times for the new approach, **GLMMadaptive**, and **lme4**. Selected such results are shown in the manuscript. In all cases, inferences stop changing after k is increased large enough. The new approach yields comparable inferences to **GLMMadaptive** and **lme4**; the former takes 1 – 5 times as long as the new method and the latter takes 3 – 8 times as long. Further, the computation times for **lme4** do *not* include the time taken to produce confidence intervals for σ , because **lme4** does not provide Wald confidence intervals for σ . Instead, it offers computationally intensive profile likelihood and bootstrap confidence intervals for σ . These are shown in Figure 63, and for larger k are very close to the Wald intervals provided by the new approach and **GLMMadaptive**. In a single run, the profile intervals took roughly 60 times longer to compute than the Wald intervals from the new method, with slight variability across values of k . The bootstrap approach requires the user to choose a number of simulated data sets to use, with 500 the recommended default. Using 200 repetitions only, a single run of the procedure took between 1300 – 1600 times as long as the new approach, depending on k , and produced very similar intervals. We remind the reader that the coverages of the Wald intervals for this parameter are found to be nominal in the simulations reported in Figure 53.

Point and interval estimates for β parameters

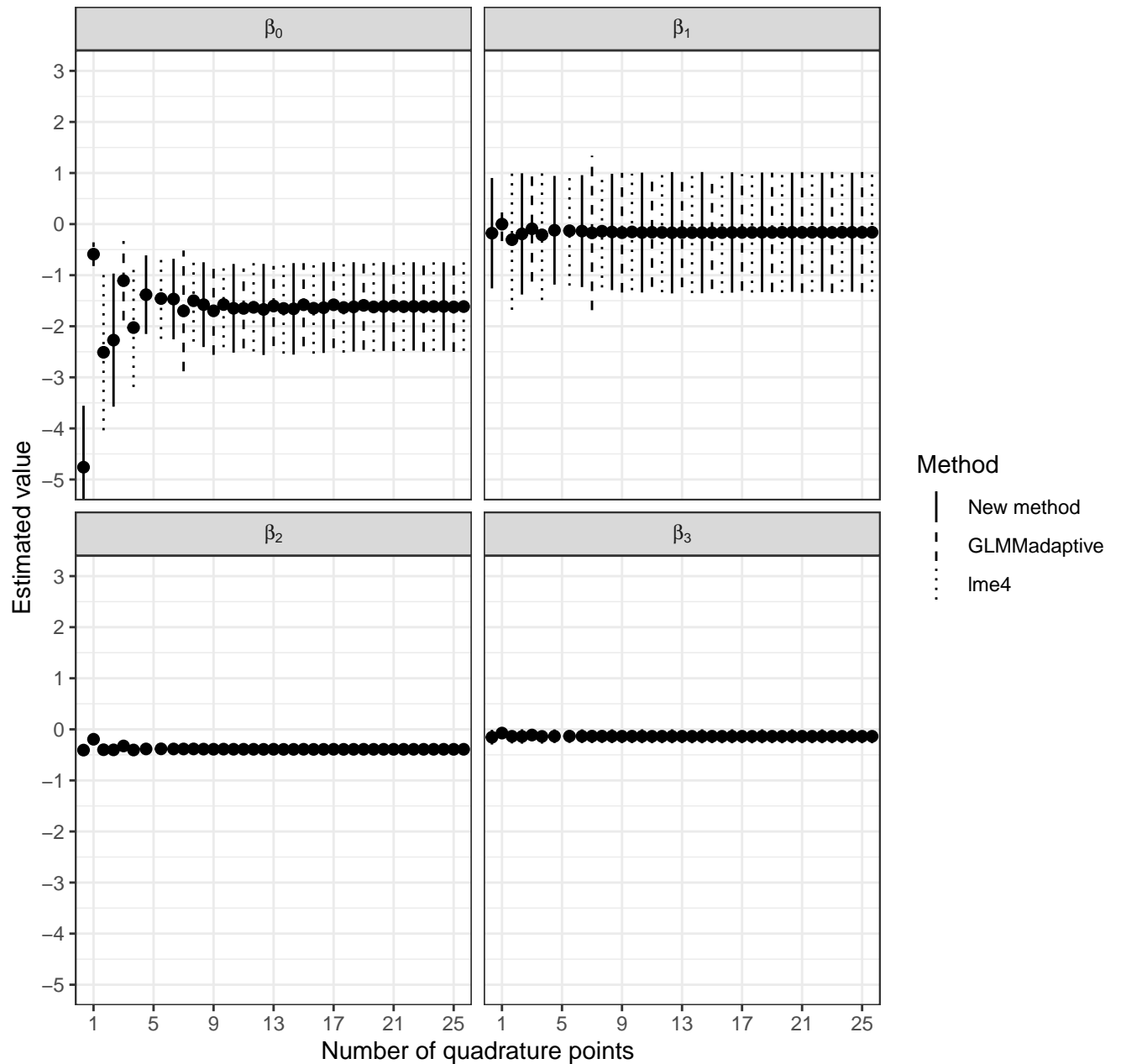


Figure 62: Point and interval estimates for regression coefficients in the toenail fungus treatment data, for the new method, `lme4`, and `GLMMadaptive`. The methods return comparable inferences at high enough values of k . For all parameters, there is a clear point at which increasing k stops changing the point and interval estimates.

Point and interval estimates for σ^2

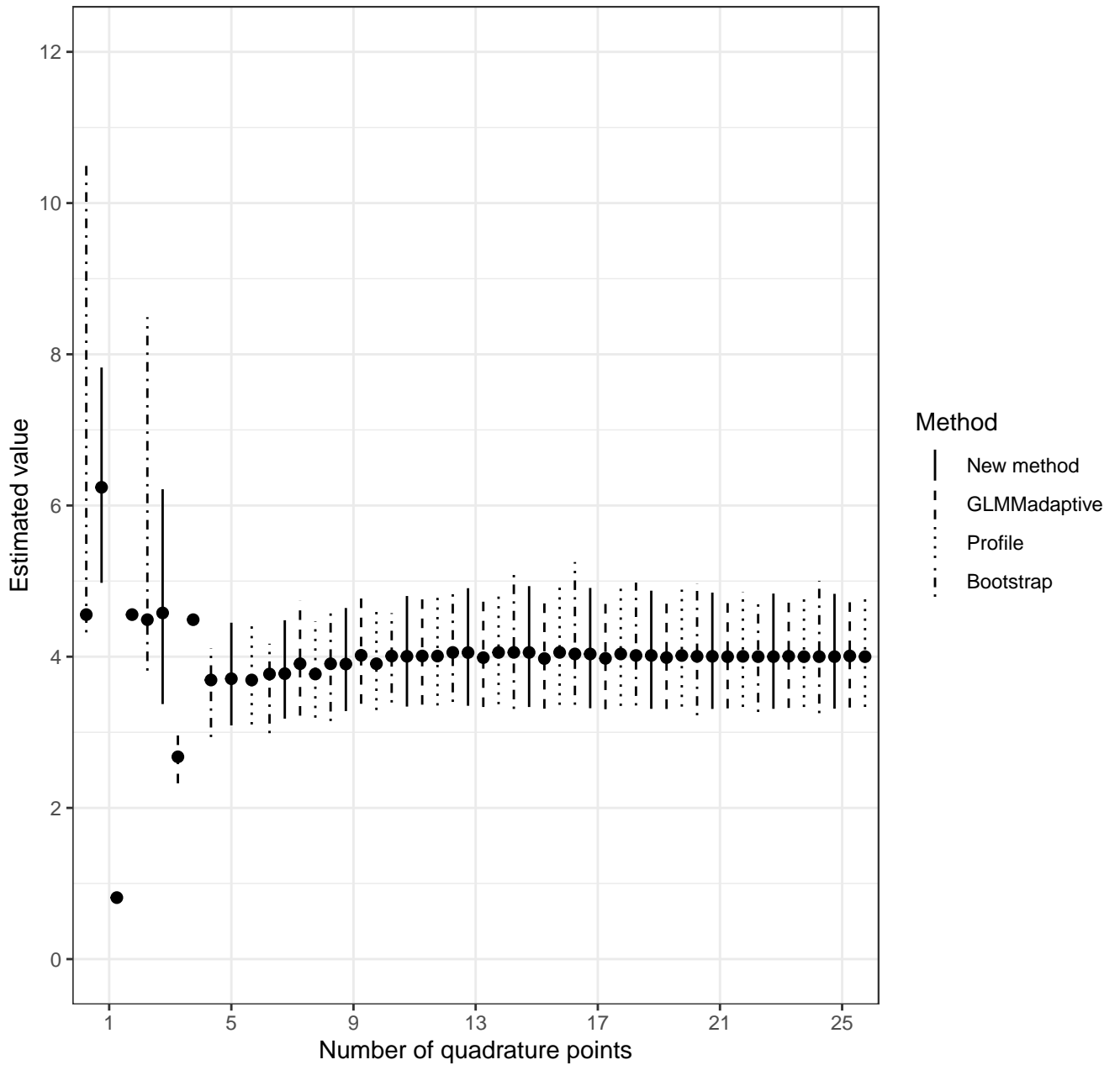


Figure 63: Point and interval estimates for σ in the toenail fungus treatment data, for the new method, `GLMMadaptive`, and `lme4` with both profile likelihood and bootstrap confidence intervals. The methods return comparable inferences at high enough values of k . For all parameters, there is a clear point at which increasing k stops changing the point and interval estimates.

Relative computation times

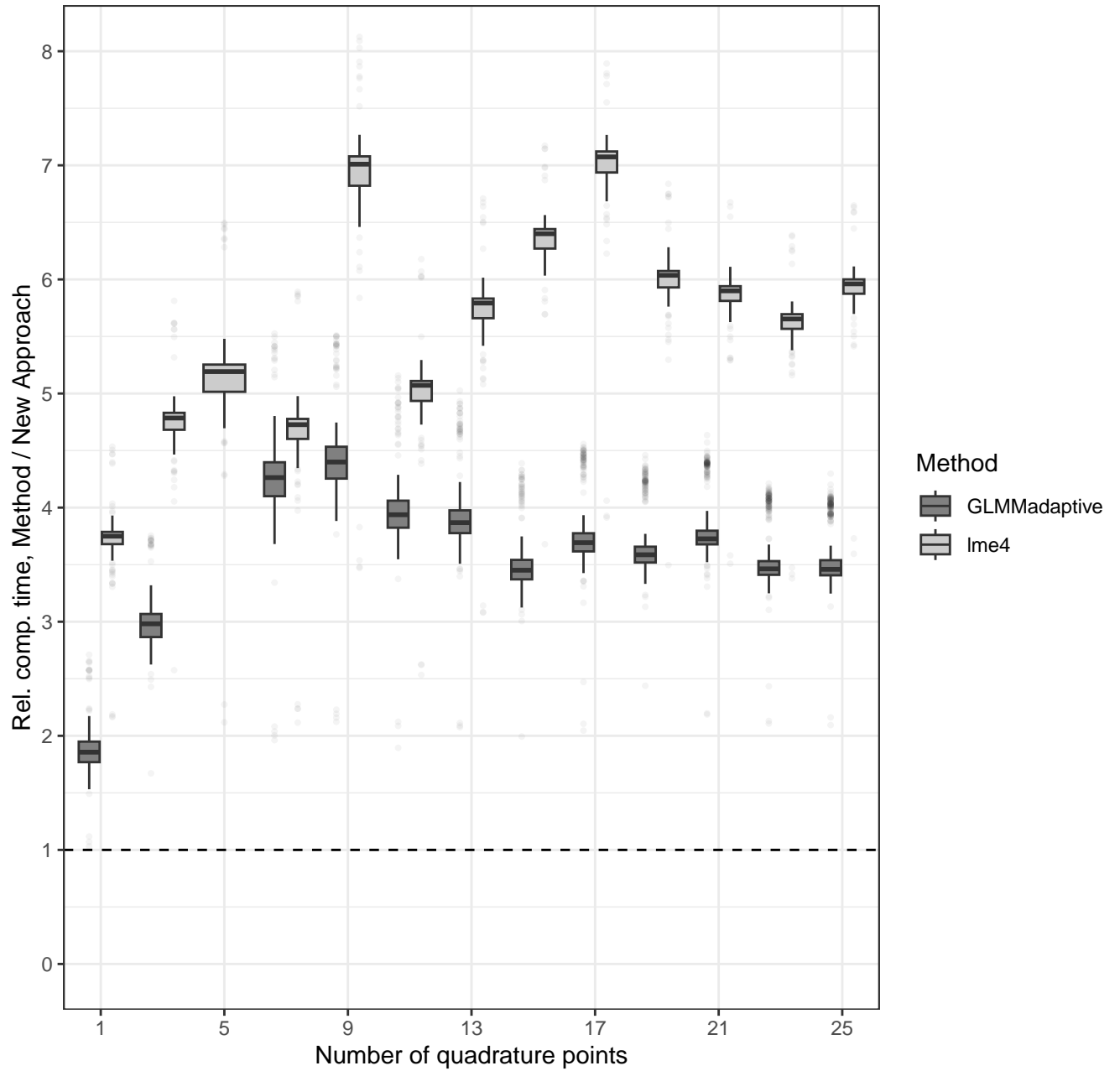


Figure 64: Relative computation times for the toenail fungus treatment data, for `GLMMadaptive` and `lme4` compared to the new method, over 500 repeated runs. The new method achieves a speedup of roughly between 2 – 7 times, which varies with k .

Absolute computation times (seconds), toenail fungus treatment data

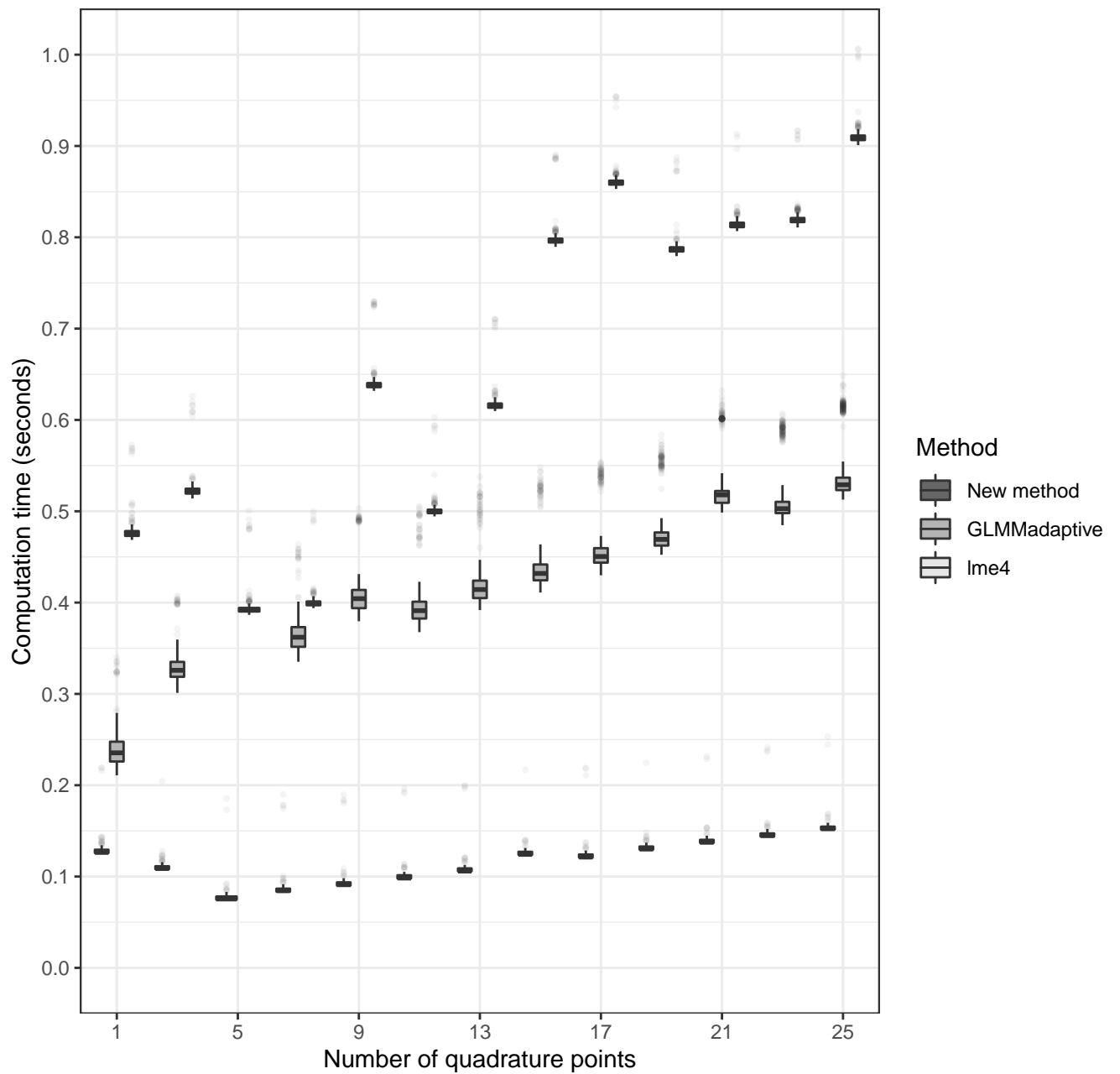


Figure 65: Absolute computation times in seconds for the toenail fungus treatment data, for the new method, `GLMMadaptive`, and `lme4` over 500 repeated runs. Both methods generally take more time for larger k , which is expected. All computations were performed on an M1 Mac book Pro laptop with 10 cores and 64Gb of RAM.